Historic, archived document

Do not assume content reflects current
scientific knowledge, policies, or practices.

Reserve
A99.9
F764U

USDA Forest Service
Research Paper INT-93
1971

U. S. DEPT. OF AGRICULTURE
NATIONAL AGRICULTURAL LIBRARY
RECEIVED

DEC 15 1971

PROCUREMENT SECTION
CURRENT SERIAL RECORDS

AIRBORNE INFRARED FOREST FIRE DETECTION SYSTEM: FINAL REPORT

INTERMOUNTAIN FOREST AND RANGE EXPERIMENT STATION
NORTHERN FOREST FIRE LABORATORY
MISSOULA MONTANA 59801

THE AUTHORS

RALPH A. WILSON is Principal Research Physicist, STANLEY N. HIRSCH is Project Leader, and FORREST H. MADDEN is Associate Research Engineer (Electronics) for the Project Fire Scan Research Program at the Northern Forest Fire Laboratory, Intermountain Forest and Range Experiment Station, Missoula, Montana.

B. JOHN LOSENSKY was the Research Forester in Project Fire Scan at the time this research was being conducted. He has since transferred to the Darby Ranger District of the Bitterroot National Forest, Darby, Montana.

ACKNOWLEDGMENTS

The authors gratefully acknowledge financial, technical, and cooperative assistance by several agencies and organizations in accomplishing the tasks included in this report. Among them are:

Bendix Corporation
Department of the Army, Office of the Secretary of the Army
Department of Defense, Advanced Research Projects Agency
The Electronic Command, U. S. Army Materiel Command
Litton Industries
Montana State Forestry Department
Texas Instrument Company
University of Michigan, Infrared Physics Laboratory, Institute of Science and Technology
USDA Forest Service, National Forest Administration

COVER PHOTOS

Front — Infrared imagery from patrol over Nezperce National Forest, Idaho. Lower fiducial mark in right margin is automatic target alarm on a wildfire in Granite Creek drainage.

Back — Photos of target area and closeup of the Granite Creek fire — still burning in the end of a fallen snag, with very little smoke.

USDA FOREST SERVICE
RESEARCH PAPER INT-93, 1971

AIRBORNE INFRARED FOREST FIRE DETECTION SYSTEM: FINAL REPORT

(Work Unit 2521A)

SUMMARY

A mathematic-functional representation of airborne infrared line scanners is used for development of an effective forest fire detection system. Conventional statistical descriptions of forest backgrounds are found to be useless for predicting detection probabilities. In situ fire detection probability measurements in 13 timber types representing the major forested areas of North America are presented. Detection probabilities approach 100 percent in the open-grown, shade-intolerant timber types; but the probabilities are marginal (50 to 60 percent) in the more shade-tolerant types, such as Douglas-fir rain forests on the West Coast and dense hardwood forests around the Great Lakes.

Also presented are the operational procedures for the system and the aircraft navigational requirements that were developed on wildfire patrol test flights made during the 1967 forest fire season in the Northern Rocky Mountains. Results of these tests indicate that approximately 50 percent of all possible wildfire targets are detected using the system. Proposed are some real time autocorrelation techniques that will significantly improve the detection capability of the system.

USDA Forest Service
Research Paper INT-93
May 1971

AIRBORNE INFRARED FOREST FIRE DETECTION SYSTEM: FINAL REPORT

Ralph A. Wilson,
Stanley N. Hirsch,
Forrest H. Madden, and
B. John Losensky

THE EVALUATION OF AN AIRBORNE INFRARED MAPPER
AS A TOOL FOR DETECTING AND MEASURING FIRES
(Work Unit 2521A)
for
Department of Defense, Office of Civil Defense
Contract OCD-OS-62-174
and
Department of Defense, Advanced Research Projects Agency
ARPA Order No. 636, Program Code No. 5860

ARPA REVIEW NOTICE

This report has been reviewed by the Advanced Research Projects Agency and approved for publication. Approval does not signify that the contents necessarily reflect the views and policies of this Agency.

INTERMOUNTAIN FOREST AND RANGE EXPERIMENT STATION
U. S. DEPARTMENT OF AGRICULTURE — FOREST SERVICE
Ogden, Utah 84401
Joseph F. Pechanec, Director

Northern Forest Fire Laboratory
Missoula, Montana 59801

AVAILABILITY NOTICE. — Distribution of this document is unlimited.

CONTENTS

Page

INTRODUCTION 1

DETECTION THEORY 8
Background and Targets 8
Equipment Development 14

PROCEDURES 17
Equipment 17
Airborne Detection Probability Tests 20
Mountaintop Tests 25
Operational Patrol Flights 27

DISCUSSION OF RESULTS 33
Percent Detection From Airborne Tests 33
Target Signal Strength and Timber Obscuration 35
Operational Tests 38

LITERATURE CITED 41

APPENDIX I — Scientific Names of Forest Species 45

APPENDIX II — Description of Test Areas 49

APPENDIX III — Mathematical Model and Detection Probability Test Data 65

APPENDIX IV — Data From Operational Patrol Tests 77

APPENDIX V — Equipment and Instrumentation 87

The use of trade, firm, or corporation names in this publication is for the information and convenience of the reader. Such use does not constitute an official endorsement or approval by the U. S. Department of Agriculture of any product or service to the exclusion of others which may be suitable.

INTRODUCTION

This work was undertaken because of a mutual interest of the Department of Defense, Advanced Research Projects Agency (ARPA), and the USDA Forest Service in the problems of detecting hot targets against natural terrain backgrounds using airborne infrared (IR) line scanning instrumentation. The study objectives were broadly defined in ARPA Order No. 544, which contains three specific task assignments that were modified from time to time during the course of the study. The basic problem was to examine the target obscuring effects of timber foliage or canopies on small charcoal fires in the forest cover types of North America. A concurrent objective was to develop an optimum system for airborne forest fire detection including the development of the operational patrol procedures.

Our work, beginning in 1962, is described in a series of three reports. This report, together with the Interim Report (1966), covers the development of the fire detection system. The third report, Fire Mapping 1968, supplements these two reports; however, it is limited to the development of the system's performance in mapping very large forest fires.

In 1962, we had planned a three-phase investigation of airborne IR fire detection problems to (1) develop the equipment; (2) measure fire detection probabilities of controlled targets in specific timber stands; and (3) develop operational patrol procedures.

The first year, 1962, was devoted primarily to acquiring and becoming familiar with the military IR line scanning equipment and adapting it to our needs. An AN/AAS-5 IR scanner was borrowed from the U.S. Army Materiel Command and installed in a Beechcraft AT-11 aircraft. We found that major modifications were needed in this hardware to accomplish the fire detection mission.

In the summer of 1963, we measured detection probabilities in only four timber types: ponderosa pine, lodgepole pine, larch–Douglas-fir, and Engelmann spruce. The idea was originated for estimating the target-obscuring effects of timber canopies using shade tolerance as a basis. We found that a standard dual-omni aircraft navigation system was inadequate for wildfire detection patrols. Also, we developed the following equipment requirements for operational patrol: (1) Rapid access to imagery; (2) a larger total field of view; (3) better optical resolution; (4) increased temperature sensitivity; and (5) more precise air navigation.

In 1964, we tried an operational test of the equipment and of navigational procedures that we had developed for wildfire patrols in a 6,000-square-mile area southwest of Missoula. Our tests failed because of IR equipment malfunctions.

The first 3 years of work are reported in the Fire Detection Interim Report (Wilson and

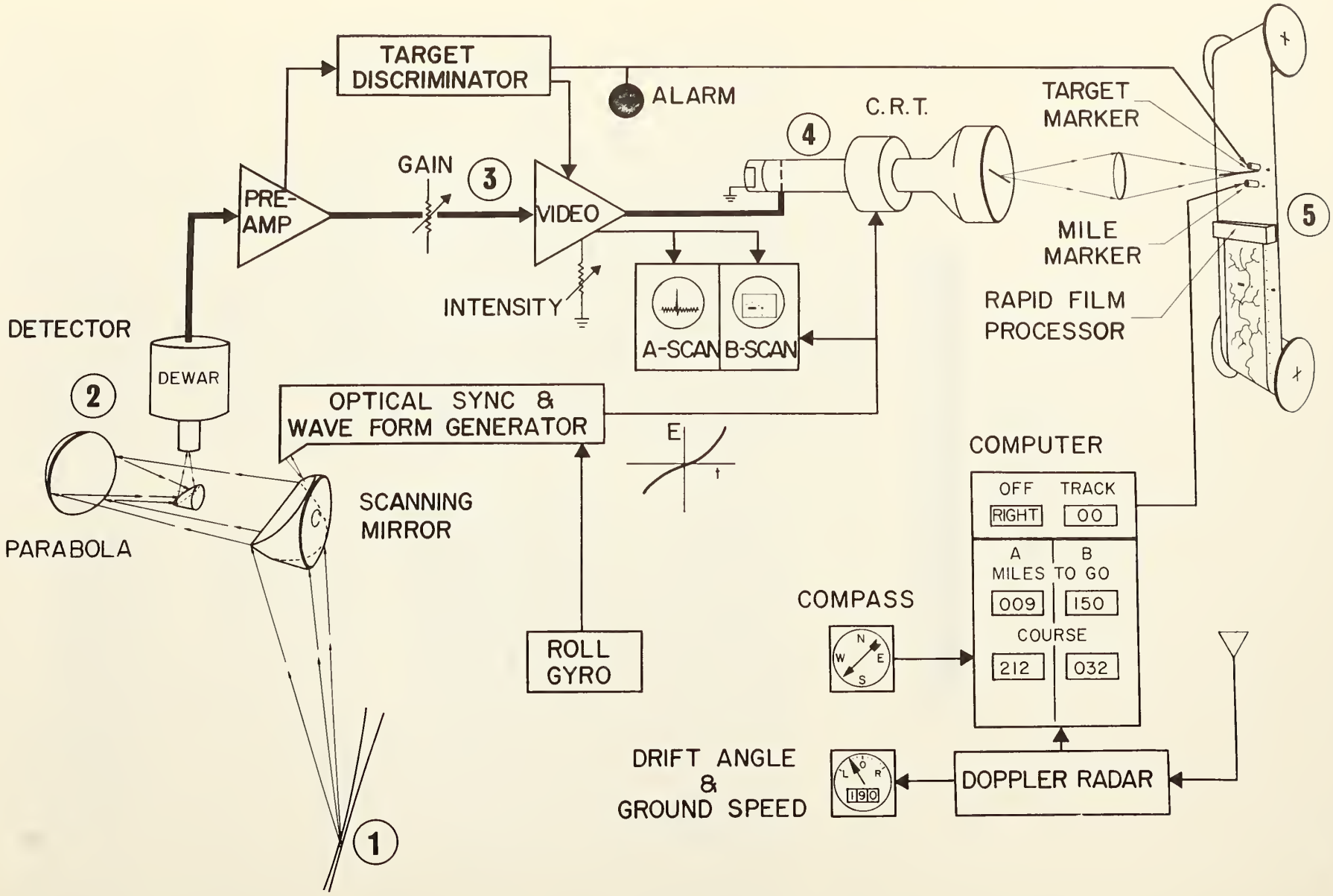

Figure 1. — Schematic of the 1967 IR detection system.

Noste 1966). From these early studies, we concluded that (1) the basic technique (i.e., airborne IR fire detection) was a sound approach; (2) detection probabilities in a wider range of timber canopies should be examined; and (3) an investment in more reliable equipment was necessary.

As a result of our 1964 work, we realized a very valuable spin-off of the detection program — the capability for mapping large wildfires. As a result, the fire mapping system was installed in an Aero Commander 500-B aircraft. In July 1966, this system was placed in operation in the Forest Service. A detailed description of the electronic signal processing required for fire surveillance is presented in Appendix V of the Fire Mapping Report.

During 1964, a Convair T-29B aircraft was obtained from the U.S. Air Force; in 1965, the fire detection instrumentation described in Appendix V was installed in this plane. This instrumentation was based on the concept illustrated in figure 1.

The study was expanded in 1965 and 1966 from the four timber types that were specified in the original ARPA task assignment to include 13 types; these were chosen to span the full range of canopy densities found in the north temperate zone of the Western Hemisphere. The Society of American Foresters (1956) recognizes approximately 150 timber types, of which about 75 types cover extensive geographic areas. Flights were made over test areas representing the 13 timber types in Louisiana, Illinois, Michigan, Montana, Idaho, Oregon, Washington, and Alaska. Figures 2 through 7 are samples of imagery of these test areas.

We realized that it was impossible to acquire enough flight data to predict reliably the detection performance at large aspect angles. As an alternative, a fixed platform was installed on a mountaintop within a larch – Douglas-fir timber stand, from which we were able to examine fire targets in detail. From the data, we developed a preliminary model for predicting detection probability based upon density differences in timber stands. In addition, recorded target signals from the mountaintop were used to develop the first automatic target alarm circuits.

The 1967 operational patrols (July 5 to September 1) encompassed the major portion of the forest fire season in the northern Rocky Mountains. The objective of these patrols was to scan as many natural wildfires as possible in order to gain operational experience and test the detection system.

While planning this report we felt that we had information to convey to three separate and distinct audiences. The first of these, of course, is the ARPA, whose support we gratefully acknowledge. That there are two other distinct audiences — forest land managers and systems design engineers — is symptomatic of the general lack of communication that often exists between systems development groups and systems user agencies which are particularly acute in forest fire detection.

In this report we have tried to show the forest land managers that small latent forest fires can be detected with reasonable probability using airborne infrared equipment. However, lookouts and visual air patrols will still find some fires that the IR scanners may miss and vice versa; and only lookouts can provide continuous surveillance of high hazard areas. On the other hand, IR systems provide new smoke penetration and nighttime detection capabilities. An integrated-combined systems approach will be necessary to achieve the most effective fire detection.

We have tried to demonstrate to the systems design engineers that forest fire detection is not a simple thermal mapping job. To be effective, this system must find the fire targets when they are very small and distributed over vast land areas. The fire targets must be precisely located to be of any use to fire suppression forces. In this report, we outline the basic requirements for a forest fire detection system and discuss the capability of the system to detect hot fire targets in natural forest backgrounds.

Our work prior to 1964 on detection probability and system development including the results of our early patrol tests is described in the Interim Report (Wilson and Noste 1966). This final report is concerned with the detection probability work we have conducted since 1965 when we adopted the detection equipment built to our specifications.

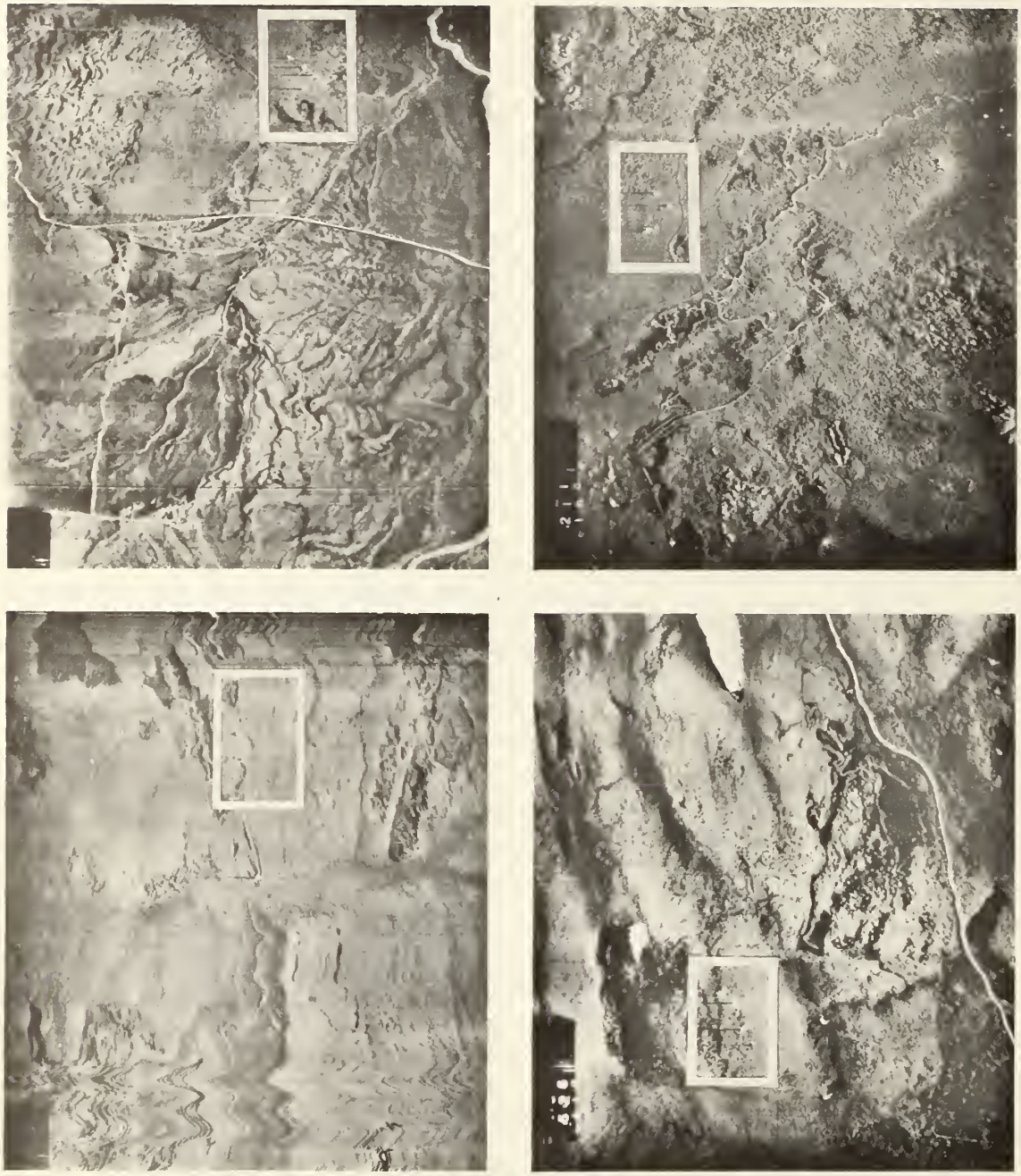

Figure 2. — Imagery shown above is from flights over ponderosa pine (932), lodgepole pine (135), Engelmann spruce (211), and larch—Douglas-fir (526) test areas. These were taken during the summer of June, July, and August 1963, using a Polaroid attachment to the AN/AAS-5 scanner. The Polaroid provided rapid access to the imagery for the detection tests, but would be inadequate for an extended patrol mission. The fire targets are observable and can be identified because we knew where to look (test areas are laid out within the white rectangles). Obviously, the targets would be difficult to discriminate from other background anomalies on a fire patrol mission because of the poor optical resolution (4 to 6 milliradians), the poor thermal resolution (3° to 5° C.), and the inadequate processing of the electronic signal.

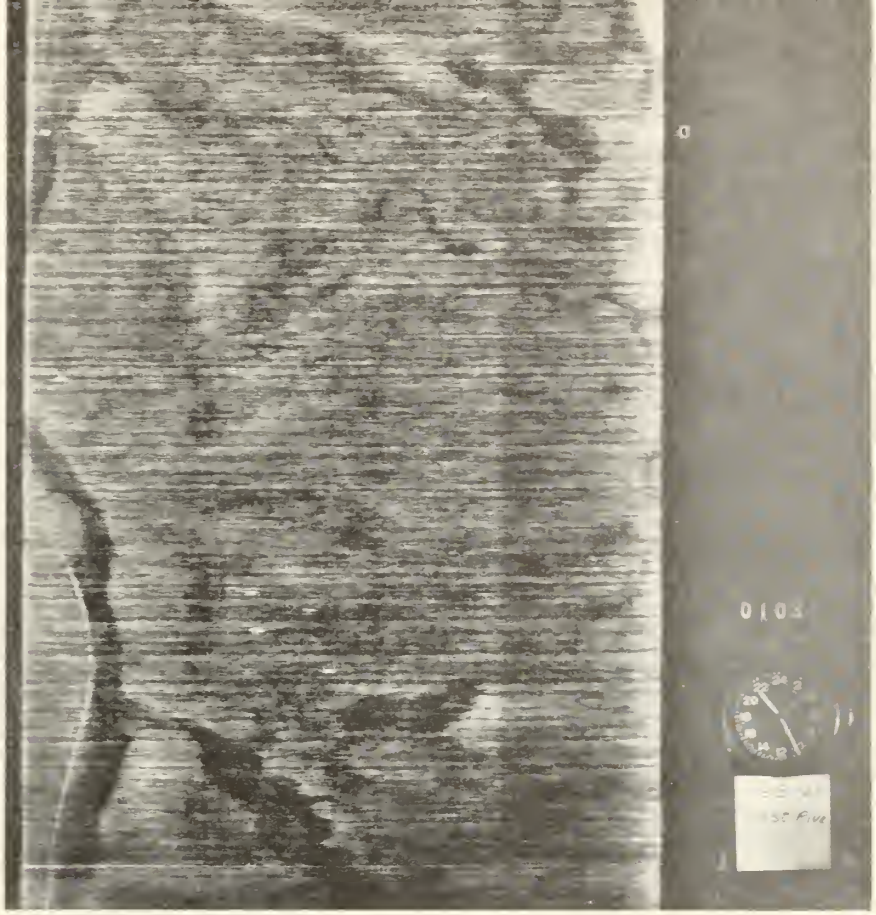

Figure 3. — Imagery of the western white pine test area on the Priest River in Idaho was made using the continuous strip camera. The excessive noise and improper response of the AN/AAS-5 system made the target difficult to locate on the imagery.

Figure 4. — Imagery of the western white pine test area was made in 1965 using the new Texas Instruments scanner and Litton electronic system. Although some instabilities are still evident in the imagery, the targets are much easier to discriminate from the background.

Figure 5. — These two pieces of imagery of the aspen test site of Michigan and the second-growth Douglas-fir in Washington, were made over terrain backgrounds having very low temperature contrast (the temperature differences measured on the ground were 4° to 7° C.). In both, the terrain detail is adequately mapped; the target signatures do not mask the surrounding background by oversaturating the electronics.

Figure 6. — This imagery was taken over the pin oak test area in 1966. Changes in the electronics improved the optical resolution and temperature resolution of this imagery over those shown in figs. 2 through 5. However, some sweep jitter and electronic instabilities are evident.

Figure 7. — The terrain adjacent to the white spruce test area along the Tanana River in Alaska is wet and boggy; it produces a flat thermal contrast. The horizontal bars are due to shifts in the electronic clamp of the CRT intensity level. Note that the bright specular reflection of the sun off the flat water surface does not affect the exposure of the surrounding terrain. The ability of the system to recover from saturation is one of the absolute requirements in fire surveillance.

DETECTION THEORY

Background and Targets

Timber provides the fuel for the fire target on the forest floor or in treetops or snags. The timber canopy attenuates the target radiance. And the timbered areas, together with grassy meadows, brush patches, barren rock faces and slides, and north-south slopes, provide the background radiant noise from which the target must be discriminated.

In addition to detection, we must locate the target relative to topographic features of the terrain background. In the sense of differentiating between desirable signals and undesirable noise, the terrain background is simultaneously a detection noise and a location signal.

Current state-of-the-art IR thermal mappers can produce imagery of background terrain with adequate resolution for the purpose of target location. Observable targets, of course, are printed in the background imagery. The detection of those targets is not a linear operation because the many possible inputs can produce only two outputs — a Yes-No dichotomy. However, IR mapping is a linear operation on orthogonal functions in the sense of superposition (i.e., the superposition of input signals provides a superposition of output signals).

No system is rigorously linear; however, the superposition requirement must hold over the dynamic range of the detection system — from significantly below the limiting background noise level up to a target signal level where the target detection probability approaches 100 percent.

We must recognize the photointerpreter (PI) as an integral part of any detection system because he makes the final decision. This decision function is also nonlinear, but the PI has an infinite advantage over an automatic line scan target discriminator (i.e., he has the facility for two-dimensional shape recognition).

Our concept of the ideal system includes an automatic target discriminator that sorts out all possible target signals. In such a system, the PI would simply review the automatic target alarms and eliminate those targets that he judged to be false alarms (campfires in campgrounds, bulldozer and construction equipment, and geothermal activity).

We should point out that false alarms may originate from two sources: (1) From thermal anomalies in the background scene, or (2) from internally generated noise in the system. Both of these types of false alarms are errors of commission. Missing a target that really exists is an error of omission that we must also avoid.

The choice of target threshold is an easy one if the automatic target discriminator can be set without concern for the relatively few false alarms caused by high peak signals. The unpredictable character of the peak signals is the major fault of statistical descriptions of non-Gaussian background noise.

Reliable estimates of minimum and maximum background temperatures can be made by judicious consideration of local meteorological data. These temperature estimates determine the peak-to-peak background contrast that is used to select the optimum detection threshold level for the automatic target discriminator. Such estimates provide a more useful criteria for threshold selection than would any conceivable statistical description of background noise.

The only remaining consideration for detection is the target radiance available at the entrance aperture of the IR system if given (1) an acceptable system capable of mapping the thermal background, (2) a realistic estimate of the peak-to-peak background radiance, and (3) a PI who can intelligently discriminate against false alarms by their unique extra-radiant character (slope, location, etc.).

The undetected, incipient forest fire has never been observed. However, the following generalizations of its character can be made:

1. It exists under a timber canopy, from which its fuels are derived.

2. For nonflaming, sustained combustion the temperature must range between 550° and 700° C.

3. In most fuels, combustion must exceed several inches in its least dimension to be self-sustaining.

4. Generally it will be located on an exposed air-fuel surface.

The typical target can be defined as not more than 5 square feet of glowing combustion.[1] This target is obscured to an unknown extent by the intervening timber canopy.

Theoretical treatments of detection probability start with a definition:

> **Detection probability is the probability that the target signal exceeds a threshold signal. The threshold signal is a signal level that the system operator may select by judicious consideration of the properties of the target, the background noise, and the IR system.**

The target signal is calculated by determining the system response to the target radiation (Wolfe 1965). The minimum acceptable threshold level is determined by fixing the maximum allowable false alarm rate. The false alarm rate is dependent on the characteristics of the background noise and the IR system's scanning function (Karr 1957; Genoud 1959).

Much has been published describing performance of IR search systems in "ideal" backgrounds (Hudson 1969; Jamieson 1963; Wolfe 1965). Almost invariably, system performance is described by a signal ratio — peak target signal (V_p) to root mean square (rms) noise (V_n) voltage ratio, V_p/V_n. Such descriptions assume that it is possible to determine the false alarm rate for any detection threshold level from incomplete statistical descriptions of the background noise (e.g., rms noise). Implicit in this assumption are the following: (1) The entire set of possible backgrounds have completely random properties (spatial and temporal); (2) these backgrounds have invariant statistical properties from one background to another; and (3) these statistical properties do not vary with the relative position of the observer (i.e., direction of view).

Robinson (1959) concludes:

> . . . **that these particular incomplete descriptions are only of value for a very restricted class of backgrounds. With most backgrounds and most systems, these methods are useless insofar as they can be used to predict performance.**

In other words, it would be very naive to consider wildland terrain backgrounds as having ideal, analytic statistical properties — they are not stationary, they are not ergodic, and they are not Gaussian.

Some have suggested more complete descriptions of backgrounds are needed (Robinson 1959; Holter and others 1962; Jamieson and others 1963). Obviously, a given background scene can be completely described by its spatial distribution of radiance, R(x). That is, R(x) is uniquely determined for every point (x) in the background. But, even a complete set of these detailed descriptions, R(x), does not meet the ergodic ensemble requirement for terrain background description (i.e., the value of a parameter — average peak radiance — is not the same when averaged over one scene or when averaged over the entire set of scenes).

The problem can be stated another way: A system should be capable of detecting targets against a wide selection of backgrounds. On any given mission, the detection threshold should be set with reference to the background that exists at that time in that locale. Thus set, the system will detect targets more reliably than if the threshold is set higher to miss false alarms for all possible backgrounds that might exist at any other time or place.

---

[1] *Reports on file at the Northern Forest Fire Laboratory indicate that five 1-square-foot combustion zones are found within a 30-foot perimeter in forest fires during the initial attack phase.*

Figures 8 through 15 show some of the effects of terrain backgrounds that are important in fire detection.

Figure 8. — An example of the spatial frequencies commonly found in the Bitterroot Mountains of western Montana is shown below. At least two distinct spatial frequency patterns are evident on this imagery. The first is the major drainage pattern of dark valley bottoms and warm exposed southern faces. The minor ridges and draws form a second distinct spatial frequency distribution.

Figure 9. — The river bottom at the top of the imagery shown above has little terrain detail which is due to low frequency spatial contours of the background. The higher alpine terrain at the lower end of the picture has much higher spatial frequency distribution caused by the minor ridges and draws and exposed rock faces. Note also that the river bottom along the top of the frame is warm relative to the background, while the higher valleys are cool.

Figure 10. — The high plateau area of eastern Oregon has a peculiar spatial distribution of backgrounds which is caused by the eroded washed drainage pattern (below). The speckled high frequency distribution of vegetation is another discrete background phenomenon.

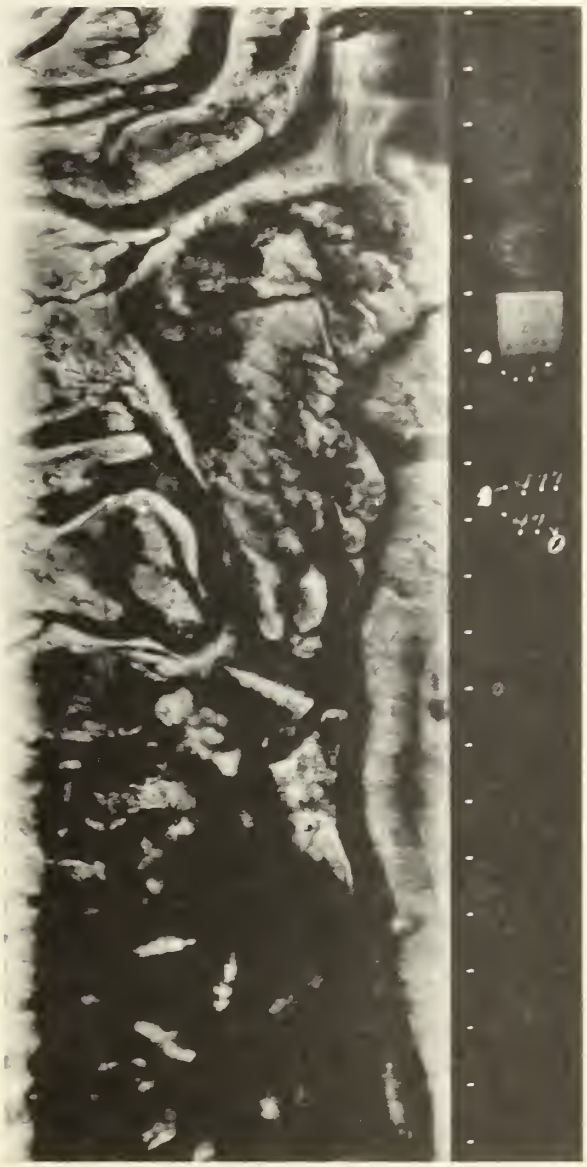

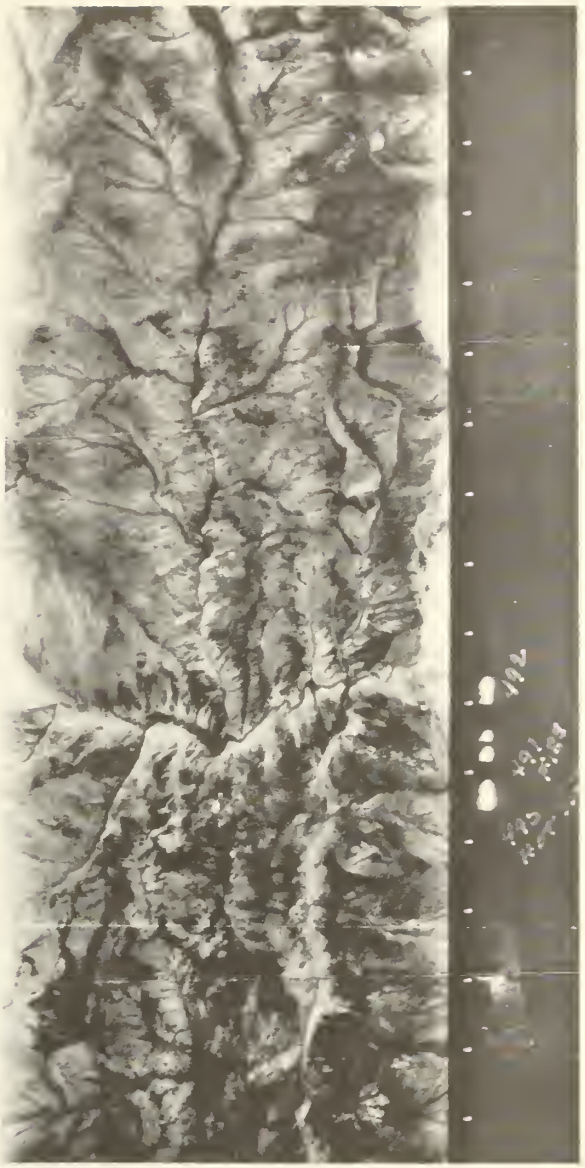

Figure 11. — The imagery shown above the exposed grassy slopes in the Salmon River country of Idaho shows the nighttime residual heat left by daytime solar radiation. The hot spring and creek can be seen in the center of the imagery just below the major river drainage pattern that runs horizontally across the frame.

Figure 12. — In the imagery below, the cool valley bottoms form a drainage pattern of low spatial frequency; the alpine meadows at the top and bottom form a spatial distribution of higher frequency.

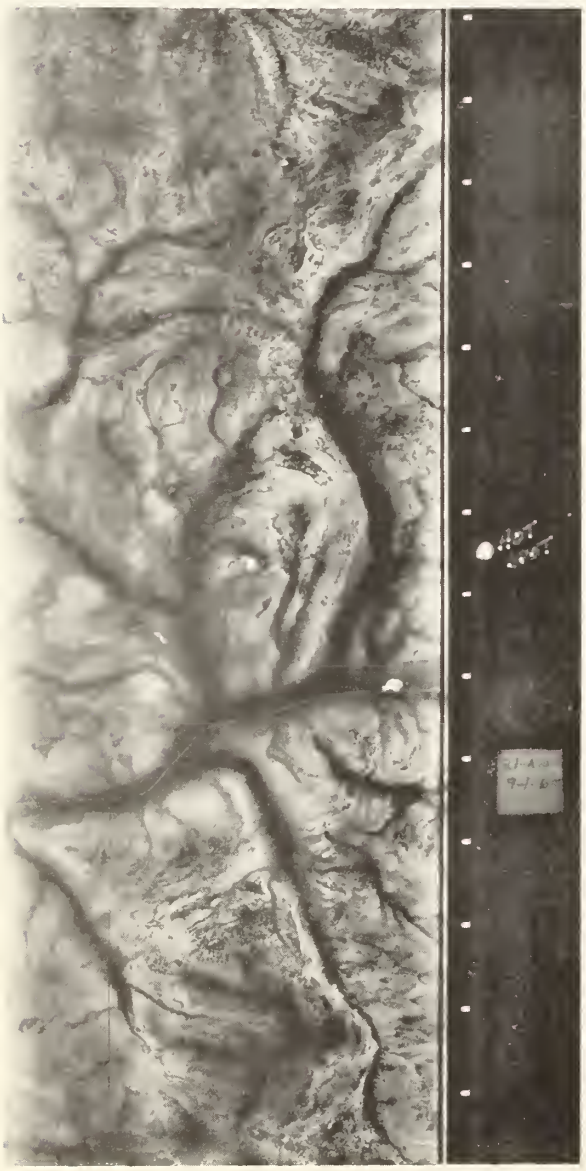

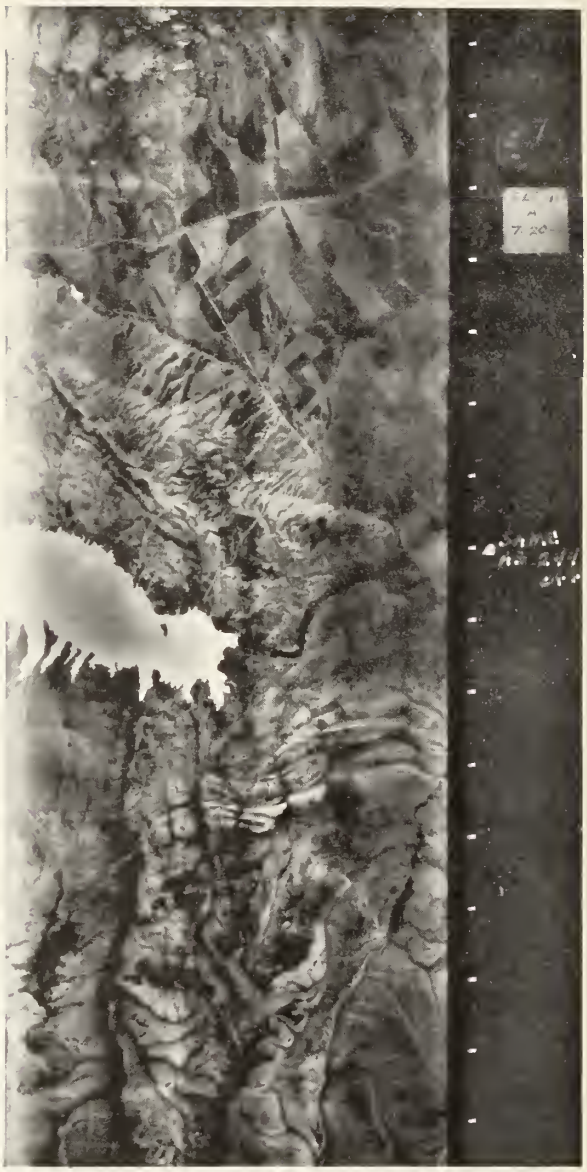

Figure 13. — Agricultural areas have a geometrical spatial pattern (above). Lakes and reservoirs are generally large; however, their shores have a sharp and discrete thermal contrast.

Figure 14. — Rockslides on southern exposures form a discrete and significant class of backgrounds, which makes fire detection difficult (below).

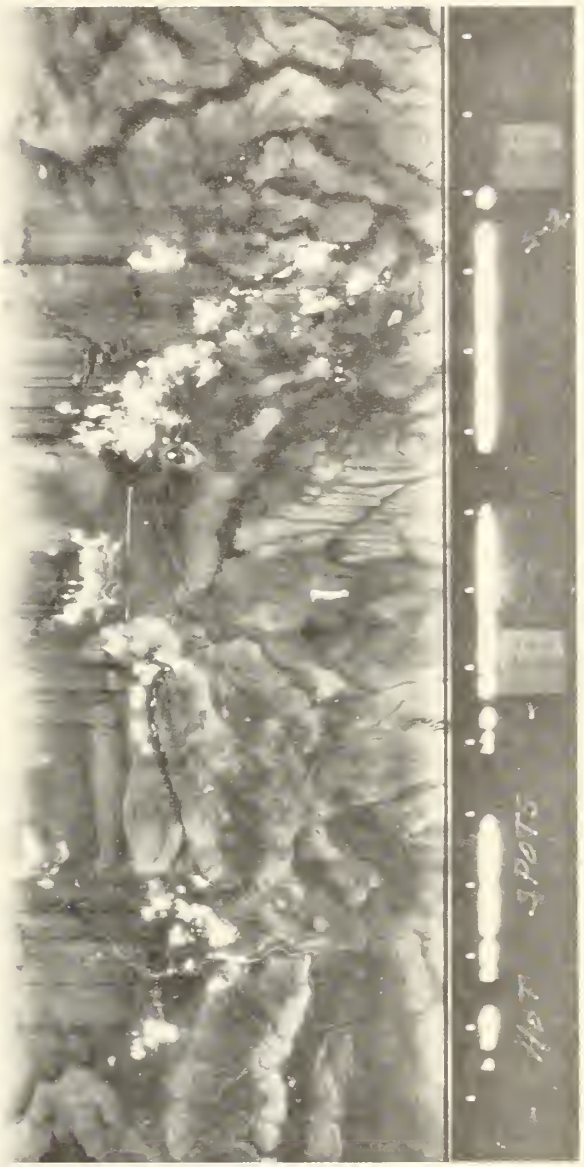

Figure 15. — This imagery is of the Gibbon Geyser Basin in Yellowstone National Park (above). Geothermal activity poses an obvious problem to fire detection.

Equipment Development

Designers of forest fire detection systems must recognize that (1) the purpose is to acquire and interpret certain information; (2) the equipment must process and reproduce the information without losing any significant detail; and (3) a well-designed system plays a major role in the decisionmaking process.

Initially, such information is a spatial distribution of cool, warm, and hot radiating surfaces. Thus, we first had to formulate a general expression for the radiant emittance distribution in the extended object plane of the terrain as Born and Wolf (1964-65) did for incoherent object illumination.

Let W(x, y) specify the radiant emittance for the point (x, y) in the object plane of the terrain. The properties of the imaging system may be characterized by a transform function, K(x,y; x′,y′). K is defined by the photographic exposure per unit area of the x, y plane at the point (x′, y′) in the reconstructed image plane. This exposure is caused by radiant emittance of unit amplitude at the object point (x, y). Thus, the spatial distribution of photoexposure on the IR imagery is given by:

$$I(x',y') = \iint W(x,y)\, K(x,y;x',y')\, dx\, dy \qquad \text{Eq. 1}$$

K is the functional transformation of the total system. K is also the product of all response and transform functions of the individual components of the system. The calibration of this function for our feasibility tests is discussed on page 22.

The total system and each identifiable system component has a characteristic input-output relationship. For this analysis, each transformation function is separable into a modulation function and a response function. For example, the input to our scanner is a radiation difference, W(x, y), between adjacent terrain areas. The detector output is a time dependent voltage, S(t). The transformation, U, for this part of the system is a product of a response function, $R\left(\frac{\text{volts}}{\text{watts}}\right)$, and a modulation function, M(x, y, t). Thus $U = R \cdot M$ such that the scalar product $S(t) = W(x,y) \cdot U(x,y,t)$. The two functions, R and M, affect the "thermal resolution" and the "optical resolution" of the system, respectively.

The performance characteristics of airborne IR thermal mappers have been adequately covered in the literature (Institute of Science and Technology 1962, 1963, 1965, 1966, 1968; Wolfe 1965; Jamieson and others 1963; Holter and others 1962). However, fire detection systems have unique operational requirements. The scanning of the terrain and the reconstruction of its image in fire detection systems follows the numbered sequence shown in figure 1. The radiant power from the source (1) traverses an optical path to the airborne scanner (2) where it is sensed by the detector and electronically processed (3). The electrical signal is applied to the CRT (4) and the CRT spot is projected onto the film (5).

An equivalent blackbody temperature, T_{BB}, is usually defined as the temperature of an "ideal" radiation source that provides the same radiant power as the "real" source being observed in the spectral region, $\Delta\lambda$, of the observation.

The total radiance emitted from a small resolution element is averaged over the elemental area, $\Delta x \Delta y$ (see 1 in fig. 1). The elemental area must include the hot target, if it is present. The following equation serves as the definition and physical interpretation of "average, effective blackbody temperature, T_{BB}, of the instantaneous field of view (IFOV)."

$$W'(\lambda,T_{BB},x,y) = \frac{1}{\Delta x \Delta y \Delta \lambda} \int_y^{y+\Delta y} \int_x^{x+\Delta x} \int_\lambda^{\lambda+\Delta\lambda} \epsilon(\lambda,x,y)\, W(\lambda,T,x,y)\, d\lambda dx dy$$

$$= \frac{1}{\Delta\lambda} \int_\lambda^{\lambda+\Delta\lambda} C_1 \lambda^{-5} \left(\exp(C_2/\lambda T_{BB}) - 1\right)^{-1} d\lambda \qquad \text{Eq. 2}$$

Note that the spectral dependence of $W'(\lambda, T_{BB})$ is not identical to that of $W(\lambda, T)$ within the element $\Delta\lambda$. Serious problems concerning T_{BB} arise when the hot target is included in the elemental area. There is always a T_{BB} that satisfies equation (2). However, T_{BB} does not approximate the true thermal temperatures of the source when the source significantly departs from the ideal blackbody conditions. When such is the case, we discard the simplified ideal blackbody assumption in favor of the actual spectral distribution (i.e., the real spectral character, $\epsilon(\lambda)$, of the source and/or the real spatial distribution of thermodynamic temperature).

From the source, the radiation traverses an optical path to the scanner's entrance aperture, A_a (at 2 in fig. 1). The spectral distribution of the transmission, $\Upsilon(\lambda)$, of radiation through the optical path is dependent on atmospheric composition. The scattering and obscuration effects of timber canopies are included in $\Upsilon(\lambda)$. The spectral responsivity, $R(\lambda)$, depends on the detector that is used. We include the spectral characteristics of the optical system in $R(\lambda)$.

The signal S_d, from the detector in response to radiant power, W, from the terrain is:

$$S_d(T_{BB},t) = \omega A a \int_{-\infty}^{\infty} \int_{-\infty}^{\infty} W'(\lambda,T_{BB},r)\, \Upsilon(\lambda)\, R(\lambda)\, \delta(r-\dot{r}t)\, d\lambda\, dr \qquad \text{Eq. 3}$$

where

$$\omega = \left(\frac{\Delta x \Delta y}{h^2/\cos^3\theta}\right)$$

$= \alpha \cdot \beta$ is the lateral angular resolution times longitudinal angular resolution[2]

r = vector notation of coordinates x, y on the terrain object plane

t = time

$\dot{r}$ = scanning rate in the object plane

δ (r - $\dot{r}$t) is the scanner-receiver modulation function

From scanner geometry,[3] $\dot{r} = \dfrac{h}{\cos^2\theta}\dot{\theta}$

where

h = aircraft altitude

θ = scan angle

$\dot{\theta}$ = rotational speed of scanning IFOV.

δ performs the space-time convolution and has a maximum value of unity and a width equal to the effective size of the resolution element of the scanner. In principle, δ includes the transform (MTF) of the point spread function, which in theory depends on optical resolution, the time constant of the detector, scan rate, etc. In most well designed IR line scanners, those spread functions are made insignificant in comparison to the size of the field stop. The rectangular area, $\Delta x \Delta y$, of δ for a square field stop projected on the ground is

$$\Delta x \cdot \Delta y = \frac{\alpha h}{\cos^2\theta} \cdot \frac{\beta h}{\cos\theta} = \frac{\omega h^2}{\cos^3\theta}$$

and the dwell time, $\tau = \Delta x/\dot{r} = \alpha/\dot{\theta}$, is constant over the full width of the scan line. The size, $\Delta x \Delta y$, of the IFOV (the projection of the resolution element onto the terrain object plane) varies as the aspect angle, θ, along the scan line.

The thermal washout at the edges of the imagery of certain discrete classes of background objects (see figs. 8 to 15) is caused by the averaging of T_{BB} over the larger IFOV at the ends of the scan lines. At the same time, other size classes may be printed with good contrast. This observation supports our contention about the non-Gaussian character of forest backgrounds.

The time dependent electric signal from the detector is amplified and processed by well known techniques (3 in fig. 1). From a practical engineering standpoint, the processing through amplifiers, filters, etc., requires that we look in detail at the time-frequency transforms of individual components (see Appendix V). For this functional representation we will define the gain, G, of time-dependent signals from the electronic system such that

$$S_o(t') = G(t, t')\, S_d(t). \qquad \text{Eq. 4}$$

[2] *Longitudinal resolution is in the direction of the aircraft flight path; lateral resolution is in the direction along the scan line, perpendicular to the flight path.*

[3] *Rigorously, θ is measured in the vertical plane of* x *(with no* y *component); $\dot{y}$ is the aircraft speed, and $\dot{x} = \theta h/\cos^2\theta$ is the scanning sweep speed and $\dot{r} \approx \dot{x}$ because the ratio $\dot{y}/\dot{x}$ is very, very small.*

Note that G need not be linear. In fact, system requirements for adequate thermal resolution at low signal levels (terrain background) and large dynamic range (hot fires) suggest a highly nonlinear, electronic gain. The first stages of signal amplification are generally the source of the limiting system noise.

The signal, S_O, is applied to the Z input of a CRT (4 in fig. 1). Thus, emittance of the source is related to the visible output — spot intensity of the CRT — and is characterized by a response, I, (e.g., luminosity per volt) and a spatial distribution δ'. The spot is focused on a photographic emulsion moving normal to the scanning direction and results in an exposure.

$$E(r') = \int S_O(t')\, I\, \delta'\, (r' - \dot{r}'t')dt'. \quad \text{Eq. 5}$$

I is the photographic exposure per unit of signal for the CRT-camera system; and $\delta'(r' - \dot{r}'t')$ is the time-position transform of the writing CRT spot on the photographic film.

The photographic film (5 in fig. 1) is processed with a characteristic, γ.

$$D(r') = \gamma \log E(r') \quad \text{Eq. 6}$$

is the film's optical density as a function of position, r' on the film.

The limiting system noise may be printed on the film. Knowing the system transfer function, we can calculate the noise equivalent input. Noise equivalent power, NEP (or NET defined in equation 2), of the system is defined as the difference in input radiant power, $\Delta W(T_{BB})$, that will produce a film density contrast equal to the density contrast produced by the limiting system noise. To determine a value of NEP, we must explicitly define our noise measurement (i.e., peak-to-peak or RMS, bandwidth, etc.) and the equivalent radiation signal (shape, size, power, etc.).

The imagery is an exact reproduction of the thermal scene, and film density is functionally equivalent to terrain temperature, $D(r') \equiv W(r')$, only to the extent that:

1. The total transformation from equation (3) to equation (6) is linear and the principle of superposition holds. The radiant power must approximate an ideal radiator in the spectral range of the observation, and the radiation contrast must significantly exceed the equivalent system noise.

2. That the δ and δ' are properly synchronized and produce complete sets of orthogonal functions, S(t) and D(r'). Note that the image resolution is determined by the total "spread" in the product of all these transforms, including those, G(t,t'), within the electronic video chain.

PROCEDURES

Equipment

The equipment installed in the Convair T-29 aircraft is shown in figures 16, 17, and 18. This aircraft was an ideal flying laboratory in which equipment development and modifications were easily performed.

The IR receiver (including mechanical mount, optics, drive motor, and InSb detector) is a stripped down version of the RS-7 IR line scanner built by Texas Instruments, Inc.

Several preamplifiers have been built and tested in attempts to resolve the video problems, such as amplifier noise, target and background dynamic range, and low thermal contrast of backgrounds. A discussion of preamplifiers is given in Appendix V.

The electronic equipment for signal processing and CRT display was built by Litton Industries, Electronic Tube Division. Slant range correction (rectilinearization), electronic roll correction and good d.c. amplification of the video signal were designed into the equipment.

The imagery is reproduced on an Ansco rapid film processor — KD-14 camera system. This camera produces continuous strip imagery that is available for viewing within a few seconds after flying over an area.

The navigation system that was in the T-29 when we obtained it from the Air Force was an AN/APN-81 Doppler radar. We replaced it in 1967 with a more reliable Bendix DRA-12/CPA-24 Doppler radar navigation system. Both of these systems compute aircraft position from the track of the Doppler radar and the aircraft compass heading.

In 1967, we added the target discrimination module (TDM) to our system. The TDM provides a marker pulse for the imagery and a trigger for an external alarm. The target markers are shown in the imagery of figure 19. The down track mileage marks from the navigation system are also shown.

Auxiliary instruments that were necessary for these tests included an extra set of flight instruments — altimeter, groundspeed indicator, etc. — for the test observer, and electronic test equipment for monitoring, processing, calibrating, and recording of the video signals.

The operational goals for the fire detection system were arbitrarily established by considering three factors: economics of fire detection, performance of alternative detection systems, and the expected capabilities of IR line scanners. The goals were as follows:

1. Detect fires as small as 1-square-foot of burning material.
2. Locate these fires relative to the thermally mapped background terrain.
3. Patrol 5,000 to 10,000 square miles per patrol mission.

As suggested by Wolfe (1965), these goals reduce to a set of system performance parameters as follows:

1. Aircraft speed of 200 miles per hour and 10-mile-wide coverage gives 2,000 square miles per hour capability.
2. 15,000 to 18,00 feet altitude with 120° wide field of view will provide 10-mile-wide coverage with adequate overlap for navigation of adjacent patrol strips.
3. The thermal and optical resolution requirements reduce to a capability of observing 1° or 2° C. background temperature differences; 30- to 70-foot objects are resolved with 2-milliradian instantaneous fields of view.

Figure 16. — Convair T-29B aircraft.

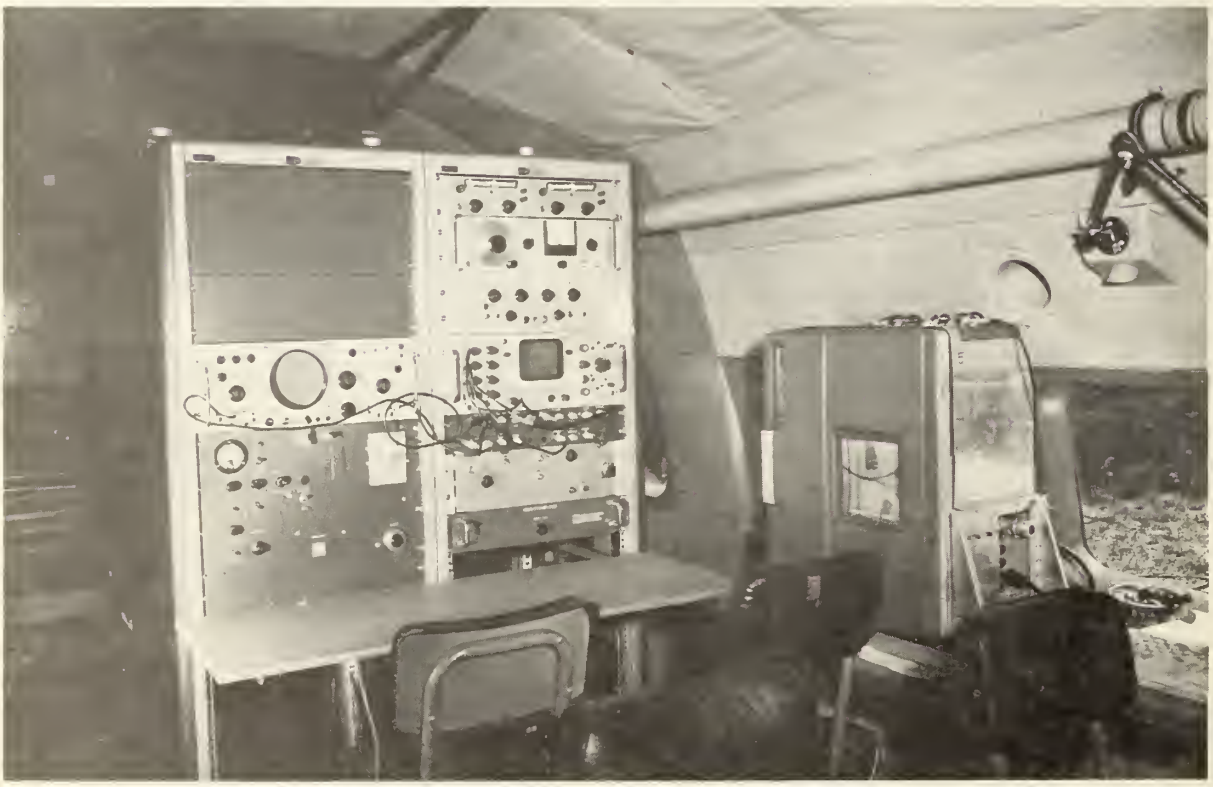

Figure 17. — Equipment racks and tape recorder installation in aircraft.

Figure 18.—Navigation and observation console containing Doppler radar and navigation computer.

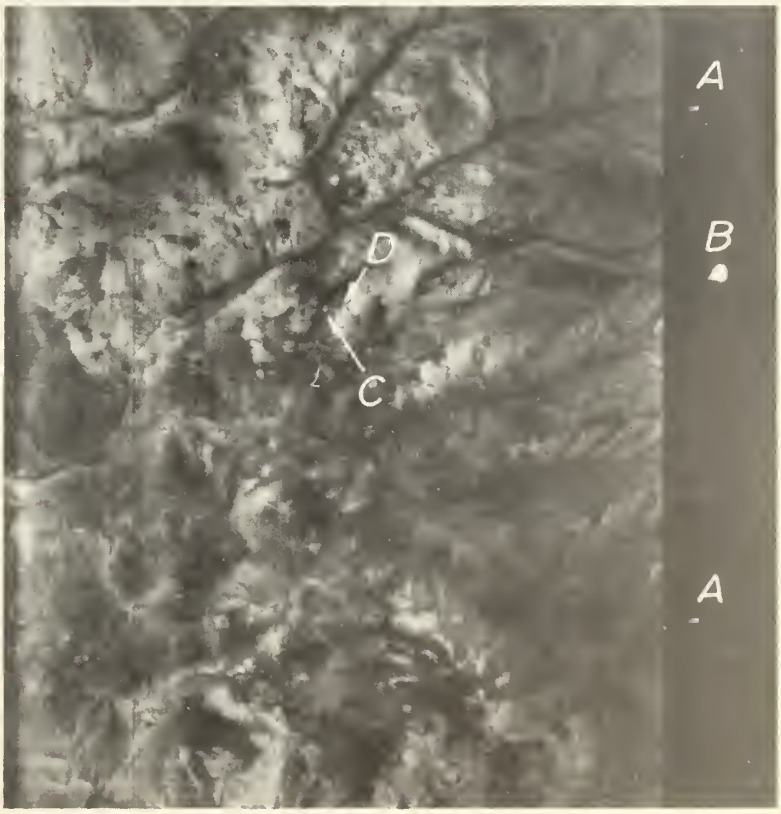

Figure 19. — This IR image, made at 12,000 feet above terrain, covers approximately 40 square miles. A, Inserted by the navigation system, these marks show 5-mile intervals along the track; B and C, automatically inserted by the TDM to indicate the presence of a fire target; and D, latent forest fire.

Airborne Detection Probability Tests

We used Baker's (1949) table for ranking tree species by shade tolerance as a qualitative indicator of crown density because species having dense crown foliage logically (1) would obscure fire targets, and (2) be more tolerant of shade. Thus shade tolerance was used as one scale of measurement for crown density. As a result of preliminary investigations, however, we found that a second scale of measurement for crown density was needed for insuring reliable prediction of detection probabilities. To do this better, we took field measurements of tree crowns in terms of height, diameter, and closure, as well as stems per acre, diameter at breast height, etc. (see Timber Cruise tables, Appendix II). These measurements were used to construct the prediction model as described in Appendix III.

The individual test areas were fully stocked. We preferred that the trees be confined to the early, mature stage and that the stands be of a basically pure type (Society of American Foresters 1954, p. 67) to allow explicit description of the composition of the test stands. These timber cruises were made in each test area using the variable radius Bitterlich plot technique (Grosenbaugh 1952, p. 32-37).

Each plot location was described according to slope, aspect, and basal area. These same plot locations were used as the test fire points.

In four of the test areas — second-growth Douglas-fir, western white pine, northern hardwoods, and lodgepole pine — the diameters and heights of each tree bole and tree crown that intercepted the scanner line of sight were measured for all aspect angles from 0° to 60°.

An analysis of 250 smokejumper reports indicated a typical spot fire consists of five 1-square-foot burning areas in a 30-foot-diameter circle. A typical spot fire spreads slowly along a broken perimeter, leaving a burned out interior and a large amount of cold or dead fire edge. Such fires in the dormant, or incipient state, maintain a fairly constant live burning area that disperses as hotspots burn apart. Therefore, we simulated these fires using five 1-square-foot buckets of burning charcoal equally spaced on the circumference of a variable radius circle. We termed these "test fire arrays." The circle radius was varied in 3-foot increments from 3 to 15 feet. Spacing of 300 feet between test fire arrays facilitated separation on the IR imagery. Fifteen to 20 test fire arrays were laid out in each of the 13 test areas.

The buckets of burning charcoal closely approximate Lambertian radiators. Temperatures of these range from highs between 850° to 900° C. 30 minutes after ignition to lows between 550° to 600° C. 5 hours after ignition. These temperatures were affected by meteorological conditions — the most apparent being the effect of wind.

During the flight tests, a ground crew monitored these target temperatures as well as terrain background temperatures. Meteorological records were kept of wind, air temperature, and relative humidity. These measurements were needed in data analysis to remove the variable effects of atmospheric water absorption and target temperatures. The ground crew also changed the radii of the test fire arrays upon instruction from the flightcrew.

In addition to the pilot, copilot, and crew chief, the flightcrew included a flight observer and an equipment operator. The flight observer monitored the IR imagery while the equipment operator adjusted system electronic controls so that terrain background contrast covered the lower half of the film gamma curve. On the film the upper portion of the gamma curve was reserved for fire target signatures. System settings corresponding to film exposure (cathode ray tube bias, or level) and temperature contrast (amplifier gain) were logged by the observer. These records proved invaluable for system development, but were inadequate for rigorous data analysis.

After 1965, most of the test data were also recorded on magnetic tape as well as film. The magnetic tape was used extensively for system development and performance checks. In addition, it provided precise data on target strength for comparison with the PI's subjective target measurements on the IR imagery.

Test flights were made at 8,000 feet over terrain. The aspect angle was varied in 10° in-

crements. The scanner optical system was tilted in pitch angle for aspect angles from 0° to 40°. The aircraft flightpath was offset for aspect angles from 40° to 60°.

For cost reasons. we simplified this procedure and adopted a "rule-of-thumb" flight plan as follows:

1. Two passes were flown over the test area from opposite directions (i.e., 30 to 40 target observations), after which the flight observer counted the targets on the imagery. This pair of passes was made looking straight down (0° aspect angle) with the targets on a 9-foot radius (halfway between 3 and 15 feet). If near 100-percent detection was observed, the aspect angle was increased to 10° and the next pair of passes was flown. As long as percent detection "looked good," two passes were made at each succeeding 10° aspect increment to a maximum of 60°.

2. When, or if, the percent detection decreased significantly, two to six additional passes were made at each 10° increment until the flight observer had established a representative average percent detection. This procedure was continued out to an aspect angle of 60°, or until the percent detection had fallen to less than one-half of its 0° aspect value.

3. If the target data were high (80- to 100-percent detection), we assumed the detection of fires over 9 feet also would be good and the ground crew was instructed to move the targets to a 3-foot radius. However, if the 9-foot data were low (less than 80-percent detection), the targets were enlarged to 15-foot radii and, the 10° angle increment procedure was repeated. Six-foot and 12-foot fire radii were tested only if it was necessary to fill in large differences of percent detection between the 3-, 9-, and 15-foot radii targets.

Figure 20. — Imagery of 20 target arrays in the aspen test area.

Imagery was recorded in flight on 5-inch film using a KD-14 rapid process camera and simultaneously on magnetic tape using an Ampex 1300 recorder. Figure 20 is sample imagery of a 20-target test area in the aspen test area. In this imagery, the test fires were placed on the circumference of a 3-foot-radius circle and viewed vertically (0° from the nadir). Forty to 100 pieces of imagery in each timber type were necessary to determine the capabilities of the detection system and to determine what fire size and aspect angle limited performance.

A simplified schematic of the test system and its associated response functions are shown in figure 21 to demonstrate our calibration technique. A density wedge was photographed on film and used to measure target strengths directly from the imagery. This wedge is the film record of calibrated signals introduced at the system input by a pulse generator. The wedge provides the PI with a scale 0 to 5 of target strengths for various background densities (fig. 21B, far right).

Figure 22 shows the video traces of individual target signals that were tape recorded simultaneously with the imagery shown in figure 20. The numbers in the upper left-hand corner of each set of traces identify individual targets. Signal strengths (0 to 5) are subjective evaluations of target intensity from filmed imagery — 0 represents no detectable target and 5 represents a saturated target. The PI's subjective measurements are well correlated with the actual signal strengths. Thus, we reliably read the target signals directly from the imagery. We then normalize these data to constant atmospheric path, target temperature, and aircraft altitude.

Adjustments made by the equipment operator proved to be a crude data normalization procedure in itself. For example, the flight observer made compensating adjustments of the imagery's thermal contrast in response to changes in environmental conditions (e.g., atmospheric H_2O absorption or target temperature). Thus, our hot target signatures as read from the imagery could not be used to determine optical attenuation coefficients of the timber canopy. This was disappointing. However, this did not seriously affect our primary objective of measuring the system's detection capability because we recognized that the calibration wedge is only a reference scale for target comparison.

The only system requirements for adequate data acquisition are (1) that the terrain background be easily observable above the system noise limit; and (2) that the flight observer must adjust the gain and level controls for optimized imagery, as described above.

It must be emphasized that the PI was always aware of the precise location of the targets in these tests; therefore, he was confident of his ability to identify targets that were hidden in the background. Actual detection of an individual fire is a yes-no dichotomy. Detection probability is the fraction of total fires that a PI observes on the output imagery. Detection probability should be related directly to the target signal strength. Even though we are primarily interested in the number of targets detected, the readings of target signal strength are better indications of system performance because we have more statistical confidence in a measure of target magnitude than we have in the yes-no dichotomy. In these tests, the PI was obviously biased by previous knowledge of target location. By requiring the observer to estimate target signal strength, a more objective measure of detectability is provided.

In the operational mode, detection performance will depend — in part — on the PI's ability to pick out submarginal targets, which in these tests were included as positive detections.

Each "piece" of imagery represents one pass over the test area and contains the target signatures of 15 to 20 test fire arrays. At least two pieces of imagery were made at each aspect angle and for each fire size in each timber type. Three different PI's read each piece of imagery; thus, each primary data point (average signal strength) represents the average of three readings of at least 30 individual target signatures. In cases where the flight observer determined "unusual" differences (number of targets on imagery or magnitude of target signals) between the first two passes, additional pairs of passes were flown until the differences were subjectively resolved. This procedure was a compromise (as we have already inferred) between statistical confidence in the data and economy of operation.

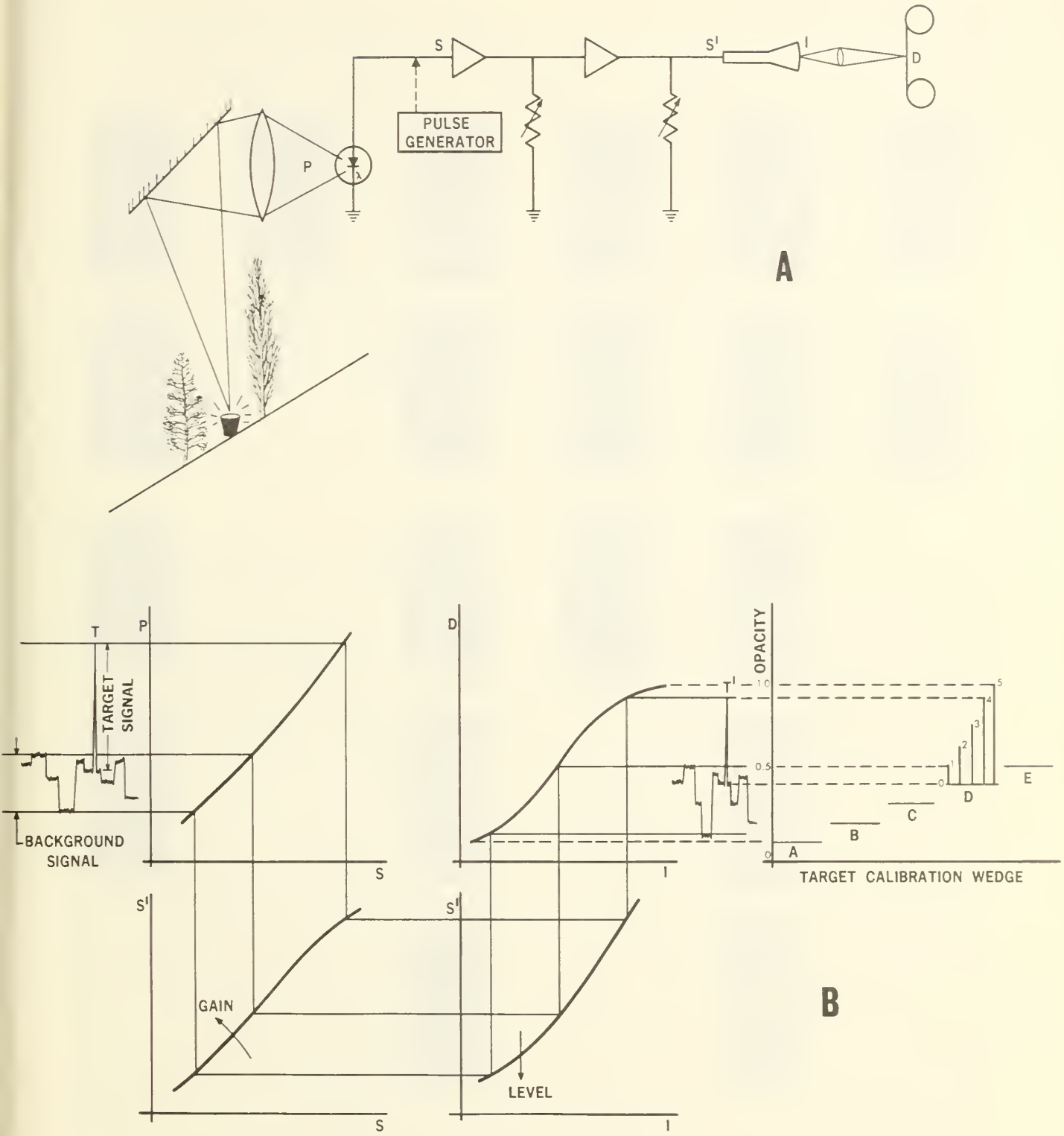

Figure 21. — A, Schematic of IR system; B, transfer function demonstrating target calibration technique.

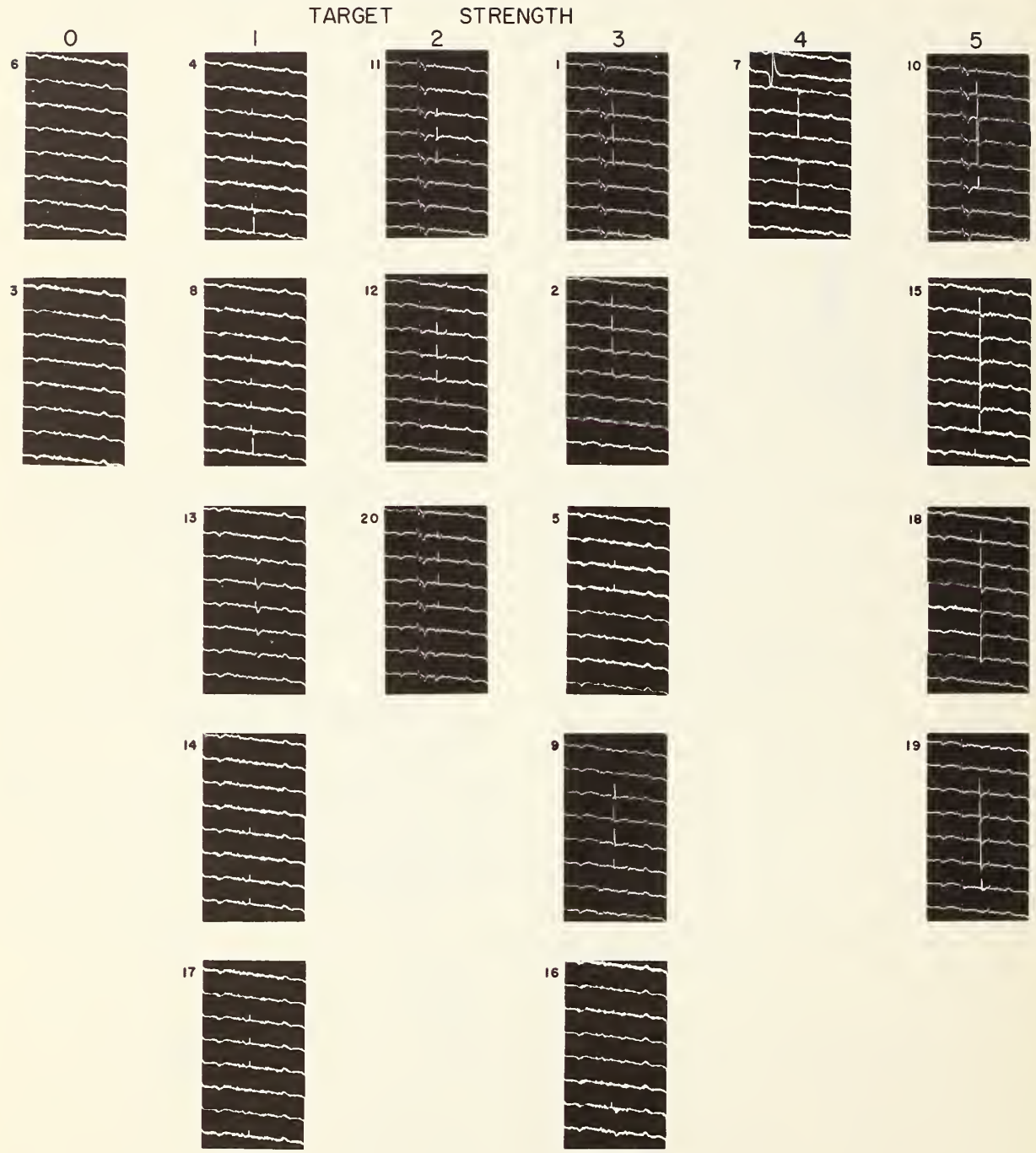

Figure 22. — Oscilloscope traces of target signals of typical test imagery (aspen, northern Michigan, August 2, 1965).

The flight observer monitored the IR imagery in "real time" for the primary purpose of directing the progress of the tests. In figure 23, his record of targets observed in flight are correlated with the later, more detailed recount by the PI's. The observer efficiency (ratio of flight observer's target count to the PI's target count) was 86 percent — average over 493 pieces of imagery from nine test areas.

Two types of error by the flight observer are possible: (1) Identification of targets that actually have no signature on the imagery (false alarms) — this error (of commission) occurred very seldom; or (2) missing or failing to count targets with identifiable signatures — this error (of omission) was far more common. Most of the missed targets (14 percent) had very weak, marginal signatures.

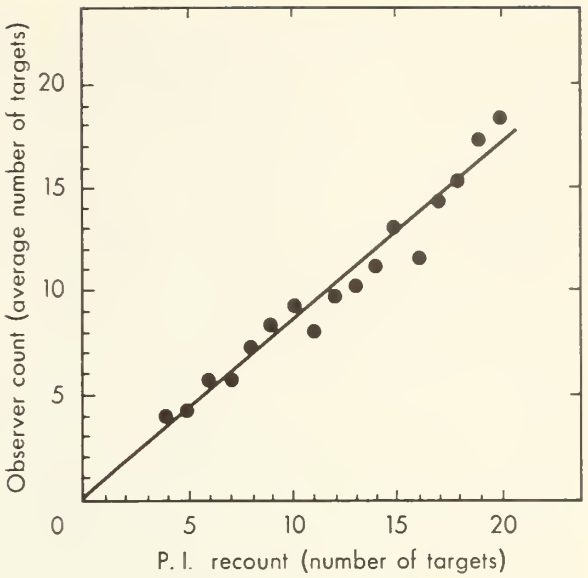

Figure 23. — Percent real time observer count versus PI recount.

Mountaintop Tests

The objective of the mountaintop tests was to measure detection probability at large vertical angles in one timber type.

The scanner was installed on a cliff overlooking the Bear Creek Drainage test area (fig. 24). This area is located west of Victor, Montana, in a well-stocked, mature larch — Douglas-fir stand associated with grand fir, Engelmann spruce, alpine fir, and lodgepole pine.

Test plots were established in the timber stand at 45°, 48°, 50°, 54°, 58°, and 60° aspect angles. Each test plot consisted of two lines 250 feet long and about 15 feet apart, oriented at right angles to the scanner line of sight. Slant ranges from the scanner to the test plots were between 2,000 and 3,600 feet.

The AN/AAS-5 scanner had been modified to improve its dynamic range and lower its noise level. The video signal was amplified by about 40 db. Target signals (A-scan traces) were recorded on Polaroid film from a Tektronix 535 oscilloscope (fig. 25). Electronic gain was periodically calibrated to compensate for drift caused by changes in environmental conditions.

A 1-square-foot burning charcoal target was moved in 1-foot increments along the test lines, providing approximately 500 individual target readings at each aspect angle (fig. 26). Radiometric tests in the laboratory wind tunnel had revealed that significant temperature fluctuations would occur as a result of wind and physical jostling of the fire bucket. Every possible precaution was taken in the field to minimize these fluctuations. Weather data, bucket temperatures, and background temperatures were recorded continuously.

Unobscured control targets were located at least 20 feet outside each end of the test line. These control targets provided an additional target calibration signal and aided the scanner operator in locating the test lines.

A detailed timber cruise was made of all trees located within 50 feet in front of each test line; each tree was identified by recording species, d.b.h., tree height, crown height, and crown width. Trees exceeding 5 inches d.b.h. also were measured that were growing between 50 and 100 feet in front of each test line. In earlier tests we had made a detailed timber crown study at the 45° test plot during which

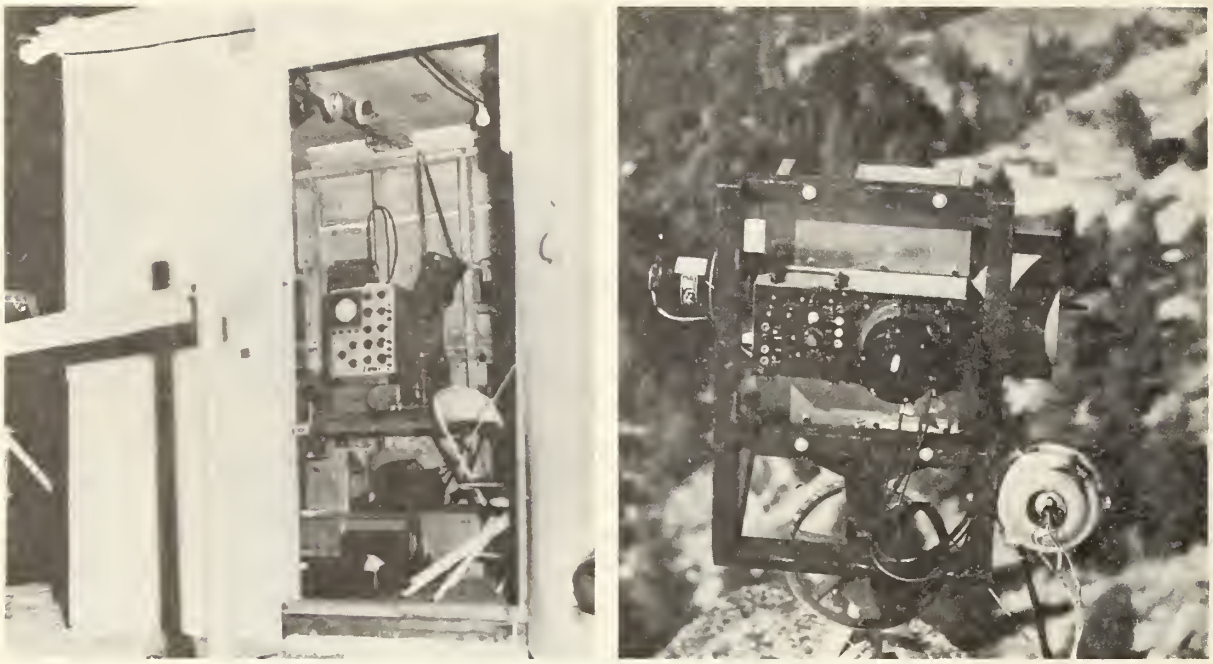

Figure 24. — Scanner installation at mountaintop location.

the horizontal profiles of all tree crowns were mapped, and studies were made of target signals received through 2,500 different optical paths from this test plot (Wilson and Noste 1966, p. 24). The profiles did not provide an accurate estimate of the amount of crown material actually intercepting the scanner-to-target line of sight. It was apparent that we needed some measurement of the vertical distribution of crown material to account for attenuation along various slant paths through the timber crowns.

In later tests on the 50°, 54°, and 60° test plots, an intercept profile cruise was made by mapping all crown material intercepting the scanner-to-target line of sight. That is, we mapped all material intercepting the plane determined by the test line and scanner location. These data provided the basic information for statistical correlation between target signals and the obscuring crown material.

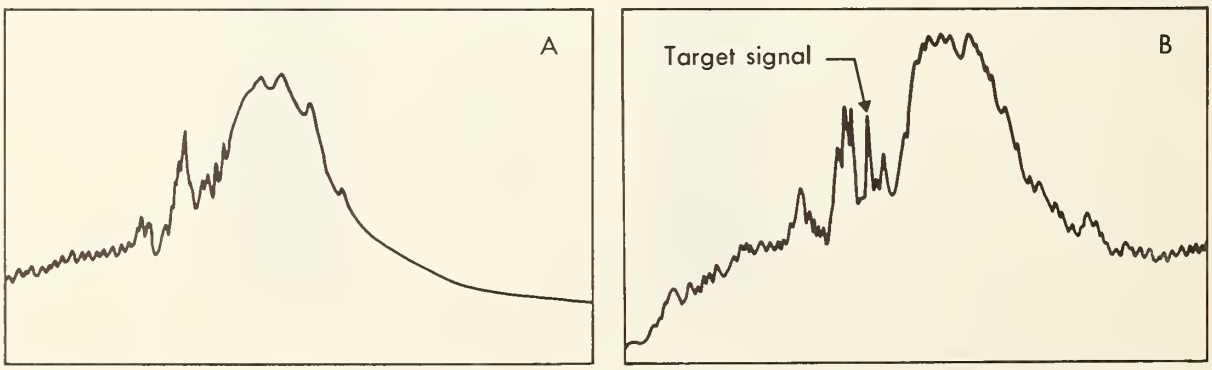

Figure 25. — Typical oscilloscope signal trace showing target signatures for mountaintop tests: A, signal trace of background adjacent to target area without target; and B, signal background with target.

Figure 26. — Burning target on 60° test line.

Operational Patrol Flights

Seven patrol flights were made during July and August of 1966. Sixty targets were detected on these seven missions — 29 campfires, 10 dwellings, 4 slash fires, 12 fire targets, and 5 false alarms. Eight fires were missed. Detailed data for the 1966 fire patrol season are given in tables 30 and 31, in Appendix IV.

A prototype pulse-height discriminator for automatic target alarm was evaluated during this patrol test season. Its performance was very encouraging. It was "alarming" on all hot targets; however, it also appeared to be "alarming" on lakes and other terrain details. The IR imagery was recorded on magnetic tape, which permitted further evaluation and development of the discriminator during the winter of 1966-67.

We concluded from the 1966 patrol tests that consideration should be given to the following:

1. The overall size of the patrol area should be enlarged to increase the likelihood of wildfire observance.

2. Forested areas should be assigned hazard priorities and graded into fire detection classes, using criteria developed in the feasibility studies.

3. Lightning storm activity and current weather information should be acquired for the patrol areas.

4. A plan for collecting fire reports from fire control personnel should be developed.

5. A pulse height/pulse width target discrimination module (TDM) should be added to the system.

6. The aircraft's navigation should be replaced.

An extensive zone 400 miles within a radius of Missoula, Montana, was established in which missions were to be flown in 1967 (fig. 27). This area was divided into eight zones, with preplanned refueling and overnight stops.

Meetings were held with personnel from the 41 National Forests located within this zone to explain the purpose of the study and to ensure timely acquisition of ground reports on wildfires. Information on lightning storms for such a large area had been extremely difficult to obtain. This problem was eased somewhat by use of the weather radar unit at Missoula and the Salt Lake City network. The Missoula radar unit provided hourly maps of individual storm cells within a 200-mile radius of Missoula; these

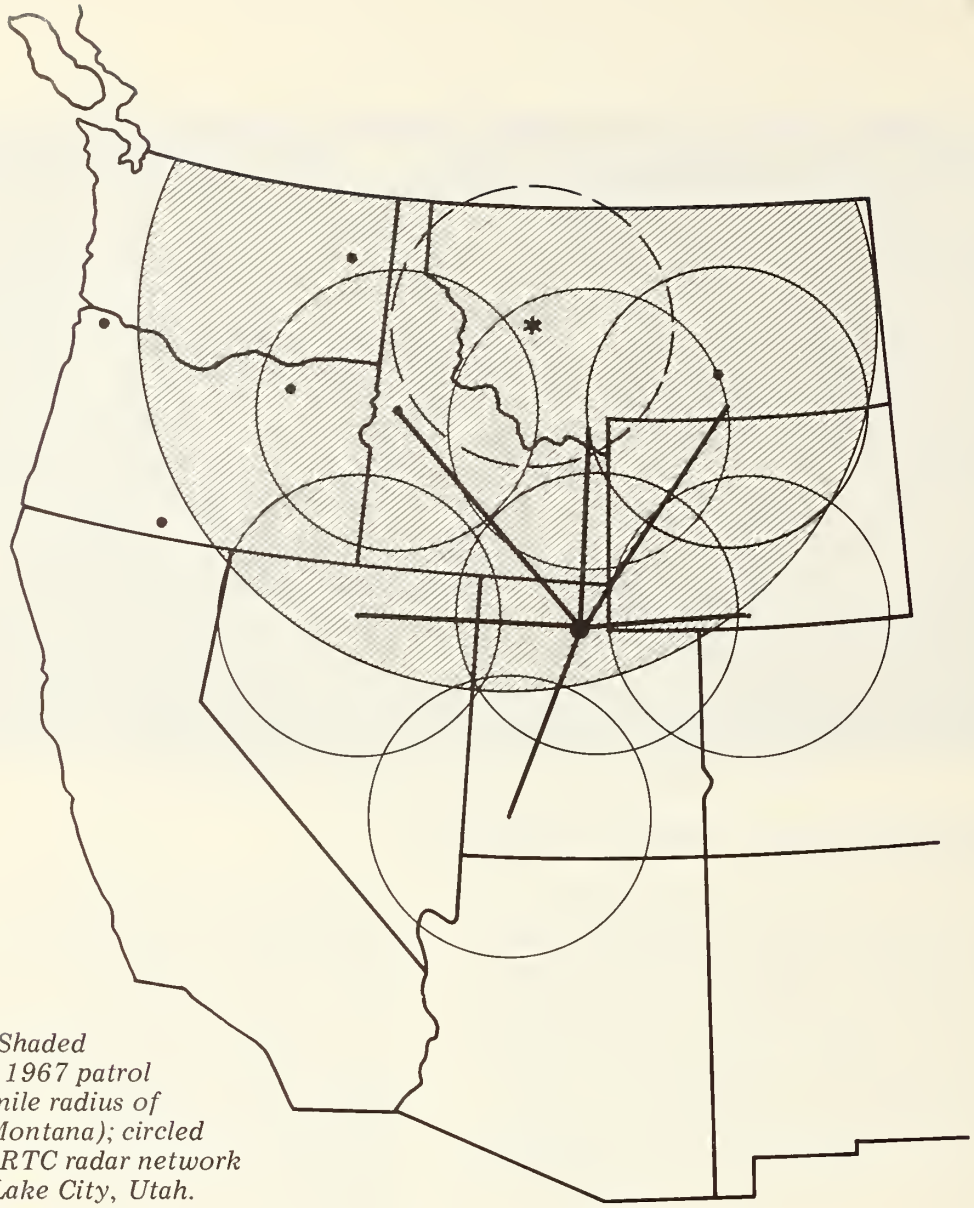

Figure 27. — Shaded area shows 1967 patrol area (400-mile radius of Missoula, Montana); circled areas are ARTC radar network from Salt Lake City, Utah.

maps were the backbone of our weather intelligence. The Salt Lake City center provided teletype reports every 2 hours of storm activity from six radar units in southern Idaho, Utah, and northwestern Wyoming. Telephone reports of lightning storms were obtained directly from National Forest personnel in the Cascade Mountain area of Washington and Oregon.

The probability was high that storms would occur simultaneously in a number of areas within the patrol zone, or would cover an area larger than could be flown on a single mission. Each National Forest was assigned a priority index in order that missions could be planned to observe a maximum number of fire targets. This priority factor (PF) was calculated from the past 10 years' fire-weather histories and expressed as a relative number of fires per storm day per million acres. The PF ranged from 0.29 for the Beaverhead National Forest to a high of 5.76 for the Malheur National Forest (table 32, Appendix II).

Inasmuch as the forest canopy plays a significant role in IR fire detection, we adjusted the PF's for species composition so that the PF value would more closely predict the number of fires that would be detected by IR. This had the effect of favoring patrols in the open timber types. The areas of timber in detection classes 1, 2, and 3 (see p. 33) were measured from USDA Forest Service maps; a weighted average of detection probability was calculated for

each of the 41 National Forests, assuming: 100 percent detection for class 1 timber; 75 percent detection for class 2 timber; and 50 percent detection for class 3 timber. We assumed fires would be equally distributed in all timber types.

The elapsed time between lightning occurrence and the time an area could be flown was determined by the rate of dissipation of clouds after a storm. We also attempted to adjust the PF to account for fires that would be detected and, in some cases, manned and controlled before they could be flown with the IR scanner. From the fire histories of each National Forest, a tabulation was made of the percent of undetected fires versus elapsed time between origin and detection. This readjustment also accounted for time lapses between different storms in different areas. Thus, the urgency of patrolling an area that had had a high PF and a storm on the previous day could be compared to an area that had a lower PF and a storm since the previous day.

In the Northern Rocky Mountain region, lightning storm activity generally occurs in the afternoon and early evening; the storm dissipates by late evening. Thus, daily storm activity, which was plotted on a planning map, was updated until 1900 hours (fig. 28). Possible mission areas were blocked out on the map and an adjusted PF assigned to each of these areas. The area with the largest probable number of target detections was selected for patrol.

A patrol mission briefing was held for the aircrew, during which flight plans were finalized based on flying conditions and lightning storm activity. On occasion, a high priority area had to be passed over because of late cloud dissipation.

Latitude and longitude of the starting and ending points of the first patrol leg were read from the planning map; values were used to compute the course and distance of the first leg of the patrol. This first leg was transferred to a sectional aeronautical chart. The remaining legs were plotted parallel to the first (fig. 29). The average altitude over terrain determined the spacing interval, which varied from 5 to 7 nautical miles. A prominent land feature was selected on each leg of the patrol grid to be used as a checkpoint. Information was provided to the navigator in the format shown in figure 40, Appendix IV. The checkpoints also were plotted on a USDA Forest Service Series A map to provide detail to the flight observer when checking the imagery.

Missions were scheduled for sometime after 2200 hours, depending on time required to fly to the beginning point of the first leg of the mission. The course and distance of the first leg were set in the Doppler computer. As the plane proceeded down the first leg, the computer showed the miles-to-go to the end of the run and the miles right or left of the desired track. This navigation system worked well during the 1967 tests.

No attempt was made to locate targets in flight. The imagery was available to the PI's by 0600 hours. Targets were located on USDA Forest Service Series A maps and recorded on data forms (fig. 41, Appendix IV). In difficult areas, Forest Service timber-type maps also were used because they have vegetation cover information.

The PI classified targets into four categories:

1. **Fire target.** — (a) If in an isolated location, any well-defined target on the film; or (b) if near roads, streams, or possible human activity, any target of greater intensity than normally expected from a campfire.

2. **Possible fire.** — (a) These are targets that may have the same characteristics as a fire target, but are possible campfires because of their location; or (b) targets that tripped the TDM, but did not appear on the film because of their location and intensity.

3. **Campfire.** — These are targets in known campgrounds or situated in an area that makes it highly probable that they are campfires (e.g., by a major road or a heavily used stream or river).

4. **Other.** — All other hot targets (e.g., hot springs, houses, mills, etc.)

Targets in the first three categories were reported to the National Forests as soon as interpretation was completed.

The reports to the National Forests included target category, location by legal description, and recognizable landmarks. A followup call was made later in the day to determine if any targets had been confirmed and if any fires had

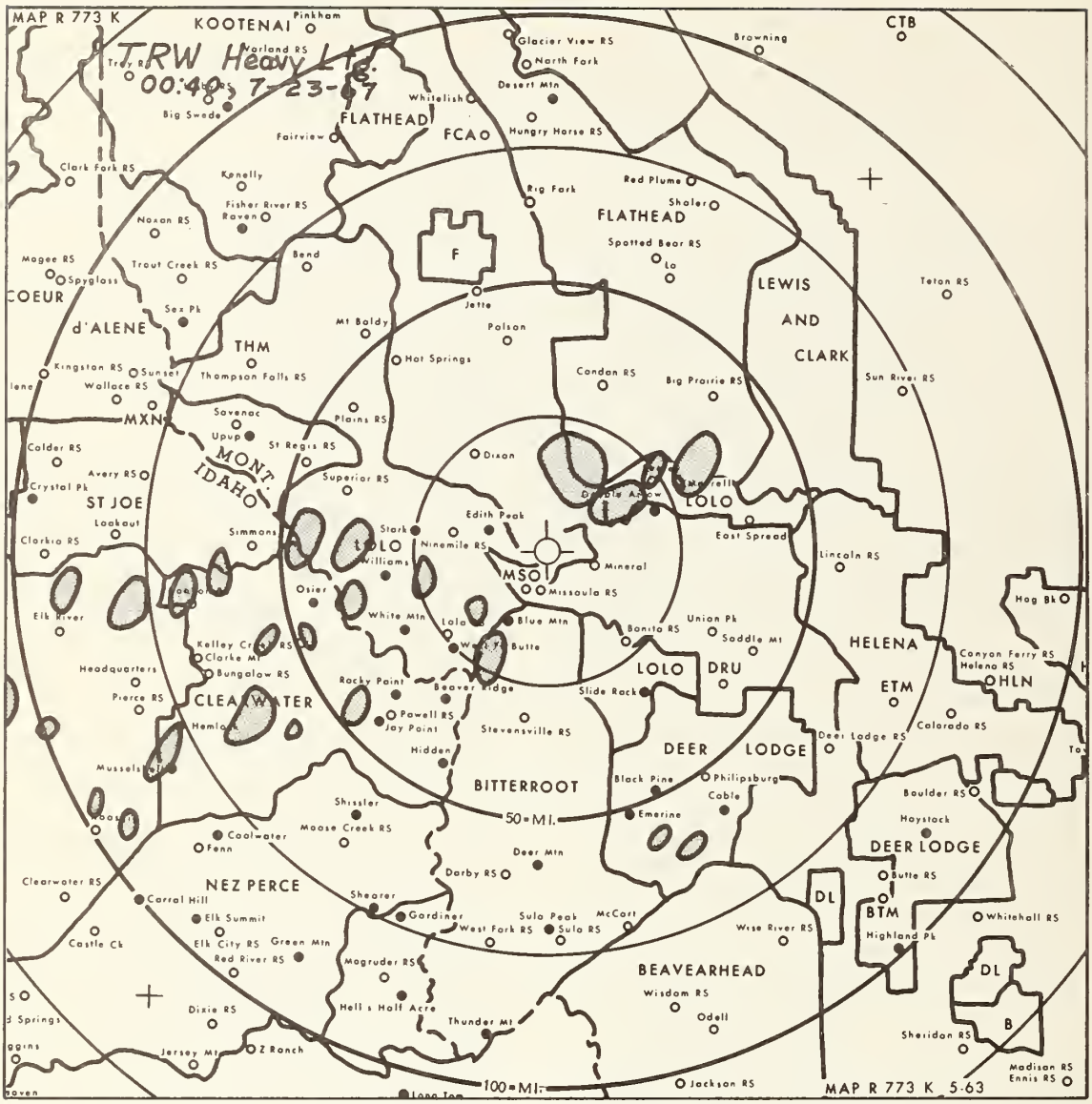

Figure 28. — Shaded areas show where lightning storms occurred on July 23, 1967, in the patrol area. This was derived using thunderstorm activity maps issued hourly by the Missoula radar unit for that day.

been missed by the scanner. The areas around fires that were accessible to our ground crew were examined to determine the type and density of crown obscuration, fire size, burning characteristics, location and fuel, and amount and type of smoke available for visual detection.

During 1967, lightning activity was limited in the western portion of the 400-mile patrol zone; thus, the number of missions flown in this area was less than anticipated. Patrol flights were made on 21 of the 35 possible operational days (table 1). Eight of the days (23 percent), on which flights were not made, had little or no lightning activity; 5 days (14 percent) had lightning but late cloud dissipation prevented scheduling a patrol mission. One mission had to be scrubbed because of restrictions on pilot hours. However, late dissipation of cloud cover caused some problems, primarily in the early part of the season. A daytime mission capability could alleviate this problem to some extent. It ap-

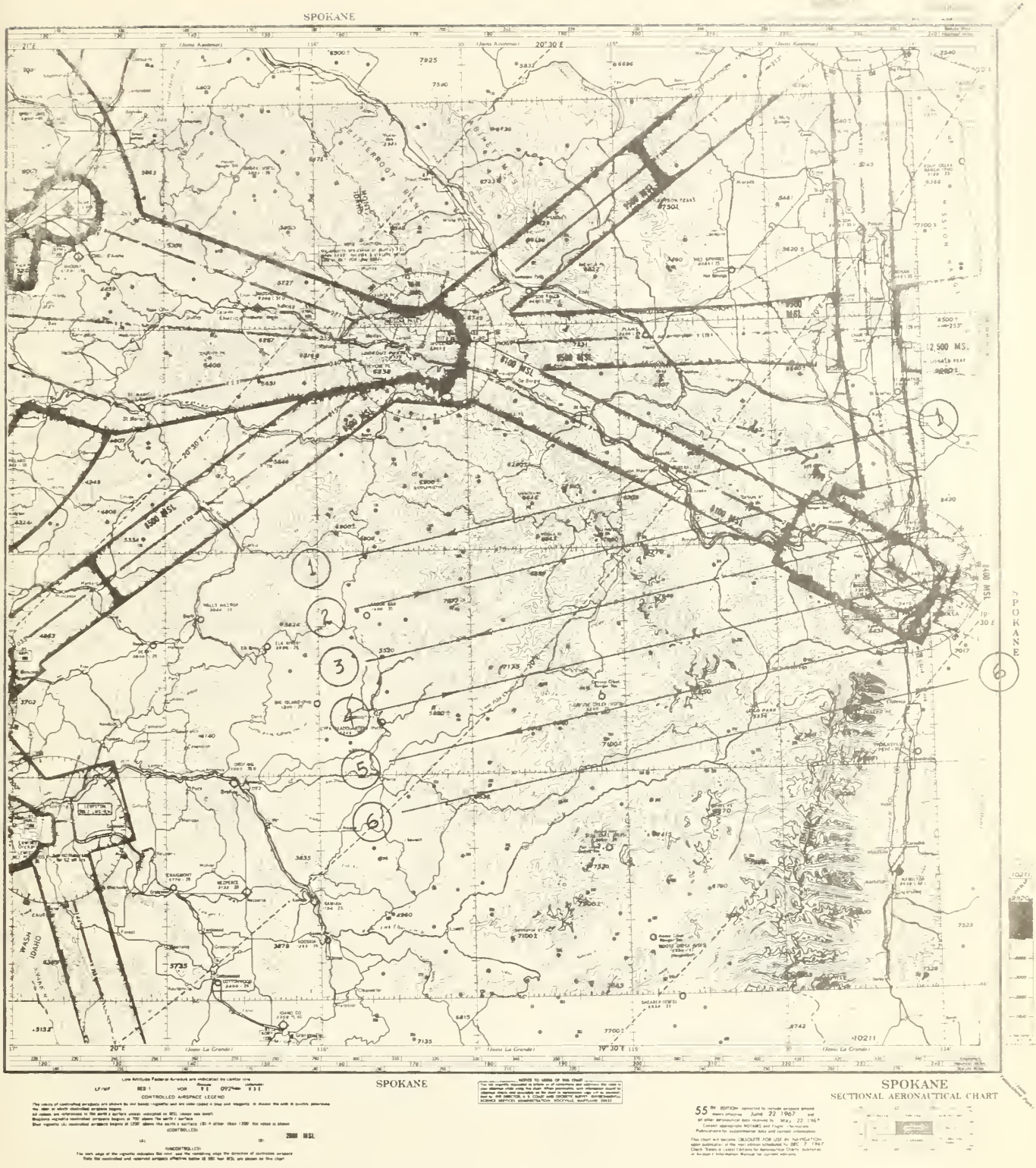

Figure 29. — Flight plan of Patrol #12, July 23, 1967. This patrol grid, of six flight legs, covers the high priority areas of lightning activity that are shown in figure 28. The imagery from this patrol is displayed on the supplemental foldout inside the back cover. Fifty-three hot targets were counted on this patrol (see table 33, Appendix IV).

pears that a normal convective storm will not cause problems. However, cloud cover associated with frontal systems may linger and prevent some missions.

The average dissipation time for thunderstorms within the patrol zone during 1967 was 1900 hours for the northwest forests, 2015 hours for the northeast forests, 2145 hours for the southwest forests, and 2315 hours for the southeast forests. Cloud cover resulted in 2-percent loss of total IR coverage. In most cases, this loss was due to patches of clouds scattered over the patrol area; however, on one flight, 25 percent of the mission was aborted because of solid cloud cover at one end of the mission area.

U. S. Weather Bureau reports were usually correct in predicting cloud dissipation. We did not miss any fires on the IR imagery because of cloud cover.

The effectiveness of the PF's that were used to plan patrol missions is difficult to evaluate. It was impossible to determine the number of fires that were started in areas that were not patrolled; consequently, we had no reference to compare to the number of fires in the partrol area. It appears that the basic premise for the PF is correct; there were no obvious errors in area selection. The information obtained from the U. S. Weather Bureau radar networks was essential for the planning of IR detection flights. Radar provides good weather information for large areas; this eliminates the need for contacting each National Forest in a proposed patrol area.

Table 1. — Difference between planned patrol coverage and area actually flown

Flight	Area planned to be flown	Area actually flown	Difference	Reason
	Square miles	Square miles	Square miles	
1	5,080	3,050	2,030	Navigational problems
2	3,910	3,910		
3	4,040	4,040		
4	2,680	2,680		
5	5,760	4,380	1,380	Low on fuel
6	5,080	3,810	1,270	Cloud cover
7	4,630	4,630		
8	2,690	2,690		
9	5,020	4,570	450	Cloud cover
10	5,740	2,870	2,870	High voltage failure
11	2,600	2,600		
12	4,320	4,320		
13	4,020	4,020		
14	3,540	2,820	720	High voltage failure
15	1,620	650	970	Aircraft engine failure
16	6,200	6,200		
17	5,510	5,510		
18	5,020	3,210	1,810	High voltage failure
19	5,140	5,140		
20	4,710	4,710		
21	2,640	2,640		
Total	89,950	78,450	11,500	
Average	4,283	3,736	548	

DISCUSSION OF RESULTS

Percent Detection From Airborne Tests

Yes-no detection probability is the percent of the existing fires that are observed and counted from the imagery. We must reemphasize that these data include, as detected fires, all targets that were observed at known locations. Detection probabilities are presented as a function of aspect angle out to 60° for fire radii of 3, 9, and 15 feet (Appendix III). Measurements of detection probability of 6- and 12-foot fire radii are included only when great differences are observed among the 3-, 9-, and 15-foot measurements. Furthermore, such measurements are incomplete beyond the aspect angle at which percent detection falls below one-half of its value at 0°.

We have discussed restraints imposed on data acquisition. The data, however, are sufficient to cover all marginal cases. For example, if a fire 3 feet in radius is detectable at 50- or 60-degree aspect angles in a particular timber type, one may infer that fires 6, 9, 12, and 15 feet in radius also are detectable at all aspect angles. Similarly, if fires 15 feet in radius are marginally detectable at the nadir, we infer that fire targets smaller than 15 feet in radius also would be difficult to detect at aspect angles greater than 0°.

The 13 timber types represented a wide range in species tolerance, composition, and crown configuration. We might expect canopy densities to be very different in other stands of the same type because of variations in species composition, age, stocking, and site quality. We can make predictions of detection probability, based on percent detection measurements, only for timber stands that are comparably stocked to our test sites. There is no basis in our data for predicting the effects of variation of timber density on detection probability within a given timber type. However, the attenuation of target signal strengths by timber crowns can be correlated with differences of stand characteristics between targets within a test area (see page 37).

The 13 timber types were divided into three categories of detection difficulty to evaluate our criterion of shade tolerance for site selection (table 17, Appendix II; fig. 30). Detection category 1 includes the generally more intolerant species, which are characterized by 95 percent detection at small vertical angles and at least 50 percent detection probability to 60°. The species in detection category 2 have a lower overall detection probability than those in category 1. Detection probability begins to drop off at smaller aspect angles than it does in category 1. The more tolerant species in category 3 exhibit poorer detection at smaller angles; detection probability rolls off with aspect angle more quickly than it does on species in either of the other two categories.

F. S. Baker (1949) states that his tolerance table is based on a general concensus of American foresters, and cautions that tolerance is not a scientifically (rigorous) defined variable. He further points out that tolerance changes with tree age and environment.

Our test sites were selected from medium to heavily stocked, mature stands. We must reemphasize that there is no rigorous basis for extrapolating our percent detection results into the broad range of stand densities within a particular timber type that one may encounter in practice.

Unaccounted variables — for example, terrain and slope — will lower the detection prob-

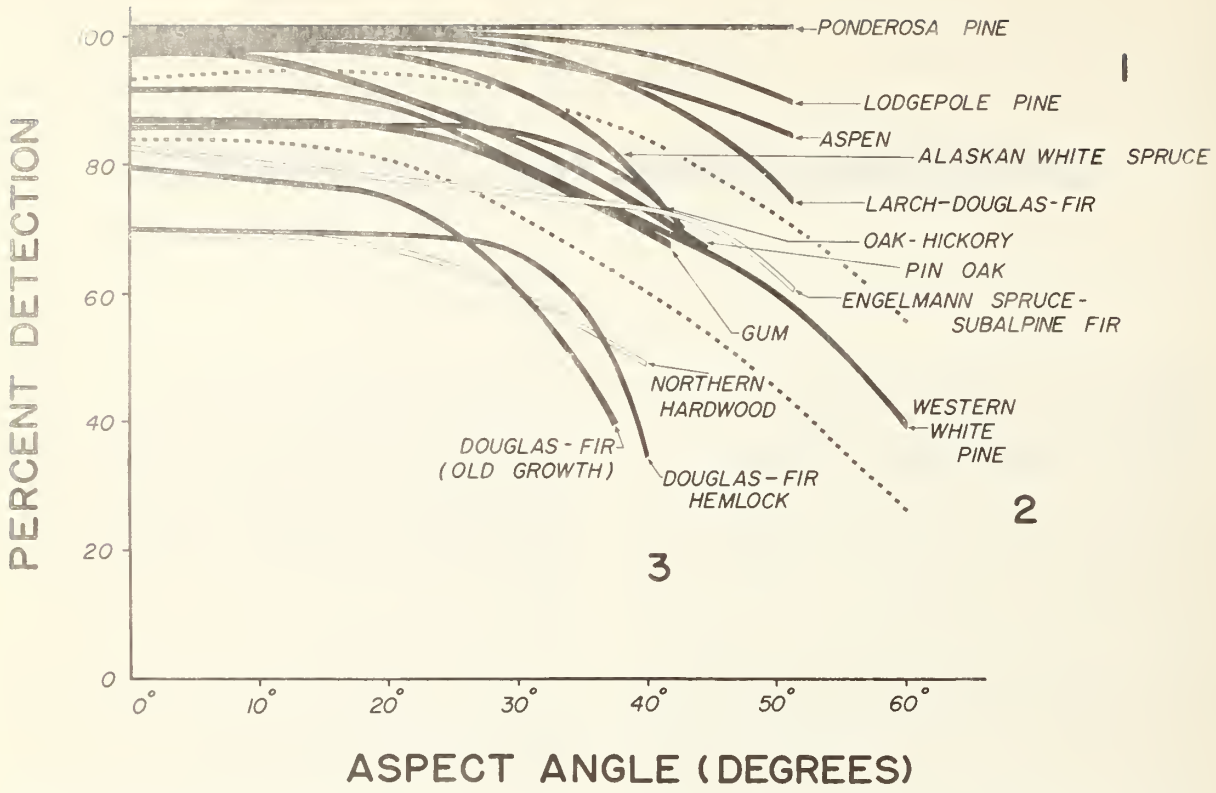

Figure 30. — Detection probability versus vertical scan angles in three major classes of timber types (9-foot fire radius).

ability curves that are shown in figure 30. PI bias (known locations of test targets) also makes these curves higher than we would expect on operational patrol. However, the heavily stocked, mature timber stands on our test sites made target detection more difficult than we would expect on patrol over typically stocked timber stands.

The mountaintop detection probabilities are shown in table 2 and in figure 31. To be detectable, a target signal must be larger than some threshold signal. This threshold signal is determined by the background signal around the target. This is analogous to the criteria used in the flight test for the five 1-square-foot targets. It permits simultaneous plotting of flight test and mountaintop test data (fig. 32).

In the Interim Report (Wilson and Noste 1966), we reported a function $(\text{Cos } \theta)^{1.40}$ as being best fit curve to the detection probability data. Our subsequent tests were more comprehensive and detection probability drops off much sharper beyond 50° than the cosine function predicted and approaches zero between 60° and 65°.

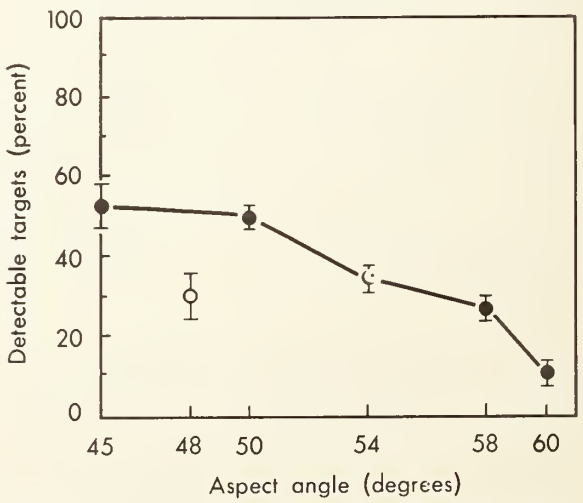

Figure 31. — Percent detection versus aspect angle for the mountaintop tests (larch — Douglas-fir timber type).

Table 2. — Detection results of the mountaintop tests

Aspect angle	Total number targets	Number observed	Percent detection	Average signal strength (relative)
45°	323	168	52.0	20.9
48°[1]	266	81	31.0	12.8
50°	486	245	50.4	25.9
54°	548	186	33.9	10.3
58°	391	105	26.9	4.8
60°	485	51	10.5	1.8

[1] *The 48° test line was in a marginal location at an azimuth nearly parallel to the cliff and was partially screened by shrubs and rocks projecting from the cliff. Also, the 48° data were taken under marginal, inclement weather conditions.*

Target Signal Strength and Timber Obscuration

The optical density of target signatures on IR imagery provides sufficient information to make estimates of attenuating effects of timber crowns and boles. Attenuation of the target signal by a denser crown canopy results in a weaker target signature on the IR imagery. Target signatures were read subjectively by three independent PI's. The first step in our analysis was a simple statistical test to demonstrate that the estimates of signal strength are a justifiable measure of the detection system capability.

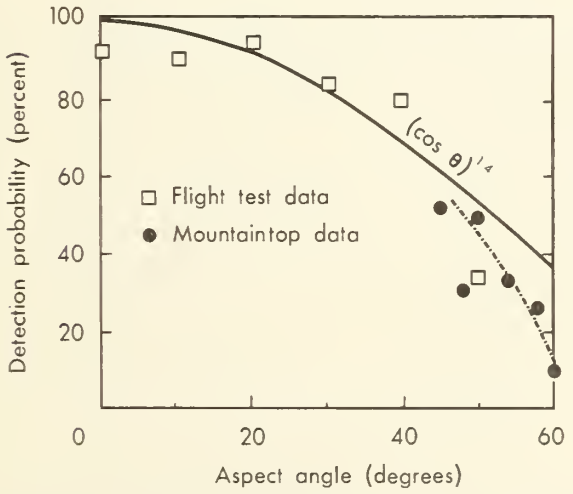

Figure 32. — Larch—Douglas-fir flight test data to 40°, extended past 60° by the mountaintop data.

This statistical test is demonstrated by plotting the average signal strength against the number of positive targets (yes detections) observed in all aspen imagery (fig. 33). Each point represents the average target signal strength that produced the given percent detection for all flight passes. A strong correlation exists between target strength and detection probability. Similar correlations exist for all 13 timber types.

Signal strengths remain constant or rise from 0° to 20° and then fall off towards 60° (fig. 34). We used an arbitrary 0 to 5 scale to estimate the fire target signatures. In so doing it is general practice to assign a signal strength of 1 to target intensities equal to or less than the maximum background density. It is these weak marginal targets (density approximately 1) that represent questionable targets counted in the percent detection results shown in figure 30. Under operational conditions, it is unlikely these targets would have been detected had their exact location not been known when the imagery was read by the PI.

Figure 35 attests to the large number of marginal tests that we counted. Indeed, successful detection in the aspen and pin oak timber types at aspect angles greater than 30° can be attrib-

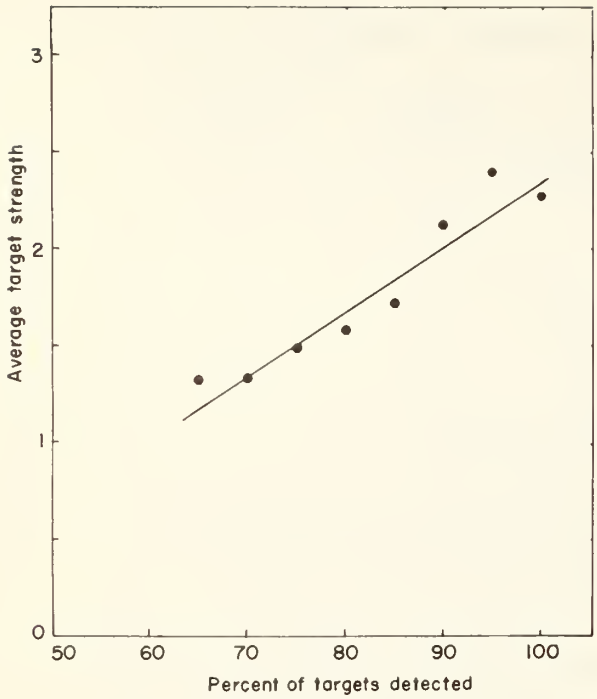

Figure 33. — Correlation of detection probability and signal strength for all aspen data.

uted directly to our ability to find a very large number of these marginal targets. Fortunately, we have a promising solution to this marginal target problem — a two-color temperature discrimination with scan-to-scan correlation (Appendix V).

If the frequency distribution of signal strength, N_S, is known (in particular, its dependence on the timber cruise parameters), then we can write a formulation for detection probability, P:

$$P = \frac{1}{N_O} \int_{S_T}^{\infty} \left(\frac{dN_S}{dS}\right) dS \qquad \text{Eq. 7}$$

where S is the signal strength and S_T is the detection signal threshold.

This distribution of signal strengths appears to depend on the spatial distribution ("patchiness") of the crown material. For example, the bimodel signal distribution of weak and strong signals in the old-growth Douglas-fir test stand is indicative of concentrated patches of crown material interspersed with patches of open spaces. On the other hand, the aspen was a homogeneous stand. Unfortunately, there is no standard forestry cruise parameter to measure this patchy effect, and we did not make provisions in our experimental design to make such measurements.

The model of timber obscurations (Appendix III) is based on the average crown density of the timber stand and thus it does not account for the variance from homogeneity in crown

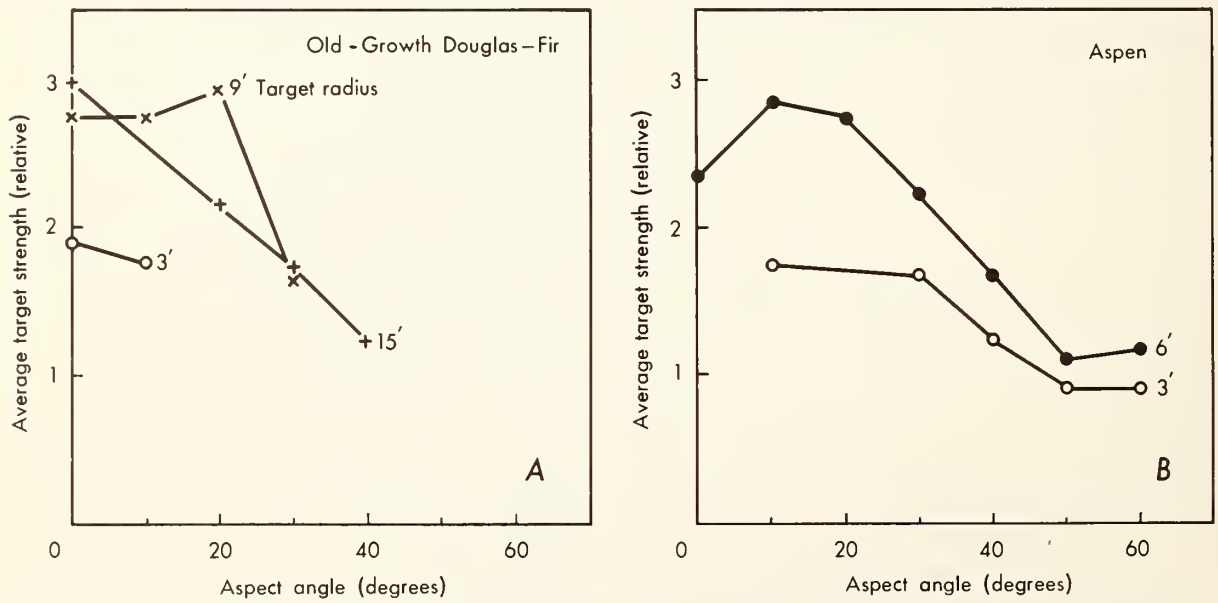

Figure 34. — Typical curves of the relative target signal strength distribution as a function of aspect angle for A, old-growth Douglas-fir and B, aspen timber types (post-1965 tests).

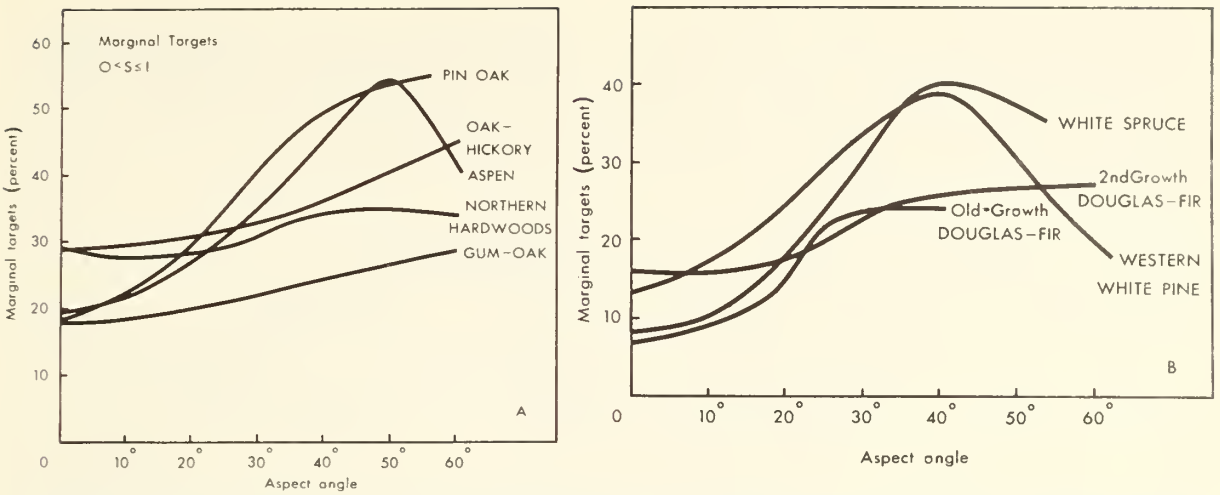

Figure 35. — Distribution of marginal targets with aspect angles ($O < S < 1$): A, Deciduous; and B, coniferous timber types.

material. The model reliably predicts the average signal strength but does not give a signal strength distribution from which we can predict a detection probability using equation (7). These signal distributions in tables 20-29 in Appendix III are also inadequate because each is measured from a single test area characterized only by an average stand density.

We established an empirical functional relation that was equivalent to equation (7) for our data. That is, detection probability, P_5 (five 1-square-foot targets), is empirically correlated with average signal strength, S:

$$P_5 = A+BS+CS^2 \qquad \text{Eq. 8}$$

The functional coefficients A, B, C and a "Coefficient of Determination," R^2 (table 3) were evaluated.[4]

[4] *The ratio of the regression sum of squares to the total sum of squares (i.e., the fraction of the total sum of squares accounted for by the regression) is sometimes called the coefficient of determination and denoted by R^2.*

Table 3. — Coefficients for target obscuration model

Timber stands	A	B	C	J	R^2
Northern hardwoods	0.233	2.503	-2.323	0.139	0.71
Oak-Hickory	.270	2.645	-2.624	.080	.67
Aspen	.452	1.946	-1.928	.113	.65
Gum-Oak	.194	2.237	-1.596	.098	.73
Pin oak	.540	1.420	-1.166	.128	.47
Western white pine	.463	1.207	-0.606	.171	.47
White spruce	.339	2.412	-2.090	.235	.79
Lodgepole pine	.463	1.710	-1.323	.194	.51
2nd-growth Douglas-fir	.136	2.737	-2.614	.106	.56
Old-growth Douglas-fir	.393	0.732	0.163	.080	.50

Coefficients A, B, and C describe the empirical fit of our data, equation (8), and should not be extrapolated beyond our observed signal strengths. The fit is not good for weak or strong average signal strengths, S. Graphs of the detection predictions, P_5, for the conifer and deciduous test areas are shown as A and B, respectively, of figure 36. These "predictions" may be compared to the measured detection probabilities in figure 30.

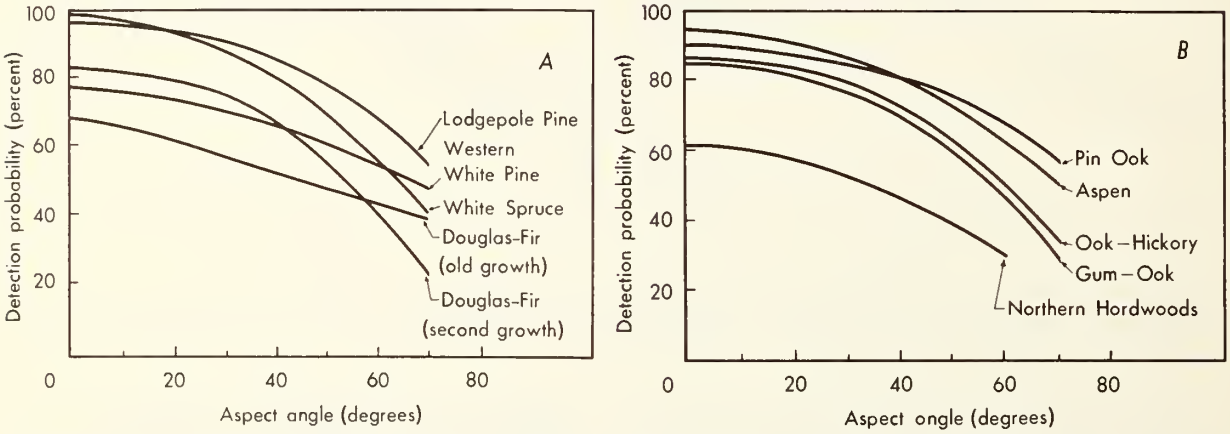

Figure 36. — Predicted detection probability (percent), P_5, versus aspect angle in A, coniferous and B, deciduous timber types.

Operational Tests

A total of 21 night detection missions was flown within the 400-mile-radius patrol zone during the 1967 fire season. Coverage per mission ranged from 650 square miles to 6,200 square miles.

There were 1,434 TDM trips on the imagery, of which 601 were interpreted as hot targets and the remaining 833 were initially interpreted as false alarms.

Hot Targets

Of the 601 hot targets, 310 were reported to the National Forests (table 34, Appendix IV) — 213 were confirmed by the ground crews and 55 could not be confirmed. Two targets reported as campfires turned out to be wildfires, 71 turned out to be other hot targets.

We flew over 134 wildfires that were possible targets of which 87 were detected (65 percent). Sixteen of the 47 fires missed registered a target on the imagery but did not trip the TDM system. These 16 fires were found on the imagery after reports were obtained from the National Forests.

False Alarms

Of the remaining 833 false alarms, 43 were roads, 56 snow, 43 ridges, 448 lakes and rivers, and 243 random noise.

In addition, 55 targets that had been reported as fires to the National Forests but could not be confirmed were later classified as errors — 34 were classed as false alarms and the remaining 21 had good target signatures on the imagery. These 21 targets were located in remote alpine areas and apparently burned out before they could be found by the ground crews.

Target Intensity

The distribution of target signal strengths for detected fires smaller than one-half acre is shown in figure 37. Signal strength is measured on a scale of 0 to 5, where 5 is a saturated target

and 2 is a normal strength required by a PI to identify a random target above the background. Using this scale, 52 percent of all hot targets and 69 percent of the 39 natural wildfires might have been missed by the PI (signal less than 1) if he didn't have the aid of the TDM.

These 39 fires are considered to be a sample of incipient fires that must be found by any detection system. Fires under suppression attack provide unknown amounts of radiation for detection; therefore, in the following analysis, only unmanned fires are considered. Our detection success in this group is 23 of 39 (59 percent).

1. **Detected by TDM.** — There were 23 unmanned wildfires detected by the TDM, of which 9 were detected previously using conventional methods (14 had not been detected). Six of the previously detected fires were detected by visual method within 2 hours after ignition; however, no fire control problems would have resulted on these six fires if detection had been delayed until the area was patrolled with the IR scanner. The other two fires burned 13 and 18 hours before detection. They were not flown earlier because they ignited during the period the aircraft was under repair for engine failure. One of these fires burned 5 acres, which was caused primarily by a delay in initial attack rather than failure of early detection.

Of the 14 fires not detected by visual methods, four were subsequently found by visual methods using target locations determined from IR scanner; six were found and suppressed by ground crews, and the remaining four were never found. None of these 14 fires became serious control problems.

2. **Undetected by TDM.** — There were five fires undetected by the TDM. These fires were judged to be marginal targets for IR detection. (On such targets a spot is seen on the IR imagery at the location given for the fire, but the TDM does not mark the imagery, which is caused by incorrect setting of the TDM.) Such marginal targets normally should be detected. One of these five fires had been detected previously by conventional methods.

3. **Fires missed by airborne IR detection system.** — There were 12 fires missed by the IR system. Four of these were detected previously by conventional means and suppressed in less than 1 hour, which indicated that the fires were small. In these four fires, the time between IR mission and initial attack was at least 8 hours. They were ground fires that could have been detectable during a second patrol on a succeeding night if they had not been suppressed. Unfortunately, during the delay between patrol flights, fires of this size could develop into major fires that could cause considerable damage.

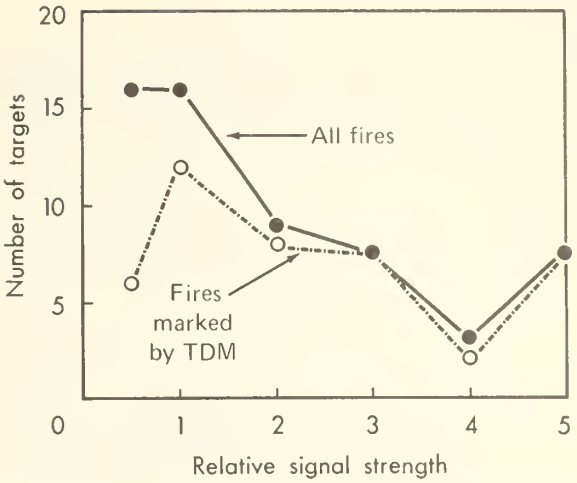

Figure 37. — Distribution of target signal strengths for detected fires smaller than one-half acre.

The remaining eight fires missed by the IR system had not been detected visually when the aircraft flew over them; they were found from 6 hours to 11 days later. Seven of these fires could have been scanned a second time before they were found (i.e., 24 hours between ignition and detection).

The unmanned fires were burning under various types of timber canopies and were scanned at various aspect angles. Of the 39 unmanned fires, 20 were burning in detection class 1 timber and 19 were in detection class 2 timber. This breakdown among classes is approximately what we had predicted because there are few detection class 3 timber stands in the patrol zone.

Fire locations read from the IR imagery were evenly distributed with regard to aspect angle — 13 were located at aspect angles of 20° or smaller, 15 were located between 20° and

40°, and 11 between 40° and 60°. This is close to what one would expect if detection probability versus angle was the only effect. However, it is quite surprising because equal angle increments do not subtend equal ground distances.

The 39 fires constitute a small sample for detailed analysis. However, we might conclude that:

1. Most of the detected fires were observed at aspect angles less than 40° and most of the misses occurred at aspect angles over 40°.

2. More targets were detected in detection class 1 timber than in detection class 2 timber; conversely, more targets were missed in detection class 2 timber.

3. Four out of the five TDM misses that had observable IR target signatures were in the detection class 2 timber. The distribution of these misses with aspect angle does not appear significant.

Many fires are started by lightning in the interior of snags and rotten trees. The size of a snag fire remains relatively small until a firebrand falls to the ground or the exterior of the tree begins to burn. We had assumed that fires confined to snags at the time of observation would be more difficult to detect than ground fires. However, 6 of 10 snag fires (60 percent) were detected; whereas, 16 of 24 (66 percent) of the ground fires were detected.

Target Location

We attempted to locate all targets to the nearest one-fourth mile, or 40-acre block, using Forest Service Series A maps which are scaled one-half inch to the mile (table 4). Targets located from the IR imagery were compared to the fire locations listed on the standard Forest Service fire report forms (5100-29).

The accuracy of location is dependent largely on image quality and terrain detail. Homogeneous timber stands and flat terrain provide little detail on IR imagery, thus, accurate location of targets is difficult. Some correlation is evident between scan angle and location accuracy; however, number of targets obtained at aspect angles over 40° is too small for reliable estimates of error.

The system must be adjusted to obtain maximum terrain contrast on the imagery. For most areas, the lack of terrain detail on available Forest Service maps poses a major problem. Aerial photographs provide better terrain detail than do these maps; however, they are not annotated so that the PI can identify targets according to legal descriptions.

Twenty-six fires within the area patrolled had not been exposed to visual detection. Eleven of these (42 percent) were detected and reported to the National Forests (table 36, Appendix IV). Three (12 percent) were detected by IR but had been detected by visual methods before the IR reports were sent to the National Forests. Four (16 percent) were recorded on the imagery but the TDM did not mark them. Eight (30 percent) were missed by the IR detection system.

The targets missed and the false alarms were due partially to our limited experience in adjusting the TDM trip level. However, the principal cause was a basic flaw in the TDM design; specifically, electronic filter differentiated the video signal thus nullifying the effect of pulse-width discrimination. This seriously affected the operator's ability to establish a satisfactory trip level.

In-flight photointerpretation is a realistic goal and would permit dispatching of fire control forces within 1 hour of detection.

Table 4.—Location accuracy for detected fires

Location error	Scan angle			
	0°-20°	20°-40°	40°-60°	Average
	Percent			
Less than 1/8 mile	24	22	6	18
1/8 mile	43	35	25	35
1/4 mile	19	13	32	20
1/2 mile	10	30	6	17
3/4 mile	4	0	19	7
1 mile	0	0	12	3

LITERATURE CITED

Baker, Frederick S.
1949. A revised tolerance table. J. Forest. 47: 179-181.

Biberman, Lucien M.
1967. Apples, oranges, and unlumens. Appl. Opt. 6(6): 1127-1128, illus.

Born, Max, and Wolf, Emil.
1964-65. Principles of optics, Ed. 3. 808 p., illus. New York: Pergamon Press.

Genoud, Richard H.
1959. Infrared search-system range performance. Inst. Radio Eng. Proc. 47(9): 1581-1586, illus.

Grosenbaugh, L. R.
1952. Plotless timber estimates — new, fast, easy. J. Forest. 50: 32-37, illus.

Harlow, William M., and Harrar, Ellwood S.
1950. Textbook of dendrology, Ed. 3. 555 p. New York, Toronto (etc.): McGraw-Hill Book Co., Inc.

Hirsch, Stanley N.
1962. Infrared as a fire control tool. Western Forest Fire Res. Counc. Proc. 1962: 5-10, illus.

———
1962. Possible application of electronic devices to forest fire detection. U. S. Forest Serv. Intermountain Forest and Range Exp. Sta. Res. Note 91, 8 p.

———
1963. Applications of remote sensing to forest fire detection and suppression. Second Symp. Remote Sensing Environ. Proc. 1962: 295-308, illus.

Hirsch, Stanley N.
1964. Forest fire detection systems. Western Forest Fire Res. Counc. Proc. 1964: 3-5, illus.

———
1965. Airborne infrared mapping of forest fires. Fire Technol. 1(4): 288-294, illus.

———
1965. Infrared line scanners — a tool for remote sensing of forested areas. Soc. Amer. Forest. Proc. 1965: 1969-1972, illus.

———
1965. Preliminary experimental results with infrared line scanners for forest fire surveillance. Third Symp. Remote Sensing Environ. Proc. 1964: 623-648, illus.

———
1968. Detecting small fires with airborne infrared line scanners (U). U. S. Atomic Energy Comm. Meeting on Search, Detection, and Recovery of Nuclear Heat Sources Proc. (U) 1968: 124-134, illus. (Classified)

———
1968. Forest fire control (in part). P. 187-188, in: 1968 McGraw-Hill Yearbook of Science and Technology. New York, St. Louis [etc.]: McGraw-Hill Book Co., Inc.

———
1968. Project Fire Scan — summary of 5 years' progress in airborne infrared fire detection. Fifth Symp. Remote Sensing Environ. Proc. 1968: 447-457, illus.

Hirsch, Stanley N., Bjornsen, Robert L., Madden, Forrest H., and Wilson, Ralph A.
1968. Project Fire Scan fire mapping final report, April 1962 to December 1966. U. S. Forest Serv. Res. Pap. INT-49. 49 p., illus.

Holmgren, Arthur H., and Reveal, James L.
1966. Checklist of vascular plants of the Intermountain Region. USDA Forest Serv. Res. Pap. INT-32, 160 p.

Holter, Marvin R., Nudelman, Sol, Suits, Gwynn H., Wolfe, William L., and Zissis, George J.
1962. Fundamentals of infrared technology. 442 p., illus. New York, London: The Macmillan Co.

Hudson, Richard D., Jr.
1969. Infrared system engineering. 642 p., illus. New York, London [etc]: John Wiley and Sons.

Institute of Science and Technology.
1962. Proceedings of the First Symposium on Remote Sensing of Environment. 124 p., illus. Ann Arbor, Mich.: Univ. Mich.

———
1963. Proceedings of the Second Symposium on Remote Sensing of Environment. 459 p., illus. Ann Arbor, Mich.: Univ. Mich.

———
1965. Proceedings of the Third Symposium on Remote Sensing of Environment. 821 p., illus. Ann Arbor, Mich.: Univ. Mich.

———
1966. Proceedings of the Fourth Symposium on Remote Sensing of Environment. 871 p., illus. Ann Arbor, Mich.: Univ. Mich.

———
1968. Proceedings of the Fifth Symposium on Remote Sensing of Environment. 946 p., illus. Ann Arbor, Mich.: Univ. Mich.

Jamieson, John A., McFee, Raymond H., Plass, Gilbert N., Grube, Robert H., and Richards, Robert G.
1963. Infrared physics and engineering. 673 p., illus. New York, Toronto [etc.]: McGraw-Hill Book Co., Inc.

Jones, R. Clark, Goodwin, Deryck, and Pullan, George.
1960. Standard procedure for testing infrared detectors and for describing their performance. 45 p., illus. Washington, D. C.: Office of Director of Defense Research and Engineering.

Karr, Philip R.
1957. Mathematical study of background "noise." 24 p., illus. Def. Doc. Center AD 608021.

Little, Elbert L.
1953. Check list of native and naturalized trees of the United States (including Alaska). USDA Forest Serv. Agr. Handbook 41, 472 p.

Losensky, B. John.
1968. A preliminary report on the infrared lightning fire patrol study. USDA Forest Serv. Fire Contr. Notes 29(2): 4-6, illus.

———
1969. An operational test of an infrared fire detection system. USDA Forest Serv. Fire Contr. Notes 30(2): 8-11, illus.

Robinson, David Z.
1959. Methods of background description and their utility. Inst. Radio Eng. Proc. 47(9):1554-1561, illus.

Society of American Foresters
1954. Forest cover types of North America (exclusive of Mexico). 67 p. Washington, D. C.: Soc. Amer. Forest. (Reprinted in 1967, 6th Edition.)

———
1956. Forestry handbook. (Reginald D. Forbes, ed.). 1143 p., illus. New York: Ronald Press.

Wilson, Ralph A.
1966. The remote surveillance of forest fires. Appl. Opt. 5(6): 899-904, illus.

Wilson, Ralph A.
1968. Fire detection feasibility tests and system development. Fifth Symp. Remote Sensing Environ. Proc. 1968: 465-477, illus.

———, and Noste, Nonan V.
1966. Project Fire Scan fire detection interim report, April 1962 to December 1964. U. S. Forest Serv. Res. Pap. INT-25, 55 p., illus.

Wolfe, William L., ed.
1965. Handbook of military infrared technology. 906 p., illus. Washington, D. C.: U. S. Government Printing Office.

APPENDIX I

Scientific Names of Forest Species

Following is a list of species, by common and scientific name (Harlow and Harrar 1950; Holmgren and Reveal 1966; Little 1953), mentioned in this report:

Common Name	Scientific Name
Alder	*Alnus B.* Ehrh.
Alpine fir	*Abies lasiocarpa* (Hook.) Nutt.
American elm	*Ulmus americana* L.
Ash	*Fraxinus* L.
Aspen	*Populus tremuloides* Michx.
	Populus grandidentata Michx.
Balsam fir	*Abies balsamea* (L.) Mill.
Balsam poplar	*Populus balsamifera* L.
Basswood	*Tilia americana* L.
Beaked hazel	*Corylus cornuta* Marsh.
Black oak	*Quercus velutina* Lam.
Cane	*Arundinaria tecta*
Cherry	*Prunus serotina* Ehrh.
Cherrybark oak	*Quercus falcata* var. *pagodaefolia* Ell.
Dogwood	*Cornus* L.
Douglas-fir	*Pseudotsuga menziesii* (Mirb.) Franco
Eastern hemlock	*Tsuga canadensis* (L.) Carr.
Elm	*Ulmus* L.
Engelmann spruce	*Picea engelmannii* Parry
Grand fir	*Abies grandis* (Dougl.) Lindl.
Hackberry	*Celtis occidentalis* L.
Hawthorn	*Crataegus* L.
Hickory	*Carya* spp.
Honeylocust	*Gleditsia triacanthos* L.
Lodgepole pine	*Pinus contorta* Dougl.
Mountain maple	*Acer spicatum* Lam.
Persimmon	*Diospyros virginiana* L.
Pin oak	*Quercus palustris* Muenchh.
Poison ivy	*Rhus radicans* L.
Ponderosa pine	*Pinus ponderosa* Laws.
Red alder	*Alnus rubra* Bong.
Red maple	*Acer rubrum* L.
Red oak	*Quercus rubra* L.
Sassafras	*Sassafras albidum* (Nutt.) Nees.
Serviceberry	*Amelanchier* Med.
Silver maple	*Acer saccharinum* L.
Soy (American) hornbeam	*Carpinus caroliniana* Walt.

Sugarberry	*Celtis laevigata* Willd.
Sugar maple	*Acer saccharum* Marsh.
Swampwhite oak	*Quercus bicolor* Willd.
Sweetgum	*Liquidambar styracitlua* L.
Sweet pecan	*Carya illinoensis* (Wangenh.) K. Koch
Vine maple	*Acer circinatum* Pursh
Water oak	*Quercus nigra* L.
Western hemlock	*Tsuga heterophylla* (Raf.) Sarg.
Western larch	*Larix occidentalis* Nutt.
Western redcedar	*Thuja plicata* Donn.
Western white pine	*Pinus monticola* Dougl.
White birch	*Betula papyrifera* Marsh.
White oak	*Quercus alba* L.
White spruce	*Picea glauca* (Moench) Voss.
Willow	*Salix* L.
Willow oak	*Quercus phellos* L.
Yellow birch	*Betula alleghaniensis* Britton

APPENDIX II

Description of Test Areas

The 13 test areas are a representative sample of the major forested areas of North America. They were chosen to cover a wide range of canopy densities on the basis of shade tolerance.

The following descriptions provide some insight into the character of these test areas (also see table 17).

Ponderosa Pine Test Area

The area is located on a bench south of the Big Blackfoot River, in the Lubrecht Experimental Forest, which is managed by the University of Montana.

The ponderosa pine type is very intolerant to shade. The timber primarily consists of a medium density stand of residual ponderosa pine interspersed with stagnated pole stands. Average height of dominant and codominant trees of the young, thrifty, and mature timber is 58 feet. In the areas of reproduction, the average height is 12 feet, consisting of about 80 percent total crown. Density of the ponderosa pine increases toward the south side of the test area (10 percent average slope with a north aspect) where it becomes intermingled with Douglas-fir. The ponderosa pine decreases to scattered clumps in a predominantly Douglas-fir stand. Basal area at target locations ranges from 0 to 190 square feet per acre; the less dense plots were on the north side of the area. The timber density can be estimated from table 5.

Lodgepole Pine Test Area

The area is located on the east side of Gold Creek approximately 6¼ miles north of State Highway 200, on the Missoula Ranger District, Lolo National Forest.

The area is situated on a bench with low ridges and minor draws. A marsh borders the northeast side of the area. No slopes exceed 20 percent.

The timber is a very dense stand of stagnated lodgepole pine; this type is very intolerant to shade. Some young ponderosa pine sawtimber grows on the northeastern portion of the area. Larch — Douglas-fir timber borders the south and east edges. Density of the lodgepole pine is fairly uniform throughout. Basal area at the target locations ranges from 0 (in small openings within the stand) to 227 square feet per acre. The timber density can be estimated from table 6.

Western White Pine Test Area

The area is located along Moores Creek in the Priest River Drainage about 5 miles northwest of the Falls Ranger Station in the Kaniksu National Forest. Terrain is variable with flat valley bottoms and abrupt steep ridges. Slopes increase to 30 percent in the southwest portion of the test area.

The timber consists of mature western redcedar and western white pine with an understory of western hemlock and cedar. The average height of dominant and codominant ma-

WILSON, RALPH A., HIRSCH, STANLEY N., MADDEN, FORREST H., AND LOSENSKY, B. JOHN

1971. Airborne infrared forest fire detection system: final report. USDA Forest Serv. Res. Pap. INT-93, 99 p., illus.

Outlines the basic requirements for an airborne infrared forest fire detection system and discusses the capability of the system to detect hot fire targets in natural forest backgrounds.

WILSON, RALPH A., HIRSCH, STANLEY N., MADDEN, FORREST H., AND LOSENSKY, B. JOHN

1971. Airborne infrared forest fire detection system: final report. USDA Forest Serv. Res. Pap. INT-93, 99 p., illus.

Outlines the basic requirements for an airborne infrared forest fire detection system and discusses the capability of the system to detect hot fire targets in natural forest backgrounds.

WILSON, RALPH A., HIRSCH, STANLEY N., MADDEN, FORREST H., AND LOSENSKY, B. JOHN

1971. Airborne infrared forest fire detection system: final report. USDA Forest Serv. Res. Pap. INT-93, 99 p., illus.

Outlines the basic requirements for an airborne infrared forest fire detection system and discusses the capability of the system to detect hot fire targets in natural forest backgrounds.

WILSON, RALPH A., HIRSCH, STANLEY N., MADDEN, FORREST H., AND LOSENSKY, B. JOHN

1971. Airborne infrared forest fire detection system: final report. USDA Forest Serv. Res. Pap. INT-93, 99 p., illus.

Outlines the basic requirements for an airborne infrared forest fire detection system and discusses the capability of the system to detect hot fire targets in natural forest backgrounds.

ture timber is 120 feet. The average diameter of the dominant species is 17 inches but the average for the stand overall is 12 inches. This site is classed as tolerant of shade because of the dominance of cedar and hemlock in the test area. The timber density can be estimated from table 7.

White Spruce Test Area

The stand is located on State land about 37 air miles southeast of Fairbanks, Alaska, on an island formed by two channels of the Tanana River.

The topography is flat — typical of the Tanana River Valley. Islands and bars are continually being built up and eroded away by the river. As these islands increase in size, brush invades and helps to stabilize them, which in turn is followed by invasions of white or black spruce. These islands will be present until erosion occurs following a shift in the river. Fire also plays a part in the ecological pattern of the land. These factors result in fairly young, even aged stands.

The test area is predominantly white spruce with a few balsam poplar. The stand is quite dense; however, the crown cover averages only 47 percent. Average height of dominants is 79 feet. The understory is generally sparse; a few willow and alder shrubs are scattered through the stand and along the shore. The ground cover is composed almost entirely of a deep, heavy cover of mosses and lichens. During the test period in late June, the frostline was about 3 feet below the ground. White spruce is a shade tolerant species.

Reproduction and understory of this stand have an average height of 7 feet and an average diameter of 3 inches. The density of the understory species in stems per acre follows: white spruce (381), balsam poplar (1.7), willow (3.4), alder (8.6).

The timber density can be estimated from table 8.

Engelmann Spruce Test Area

The area is located on a plateau about 2 miles southeast of Skookum Butte Lookout on the Powell Ranger District, Clearwater National Forest, in Idaho. Terrain is slightly rolling, and no slopes exceed 10 percent.

The timber is a heavy density stand of overmature Engelmann spruce with scattered grand fir and alpine fir in association. The average height of dominant and codominant trees is 98 feet. Basal areas around the test targets range from 120 to 360 square feet per acre, averaging 225 square feet per acre. The Engelmann spruce cover type is tolerant to shade. The timber density can be estimated from table 9.

Oak-Hickory Test Area

The test area is located in the Stinchfield Wood Management Unit, which is maintained by the University of Michigan, approximately 15 miles northwest of Ann Arbor. The area is characterized by a morainic topography. which is rolling with deep depressions. The soils are generally of the Bellefontaine sandy loam type and their quality has been reduced by severe grazing and fire treatments carried on before 1925. In addition to the fire treatments, selective cutting carried on prior to 1925 contributed to a marked reduction in the quality of the stand.

Until 1952, management activities were limited to protective measures to control fire and prohibit grazing. In 1952, a hardwood management unit was established and cutting treatments have been made periodically to remove inferior trees and thus the quality of the stand has been improved. As a result of the prohibition against grazing, a hardwood understory has now become established.

The present overstory is composed largely of black oak. White oak, cherry, and a minimal amount of hickory and miscellaneous species make up the remainder of the stand. We judged the site to be in the intermediate shade tolerance class. The reproduction and understory average 7 feet in height and 3 inches diameter.

The average density of the understory species in stems per acre follows: cherry (262), ash (111), hickory (95), sugar maple (90), sassafras (57), serviceberry (42), silver

maple (28), white oak (23), basswood (14), red oak (9), elm (9), and black oak (7).

The timber density can be estimated from table 10.

Larch–Douglas-fir Test Area

The area is approximately 1¼ miles east of State Highway 31, and 1½ miles north of Pierce Lake on the Condon Ranger District, Flathead National Forest, in Montana. Terrain is moderately rolling slopes.

Timber on the area is medium density old-growth Douglas-fir and larch, which is classed as intolerant to shade. Reproduction is sparse and predominantly Douglas-fir, an average of 40 feet high and almost 100-percent crown closure. Density of the timber is uniform over the entire area, varying only in species composition. Basal area ranges from 20 square feet to 260 square feet; average overall basal area was 149 square feet per acre. The timber density can be estimated from table 11.

Aspen Test Area

The stand is located about 10 air miles southwest of Kenton, Michigan, on the Kenton Ranger District, Ottawa National Forest, in Ontonagon County. The topography is flat to gently rolling, interspersed by boggy areas. The soil type is a Gogebic fine sandy loam. Repeated burning has depleted the soil quality.

The original stand was composed of a mixture of white pine and northern hardwoods with white pine predominating. The white pine was logged about 1898 — and the hardwoods about 1907. Until 1928, the area was burned every year to "green up the woods" so it could be used as pasture.

The present stand is composed predominantly of aspen and red maple with some scattered white birch and balsam fir. The dominant trees average 69 feet in height. It appears that the site has not recovered sufficiently to support much more than aspen and at least one more cycle of aspen may be expected. We classified this site as very intolerant of shade.

The reproduction and understory have an average height of 7 feet and an average diameter of 3 inches. The average density of the understory species in stems per acre follows: red maple (127), aspen (64), cherry (35), balsam fir (28), silver maple (24), sugar maple (21), serviceberry (7), white spruce (5), and white birch (5).

The timber density can be estimated from the table 12.

Second-Growth Douglas-fir Test Area

The test area is located on State land in the Toutle River Drainage, approximately 35 miles east of Castle Rock, Washington. The test site is located on the river bottom land and has no major land relief.

The stand was originally composed of Douglas-fir with some western hemlock. Cutting occurred at a very early date (around 1900). It is apparent from the old stumps and the present stand that fire did not follow the logging. The present stand is composed of a mixture of Douglas-fir and hemlock with minor amounts of western redcedar. The understory is composed of hemlock, vine maple, and red alder, varying in density from light to medium stocking. With the continued exclusion of fire, the stand will eventually revert to western hemlock and western redcedar. It is a shade tolerant site. The timber density can be estimated from table 13.

Old-Growth Douglas-fir Test Area

The test area is located 2 miles south of Willow Flats on the Glide Ranger District of the Umpqua National Forest in Oregon, on a high, rolling plateau, bordered on the east and west by clearcuts. It is bisected by a ridge approximately 30 feet high. Test plots were placed along the top and bottom of this ridge on relatively flat ground.

The timber is composed of well stocked old-growth Douglas-fir with some scattered western hemlock. The understory is composed of hemlock poles and some scattered vine maple and rhododendron, varying in density from light to medium stocking. The stand

is approximately 450 years of age, and averages 187 feet in height. The shade tolerance is intermediate.

Data derived from the timber cruise on this area were limited. The gross volume figures in board feet per acre are as follows: Douglas-fir, 150,000; hemlock, 32,000. The basal area is 392 square feet per acre.

Sweetgum-Water Oak Test Area

The stand is located in Madison Parish about 12 air miles southwest of Tallulah, Louisiana, on land owned by the Chicago Mills and Lumber Company. The topography is flat. Relics of drainage ditches constructed during the period it was farmed are still discernible.

The stand is typical of a river bottom hardwood type. Prior to the Civil War the area was cultivated primarily for cotton. After the war, the land was left idle and reverted to timber.

The stand is even aged; however, current cutting practices and the maturation of the stand are changing it to an uneven aged stand. The soils are quite deep and heavy; as a result, large areas of similar stands are being cleared and planted to soybeans. The stand is well stocked (68 percent sweetgum and water oak), averaging 118 feet high and 70 percent crown closure. The remainder is composed of a wide mixture of sweet pecan, willow oak, honey locust, red maple, elm, red oak, and hackberry. It is classed as intolerant to shade. Intermediate and improvement cuts have been made in the stand; as a result, the residual volume is generally of high quality.

The understory is light to medium and parts of the stand have a heavy cover of cane. Lianas are common throughout the stand; however, few dense tangles are found. The reproduction and understory of this stand have an average height of 7 feet and an average diameter of 3 inches. The average density of understory species in stems per acre follows: dogwood (121), hackberry (81), water oak (71), elm (34), ash (26), sweetgum (24), and soy hornbeam (16).

The timber density can be estimated from table 14.

Pin Oak-Sweetgum Test Area

The stand is located about 19 air miles west of Carbondale, Illinois, on the Murphysboro Ranger District, Shawnee National Forest, in Jackson County. The topography is flat; about half of the area was under water to a depth of up to 4 inches during the test period.

The stand is situated between the Mississippi and the Big Muddy Dikes on the Mississippi flood plain. Periodic inundation occurs on most of the stand during high water periods, which normally occur in the spring of the year. As a result, tree growth is restricted to water tolerant trees (such as pin oak) on a large portion of the stand.

The stand is well stocked, primarily with pin oak, cherrybark oak, and swampwhite oak (83 percent). The remainder includes varying amounts of red maple, sweetgum, hickory, and elm. The average height of the dominant species is 101 feet; their average crown closure is 76 percent. The understory is relatively light, made up primarily of elm and red maple. The ground cover is dense in some areas, composed primarily of poison ivy; it is bare where inundation occurs. Except for the cherrybark oak on the drier sites, the timber is short and of poor form. Logging has been limited since the formation of the present stand, which is of intermediate shade tolerance.

Reproduction and understory have an average height of 7 feet and an average diameter of 3 inches. The density of the understory species in stems per acre follows: elm (71), red maple (66), hickory (17), ash (17), sweetgum (10), pin oak (7), and swampwhite oak (7).

The timber density can be estimated from table 15.

Northern Hardwoods Test Area

The test area is located 4 miles south of Kenton, Michigan, on the Kenton Ranger District, Ottawa National Forest, in Ontonagon County. The topography is flat; a few dry streams intersect the area. The soil types are

of the Gogebic-Munising association, which have a relatively deep, fine sandy loam surface soil.

The original stand on the test area was composed of a mixture of conifers and hardwoods. The conifers were logged during the period 1890-1910. Logging of the hardwoods started about 1910 and continued through 1925. The area was covered with seedlings about 8 feet high and a few old culls when it was acquired by the Forest Service in 1931.

In 1961, the stand was cut and thinned to improve its quality. The present stand is in excellent condition, composed primarily of sugar maple with minor amounts of birch, cherry, hemlock, red oak, and silver maple, all in excellent condition. The test stand is classified as very tolerant to shade. The reproduction and understory have an average height of 7 feet and an average diameter of 3 inches.

The average density of the understory species in stems per acre follows: sugar maple (364), silver and red maple (58), and miscellaneous (12).

The timber density can be estimated from table 16.

Table 5. — Data derived from timber cruise of ponderosa pine test area

Timber measurements	Ponderosa pine	Larch—Douglas-fir	Average or total
Trees/acre	67	0.1	67.1
Volume (bd. ft./acre)[1]	5,316	13	5,330
Average basal area/tree (sq.ft.)	1.14	1.06	1.13
Average diameter (inches), weighted	14.5	14	14.5
Average tree height (ft.), weighted	58	60	58.1
Average lower crown limit, both species in mixed stand (ft.)	—	—	18
Average crown thickness (ft.), both species	—	—	40
Cumulative stem density, all plots (inches)	6,540	82	6,622
Apparent crown cover density (percent) from aerial photos over test fire areas	—	—	60

[1] *Scribner log rule was used for all merchantable volumes. Cruise includes all merchantable trees 8 inches diameter and larger (by 2-inch classes).*

Table 6. — Data derived from timber cruise of lodgepole pine test area

Timber measurements	Lodgepole pine	Ponderosa pine	Average or total
Trees/acre	156	5.2	161.2
Volume (bd. ft./acre)[1]	8,730	320	9,050
Average basal area/tree (sq. ft.)	.57	1.02	.795
Average diameter (inches), weighted	10	14	10.1
Average tree height (ft.), weighted	62	53	61.7
Average lower crown limit, both species in mixed stand (ft.)	—	—	28
Average crown thickness (ft.), both species	—	—	44
Cumulative stem density, diameter. Trees in each diameter class (inches)	—	—	2,662
Crown cover density (percent) as estimated by aerial photos over test fire area	—	—	80

[1] *Scribner log rule was used for all merchantable volumes. Cruise includes all merchantable trees 8 inches diameter and larger (by 2-inch classes).*

Table 7. — Data derived from timber cruise of western white pine test area

Timber measurements	Western white pine	Western hemlock	Western redcedar	Grand fir	Average
Trees/acre	126.8	75.0	156.5	61.1	104.9
Volume (bd. ft./acre)[1]	12,611	4,361	13,287	3,333	8,398
Volume (cu. ft./acre)	2,281.25	1,004.73	2,791.50	704.00	1,695.37

[1] *Scribner log rule was used for all merchantable volumes. Cruise includes all merchantable trees 8 inches diameter and larger (by 2-inch classes).*

Table 8. —Data derived from timber cruise (size class: 3+ inches) of white spruce test area

Timber measurements	White spruce	Balsam poplar	Average or total
Volume (cu. ft./acre)	4,542	31	4,573
Average diameter (inches)	5.8	9.5	5.8
Basal area (sq. ft./acre)	185.5	1.5	187.0
Average height (ft.)	53.4	58.7	53.4
Trees/acre	892	3	895
Percentage of species in area	99.6	0.4	

Table 9. — Data derived from timber cruise of Engelmann spruce test area

Timber measurements	Larch—Douglas-fir	Grand fir	Alpine fir	Engelmann spruce	Average or total
Trees/acre	0.7	6.3	20.7	133.0	160
Volume (bd. ft./acre)[1]	63	1,621	3,841	35,864	41,208
Average basal area/tree (sq. ft.)	1.48	1.74	1.47	1.71	1.6
Average diameter (inches), weighted	16.5	18	16.5	18	17.5
Average height (ft.), weighted	48	83	82	88	86
Average lower crown limit (ft.), all species in mixed stand	—	—	—	—	23
Average crown thickness (ft.), all species	—	—	—	—	62
Cumulative stem density (inches), all plots	—	—	—	—	10,344
Crown cover density (percent) from aerial photos over test areas	—	—	—	—	100

[1] *Scribner log rule was used for all merchantable volumes. Cruise includes all merchantable trees 8 inches diameter and larger (by 2-inch classes).*

Table 10. — Data derived from timber cruise of oak-hickory test area

Timber measurements	Size class	Black oak	White oak	Cherry	Hickory	Miscel-laneous	Average or total
	Inches						
Volume (cu. ft./acre)	3+	816.4	399.9	69.3	66.5	92.8	1,444.9
Volume (bd. ft./acre)[1]	9+	3,156	1,410	—	—	128[2]	4,694
Density (stems/acre)	3+	51.5	43.0	42.8	60.6	88.6	286.5
Basal area (sq. ft./acre)	3+	38.5	18.5	4.5	7.0	6.5	75.0
Average diameter (inches)	3+	12	8	4	4	4	6

[1] *Scribner log rule was used for all merchantable volumes. Cruise includes all merchantable trees 8 inches diameter and larger (by 2-inch classes).*

[2] *Includes cherry and hickory.*

Table 11. — Data derived from timber cruise of larch—Douglas-fir test area

Timber measurements	Douglas-fir	Lodgepole pine	Engelmann spruce-alpine fir	Larch	Average or total
Trees/acre	71.1	14.9	11.0	23.8	120.8
Volume (bd. ft./acre)[1]	8,168	1,316	1.800	5,639	16,923
Average basal area/tree (sq. ft.)	1.20	.69	1.25	1.73	1.21
Average diameter (inches), weighted	15	11	15	17	14.9
Average height (ft.), weighted	75	77	80	97	82
Average lower crown limit, all species in mixed stand (ft.)	—	—	—	—	35
Average crown thickness (ft.), all species	—	—	—	—	47
Cumulative stem density, all plots (inches)	2,656	238	450	1,536	2,224
Apparent crown cover density (percent) from aerial photos over test areas	—	—	—	—	80

[1] *Scribner log rule was used for all merchantable volumes. Cruise includes all merchantable trees 8 inches diameter and larger (by 2-inch classes).*

Table 12. — Data derived from timber cruise (size class: 3+ inches) of aspen test area

Timber measurements	Aspen	Red maple	White birch	Balsam fir	White spruce	Average or total
Volume (cu. ft./acre)	3,092.7	395.2	184.7	63.5	20.6	3,756.7
Basal area (sq. ft./acre)	154	47	10	7	2	220
Trees/acre	529	166	34	18	2	749
Average diameter (inches)	8.2	6.5	7.9	6.8	9.5	7.9
Cords/acre	39.1	5.0	2.3	.8	.3	47.6

Table 13. — Data derived from timber cruise of second-growth Douglas-fir test area

Timber measurements	Size class	Douglas-fir	Hemlock	Western redcedar	Hardwood	Average or total
	Inches					
Volume (bd. ft./acre)[1]	12+	40,097	25,200	1,031	900	67,230
Volume (cu. ft./acre)	3+	6,559.10	4,402.92	245.88	114.17	11,327.55
Average diameter (inches)	3+	24.7	14.9	11.1	6.3	17.1
Average height (ft.)	3+	172	113	61	40	123
Trees/acre	3+	30	56.2	9.6	6.4	102.2

[1] *Scribner log rule was used for all merchantable volumes. Cruise includes all merchantable trees 8 inches diameter and larger (by 2-inch classes).*

Table 14. — Data derived from timber cruise of sweetgum-water oak test area

Timber measurements	Size class	Sweet-gum	Water oak	Sweet pecan	Willow oak	Miscel-laneous[1]	Average or total
	Inches						
Volume (bd. ft./acre)[2]	3+	4,907	3,584	576	579	466	10,112
Volume (cu. ft./acre)	3+	1,626	977	174	168	236	3,181
Average diameter (inches)	3+	10.9	11.1	16.0	7.2	6.4	9.7
Average diameter (inches)	10+	12.9	15.1	16.0	17.6	13.3	13.7
Average height (ft.)	10+	78.5	79.0	106.0	51.0	44.0	69.0
Basal area (sq. ft./acre)	3+	47.5	24.5	4.0	4.5	9.5	90.0
Trees/acre	10+	43.3	16	2.7	1.7	3.9	68.0
Trees/acre	3+	65.3	28.1	2.7	10.7	30.7	137.5
Species percentage in area	All	48	20	2	8	22	

[1] *Includes honey locust, sugar berry, red oak, red maple, and elm.*

[2] *Scribner log rule was used for all merchantable volumes. Cruise includes all merchantable trees 8 inches diameter and larger (by 2-inch classes).*

Table 15. — Data derived from the pin oak-sweetgum test area

Timber measurements	Size class	Pin oak	Cherry-bark oak	Swamp-white oak	Red maple	Sweet-gum	Hickory	Elm	Average or total
			Inches						
Volume (bd. ft./acre)[1]	3+	3,729	1,456	—	—	1,143	—	—	6,328
Volume (cu. ft./acre)	3+	1,509	561	169	152	127	70	60	2,648
Average diameter (inches)	3+	10.1	10.7	7.4	10.8	8.0	8.1	9.1	9.7
Basal area (sq. ft./acre)	3+	51	19	6.5	5.0	4.0	2.5	2	90.0
Trees/acre	10+	46.4	14.1	—	—	13.9	—	—	74.4
Trees/acre	3+	80.1	26.6	18.7	7.5	9.3	5.0	3.8	151.0
Species percentage in area	All	53	17.6	12.4	5.0	6.2	3.3	2.5	

[1] *Scribner log rule was used for all merchantable volumes. Cruise includes all merchantable trees 8 inches diameter and larger (by 2-inch classes).*

Table 16. — Data derived from timber cruise of Northern Hardwoods test area

Timber measurements	Size Class	Sugar maple	Red oak	Hemlock[1]	Yellow birch	Red and silver maple	Cherry	Miscel-laneous	Average or total
	Inches								
Volume (cu.ft. /acre)	3+	1,522.7	188.3	296.4	56.2	95.4	51.1	32.3	2,242.4
Volume (bd. ft./acre)[2]	9+	4,835	—	1,015	—	—	—	294[3]	6,144
Density (stems/acre)	3+	167.9	41.7	16.3	6.3	39.8	6.9	10.8	289.7
Basal area (sq. ft./acre)	3+	58.84	8.31	12.45	2.15	4.94	2.00	1.68	90.38
Average diameter (inches)	3+	6.6	5.7	10.8	6.7	4.4	6.9	4.9	6.59
Average height (ft.)	3+	50.2	52.7	44.6	51.8	44.5	55.0	41.4	48.6

[1] *Includes all conifers.*

[2] *Scribner log rule was used for all merchantable volumes. Cruise includes all merchantable trees 8 inches diameter and larger (by 2-inch classes).*

[3] *Includes all hardwoods except sugar maple.*

Table 17. — Pertinent physical factors of test areas used in study

Timber cover type[1]	No. of test plots	Elevation m.s.l.	Flight path direction[2]	Legal description
		Feet		
Interior ponderosa pine (I)[3]	8	3,650	East & west	NE ¼ sec. 35, T. 14 N., R. 15 W., Principal meridian of Montana (PMM) (Montana)
Lodgepole pine (I)	8	4,200	North & south	S ½ SW ¼ sec. 6, N ½ NW ¼ sec. 7, T. 14 N., R. 16 W., PMM (Montana)
Engelmann spruce-Alpine fir (IV)	8	5,800	North & south	SW ¼ sec. 7, T. 38 N., R. 22 W., Bench mark (BM) (Idaho)
Larch—Douglas-fir (II)	8	4,500	North & south	NE ¼ or SW ¼ sec. 10, T. 19 N., R. 16 W., PMM (Montana)
Western white pine (IV)	20	2,450	North & south	SW ¼ sec. 21 and NW ¼ sec. 28, T. 58 N., R. 5 W., BM (Idaho)
Oak-Hickory (III)	20	1,000	North & south	N ¼ of NE ¼ sec. 14 and SE ¼ of SE ¼ sec. 11, T. 1 S., R. 4 E., Washteneaw Co. (Michigan)
Northern hardwoods (V)	20	1,500	North & south	N ½ sec. 35, T. 47 N., R. 37 W., Michigan Meridian, Ontonagon Co., (Michigan)
Aspen (I)	20	1,500	North & south	SE ¼ of sec. 5, T. 46 N., R. 38 W., Michigan Meridian, Ontonagon Co. (Michigan)
Second-growth Douglas-fir (IV)	20	1,400	East & west	NE ¼ sec. 2, T. 9 N., R. 3 E., Willamette Meridian (Washington)
Old-growth Douglas-fir (III)	15	4,000	North & south	SE ¼ of sec. 3, T. 27 S., R. 1 W., Willamette Meridian (Oregon)
Sweetgum-Water oak (II)	20	50	East & west	SE ¼ sec. 15, T. 15 N., R. 11 E., Washington Meridian, Madison Parish (Louisiana)
Pin oak-Sweetgum (III)	20	500	North & south	Sec. 19, T. 10 S., R. 3 W., 3rd Principal Meridian, Jackson Co. (Illinois)
White spruce (IV)	20	700	North & south	Sec. 17 and 18, T. 6 S., R. 4 E., Fairbanks Meridian (Alaska)

[1] *Society of American Foresters. Forest cover types of North America (exclusive of Mexico). 67 p. Washington, D. C.: Soc. Amer. Forest. (Reprinted in 1967, 6th Edition).*

[2] *Flight directions are precisely 0°, 90°, 180°, and 270°, true azimuth.*

[3] *I — very intolerant; II — intolerant; III — intermediate; IV — tolerant; V — very tolerant. Frederick S. Baker. 1949. A revised tolerance table. J. Forest.*

Table 18. — Log of detection probability test flights

Test area	Flight		Test area	Flight	
	Date	No.		Date	No.
Interior	6/17/63	4	Oak-Hickory	7/17/65	64
ponderosa pine	6/18/63	5	(52)[1]	7/18/65	75
(237)[1]	6/26/63	6		7/19/65	76
	6/27/63	7		7/20/65	77
	7/1/63	8			
			Northern	7/28/65	80
Lodgepole pine	7/9/63	11	hardwoods	7/29/65	81
(218)	7/12/63	12	(25)		
	7/16/63	14			
	7/19/63	15	Aspen	8/2/65	82
	6/25/64	20	(16)		
	7/9/64	23			
	8/4/64	29	Second-growth	9/20/65	95
	8/6/64	31	Douglas-fir		
	6/22/65	67	(230)		
	7/9/65	71			
	7/10/65	72	Old-growth	9/25/65	97
	6/28/67	195	Douglas-fir		
			(229)		
Engelmann	7/25/63	18			
spruce	7/26/63	19	Sweetgum-	5/20/66	130
(206)	7/29/63	20	water oak	5/21/66	131
	7/31/63	22	(92)	5/24/66	132
	8/1/63	23			
	8/21/63	33	Pin oak-Sweetgum	5/31/66	135
			(65)		
Larch—Douglas-fir	8/27/63	34			
(212)	8/28/63	35	White spruce	6/18/66	143
	8/29/63	36	(Interior Alaska)	6/20/66	144
	9/3/63	37	(201)	6/22/66	145
	9/6/63	38			
	9/18/63	41			
Western	7/22/64	2			
white pine	7/23/64	3			
(215)	8/30/65	91			
	8/31/65	92			
	9/1/65	93			

[1] *Numbers in parentheses are type designations assigned by the Society of American Foresters, "Forest cover types of North America (exclusive of Mexico)," 67 p. Washington, D. C.: Soc. Amer. Forest. (Reprinted in 1967, 6th Edition).*

Table 19. — Detection probability classes for forest cover types of North America

CLASS 1

SAF[1] type no.	Timber type	SAF type no.	Timber type
	WESTERN UNITED STATES		
202	White spruce-Birch	234	Oak-Madrone
203	Poplar-Birch	235	Cottonwood-Willow
204	Black spruce	236	Bur oak
205	Mtn. hemlock-Subalpine fir	*237	Interior ponderosa pine
208	Whitebark pine	238	Western juniper
209	Bristlecone pine	239	Pinyon-Juniper
*212	Larch—Douglas-fir	240	Arizona cypress
214	Ponderosa pine—Larch- Douglas-fir	241	Interior live oak
217	Aspen	242	Mesquite
*218	Lodgepole pine	245	Pacific ponderosa pine
219	Limber pine	246	California black oak
220	Rocky Mtn. juniper	247	Jeffrey pine
221	Red alder	248	Knobcone pine
222	Black cottonwood-Willow	249	Canyon live oak
233	Oregon white oak	250	Digger pine-Oak
	EASTERN UNITED STATES		
1	Jack pine	51	White pine-Chestnut oak
2	Black spruce-White spruce	57	Yellow-poplar
3	Jack pine-Paper birch	61	River birch-Sycamore
6	Jack pine-Black spruce	66	Ashe juniper
8	Jack pine-Aspen	67	Mohrs oak
9	White spruce-Balsam fir-Aspen	68	Mesquite
10	Black spruce-Aspen	69	Sand pine
11	Aspen-Paper birch	70	Longleaf pine
13	Black spruce-Tamarack	71	Longleaf pine-Scrub oak
15	Red pine	72	Southern scrub oak
* 16	Aspen	73	Southern redcedar
17	Pin cherry	74	Sand live oak-Cabbage palmetto
18	Paper birch	75	Shortleaf pine
19	Gray birch-Red maple	77	Shortleaf pine-Virginia pine
21	White pine	78	Virginia pine-Southern red oak
36	White spruce-Balsam fir-Paper birch	79	Virginia pine
38	Tamarack	80	Loblolly pine-Shortleaf pine
42	Bur oak	81	Loblolly pine
43	Bear oak	83	Longleaf pine-Slash pine
45	Pitch pine	84	Slash pine
46	Eastern redcedar	86	Cabbage palmetto-Slash pine
47	Eastern redcedar-Pine	95	Black willow
49	Eastern redcedar-Pine-Hardwood	98	Pond pine
50	Black locust		

(con. next page)

Table 19. — (con.)

CLASS 2

SAF type no.	Timber type	SAF type no.	Timber type
	WESTERN UNITED STATES		
*201	White spruce	216	Blue spruce
*206	Engelmann spruce-Subalpine fir	226	Pacific silver fir-Hemlock
210	Interior Douglas-fir	227	Western redcedar-Western hemlock
211	White fir	228	Western redcedar
213	Grand fir-Larch-Douglas-fir	243	Ponderosa pine-Sugar pine-Fir
*215	Western white pine	244	Pacific ponderosa pine–Douglas-fir
	EASTERN UNITED STATES		
4	White spruce-Balsam fir	54	Northern red oak-Basswood-White ash
5	Balsam fir	55	Northern red oak
7	Black spruce-Balsam fir	56	Northern red oak-Mockernut hickory-Sweetgum
14	Northern pin oak		
20	White pine-Northern red oak-White ash	58	Yellow-poplar–Hemlock
22	White pine-Hemlock	59	Yellow-poplar–White oak–Northern red oak
29	Black cherry		
30	Red spruce-Yellow birch	76	Shortleaf pine-Oak
32	Red spruce	82	Loblolly pine-Hardwood
33	Red spruce-Balsam fir	85	Slash pine-Hardwood
34	Red spruce-Fraser fir	87	Sweetgum–Yellow-poplar
35	Paper birch-Red spruce-Balsam fir	88	Laurel oak-Willow oak
37	Northern white-cedar	89	Live oak
40	Post oak-Black oak	93	Sugarberry-American elm-Green ash
41	Scarlet oak	94	Sycamore-Pecan-American elm
48	Eastern redcedar-Hardwood	96	Overcup oak-Water hickory
* 52	White oak-Red oak-Hickory	97	Atlantic white-cedar
53	White oak		

CLASS 3

	WESTERN UNITED STATES		
207	Red fir	*229	Pacific Douglas-fir
223	Sitka spruce	*230	Douglas-fir–W. hemlock
224	Western hemlock	231	Port-Orford-cedar–Douglas-fir
225	Sitka spruce-Western hemlock	232	Redwood
	EASTERN UNITED STATES		
23	Hemlock	39	Black ash-American elm-Red maple
24	Hemlock-Yellow birch	60	Beech-Sugar maple
* 25	Sugar maple-Beech-Yellow birch	* 65	Pin oak-Sweetgum
26	Sugar maple-Basswood	62	Silver maple-American elm
27	Sugar maple	90	Beech-Southern magnolia
28	Black cherry-Sugar maple	91	Swamp chestnut oak-Cherrybark oak
31	Red spruce-Sugar maple-Beech	* 92	Sweetgum-Nuttall oak-Willow oak

[1] *Society of American Foresters' type designation.*
**Flight tests conducted.*

APPENDIX III

Mathematical Model and Detection Probability Test Data

As noted on page 33, we concluded that detection probability cannot be predicted reliably from our data for other stand densities. However, we can show that the effect of stand density on signal attenuation is predictable.

In actuality, timber stands are quasirandom distributions of trees of various sizes and species. In order to develop a mathematical model to predict the obscuration of targets by timber canopy we will define an ideal timber stand as having randomly distributed trees of the same species. All of the trees will have the characteristics of the average tree; i.e., diameter, crown height, etc. In such a stand we recognize that there are two mechanisms that will obscure a fire target from an airborne IR line scanner: (1) the total attenuation of the target by very large obscuring material (single tree boles, combinations of tree boles, etc.); and (2) the partial attenuation due to smaller (finer) canopy material (small limbs and foliage).

In any natural timber stand an individual target may be completely unobscured, partially attenuated, or totally obscured. We cannot expect to predict the signal strength from a target for a given single observation. The following formulation is to predict a probable target signal — the signal one would expect to observe on an "average" observation. We consider that the timber stand is made up of a random stand of trees boles (large material) that support a homogeneous and spatially continuous canopy (fine material) as diagramed in figure 38.

The total expected transmission, T, for the timber stand is equal to the product, $T_C T_B$, of the expected transmissions through the canopy (T_C) and boles (T_B), respectively. The attenuation density of the obscuring media must be expressed in terms applicable to forest mensuration in order that the model be of practical use.

A tree bole closely approximates an inverted paraboloid of revolution whose vertical cross-sectional area is 2/3 dh, where d = tree diameter, h = tree height. When viewed from an aspect angle, Θ, the horizontal ground area, a, obscured by the tree, $a = 2/3\ dh \tan \Theta$.

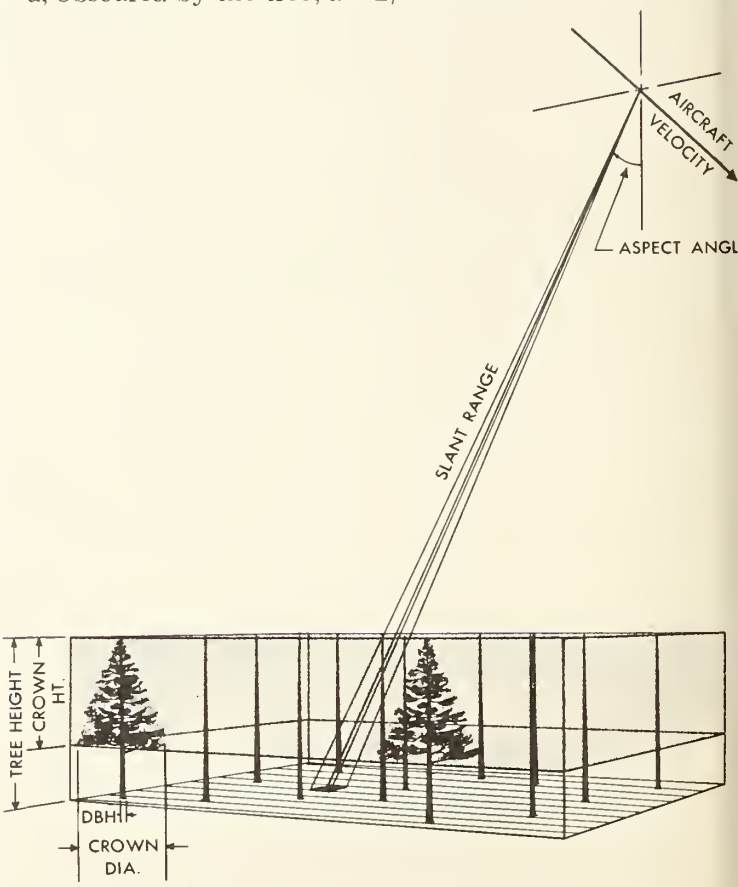

Figure 38. — Conceptual model showing obscuration effects of timber canopies.

The observable, or unobscured part of a unit area in which there is one obscuring tree bole is $T_B = (1\text{-}a) = \left(1 - \frac{2/3\ dh \tan \Theta}{43{,}560}\right)$ Eq. 9

In this equation we have defined unit area (1 acre = 43,560 square feet) in forest mensuration terms. This means that d and h must be measured in feet to satisfy this equation.

The probable transmission through the tree boles for a stand of n (tree boles/acre) with individual characteristics d_i, h_i, is equal to the probable unobscured ground area,

$$T_B = \prod_{i=1}^{n} \left(1 - \frac{2/3\ d_i h_i \tan \Theta}{43{,}560}\right).$$

If all trees are of average size as we have assumed, then

$$T_B = \left(1 - \frac{2/3\ dh \tan \Theta}{43{,}560}\right)^n$$

If an adjustment is made for the orientation of the shadows thrown by the bole (all oriented in the same direction), this equation is more properly of the form

$$(1 - d)^n (1 - h \tan \Theta)^n.$$

Similar adjustments could be made for the nonrandom spacing of trees, the vignetting of a target on the edge of a shadow, the exclusion of fire from the basal area, etc.

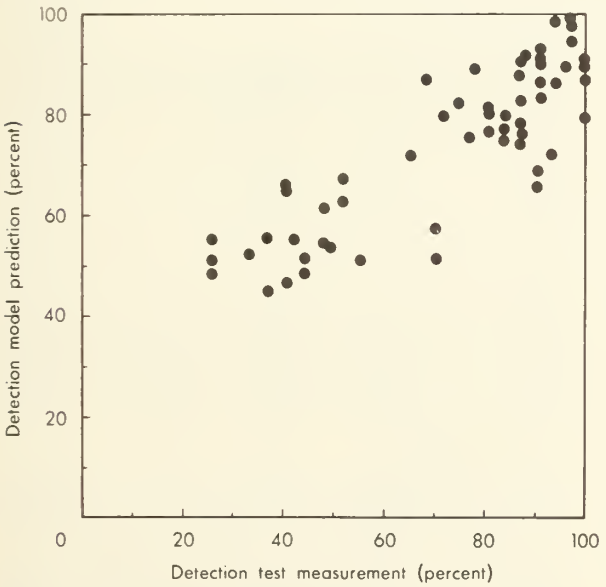

Figure 39. — Correlation of detection probabilities between model predictions and test measurements.

This formulation provides the mechanism for handling several size classes of trees in the same stand (e.g., different species in an understory-overstory association). One might have n_1 trees/acre of size class d_1, h_1; n_2 trees/acre of d_2, h_2; and n_3 trees/acre of d_3, h_3. Obviously, the expected tree bole transmission for such an association would be

$$T_B = \left(1 - \frac{2/3\ d_1 h_1 \tan \Theta}{43{,}560}\right)^{n_1} \times \left(1 - \frac{2/3\ d_2 h_2 \tan \Theta}{43{,}560}\right)^{n_2} \times \left(1 - \frac{2/3\ d_3 h_3 \tan \Theta}{43{,}560}\right)^{n_3}$$

In general, the finer material of the timber crowns only partially attenuates the target radiation (by absorption and scattering phenomena). A continuous and homogeneous attenuating material suggests an exponential transmission model. In such a material, the differential intensity, -dI, absorbed out of a small optical path, is proportional to the path length, dx, and the incident intensity, I. Thus,

$$dI = -\sigma I dx$$

$$\text{or } T_C = I/I_O = e^{-\sigma x}$$

where the constant of proportionality, σ, is the attenuation coefficient of the material (i.e., σ is similar to a loosely defined optical density). It remains for us to determine this "optical density" and path length through the timber crowns.

Consider a unit volume, V = aH, where a = 1 acre and H = one average crown height. And, consider the volume of one average tree crown, $v_c = 2/3(\frac{\pi}{4} D^2 H)$ for deciduous trees (ovaloids of revolution).

Given n trees per acre, the ratio nv_c/V is the fraction of unit volume that is filled with obscuring crown material. The slant path, r, through the unit volume is H sec Θ (aspect angle is measured from the vertical). Thus, the expected (or probable) path length, X, intercepted by crowns is

$$X = \left(\frac{nv_c}{V}\right) r = \frac{nG\frac{\pi}{4} D^2 H}{a \cdot H} H \sec \Theta$$

or

$$X = G \frac{n\frac{\pi}{4}D^2}{43{,}560} H \sec \Theta$$

where G is geometrical factor (1/3 for conifers, 2/3 for deciduous).

The factor, $\frac{n\frac{\pi}{4}D^2}{43{,}560}$, is equal to crown closure, cc, (in percent). The individual crowns are not opaque but have an optical density, J; thus, the average or expected transmission through the crowns is

$$T_C = \exp(-JG\,(cc)\,H \sec \Theta).$$

The optical density, J, is independent of timber stand density (J will vary from one timber type to another but will not vary with the number of trees or their size).

To complete the exposition of the concept, one may conceive of the attenuation coefficient, σ, and path length, x, [$\sigma = JG(cc)$ and $x = H \sec \Theta$], as representing the transmission through a continuous and homogeneous attenuating media. Note here also that the product $\sigma x = \sigma_1 x_1 + \sigma_2 x_2 = [J_1 G_1 (cc)_1 H_1 + J_2 G_2 (cc)_2 H_2] \sec \Theta$ provides for several possible crown classes.

The expected transmission, T, of target radiation through the timber is

$$T = e^{-JG\,(cc)H \sec\Theta} \left(1 - \frac{2/3\ dh \tan \Theta}{43,560}\right)^n. \qquad \text{Eq. 10}$$

Estimates of T were made by measuring the signal strength of the target signature. These estimates were made from the voltage output of the scanning system for the mountaintop tests, and from the film density on the airborne IR imagery.

The primary reason for constructing the obscuration model was to predict the dependence of detection probability on measurable timber cruise parameters.

The timber cruise parameters from the white spruce test plots were used in equation (10) to generate transmission predictions for each target at each aspect angle. These calculated canopy transmissions were used in equation (8), page 37, to generate a set of detection probability predictions. In figure 39, these probability predictions are plotted in comparison with the actual measurements of percent detection from the test flights.

Detection probability measurements, P_5, are made from observations of an array of five 1-square-foot targets (see page 37). The coefficients A, B, and C in the correlation equation (8) are valid only for signal strengths that are comparable to the five 1-square-foot target configurations. However, we can estimate the probability of detecting any number of 1-square-foot targets.

Assume (1) that the obscuring media are randomly oriented relative to the five individual 1-square-foot targets, and (2) that the probability of detecting a single target is P_1, then the following logical sequence gives the probability of detecting m targets. The probability of *not detecting one target* is $(1\text{-}P_1)$. The probability of *not detecting at least one of m targets* is $(1\text{-}P_1)^m$. The probability, P_m, of *detecting at least one of m targets* is $P_m = 1 - (1\text{-}P_1)^m$.

The assumption of randomness is not rigorously true in actual timber stand distributions. Any formulation based on this assumption will only predict a lower limit for detection probability when the size of openings between trees, size of the tree crowns, and size of the target arrays are similar. That is, with actual spatial distribution it is *more likely* that one of the m targets is observable; thus, in practice, actual detection probabilities should be higher.

Measurements of signal strength (or timber obscuration) and measurements of percent detection must be considered as two separate and independent sets of data for statistical analysis. A rigorous formulation of detection probability as a function of target signal strength is impossible because (1) the spatial distribution of timber crown material was not known in the airborne tests; (2) the meteorological and environmental conditions were not constant; and (3) calibration controls for the several mountaintop and airborne systems were inadequate.

In principle, such a formulation should be possible. A questionable example is our comparison of airborne and mountaintop data in figure 32. In this example, the comparison is based on target signal-to-background signal ratios, but the control measurements of the backgrounds are inadequate.

Table 20.—Signal strength frequency distribution by aspect angle for old-growth Douglas-fir test area[1]

Relative signal strength	Aspect angle (degrees)						
	0	10	20	30	40	50	60
0	25.33	31.85	9.33	28.33	43.33	0	0
.33	2.22	1.48	2.67	10.00	0	0	0
.67	2.22	1.48	8.00	2.50	6.67	0	0
1.00	4.44	5.19	9.33	11.67	16.67	0	0
1.33	4.00	2.22	4.00	5.83	0	0	0
1.67	2.22	.74	6.67	3.33	3.33	0	0
2.00	5.78	9.63	4.00	2.50	10.00	0	0
2.33	7.56	2.22	6.67	3.33	3.33	0	0
2.67	3.11	3.70	2.67	2.50	0	0	0
3.00	2.67	5.19	10.67	1.67	0	0	0
3.33	7.56	4.44	4.00	6.67	3.33	0	0
3.67	4.89	4.44	10.67	6.67	6.67	0	0
4.00	7.11	3.70	1.33	3.33	0	0	0
4.33	3.11	2.96	4.00	4.17	3.33	0	0
4.67	6.67	9.63	10.67	4.17	0	0	0
5.00	11.11	11.11	5.33	3.33	3.33	0	0

[1] *Society of American Foresters forest cover type designation No. 229.*

Table 21.—Signal strength frequency distribution by aspect angle for second-growth Douglas-fir test area[1]

Relative signal strength	Aspect angle (degrees)						
	0	10	20	30	40	50	60
0	22.73	23.00	27.50	28.08	32.31	36.67	0
.33	6.36	3.00	4.50	7.31	7.31	6.67	0
.67	4.55	3.00	4.00	6.54	6.15	13.33	0
1.00	5.91	9.00	9.00	11.54	14.23	6.67	0
1.33	3.18	5.00	4.50	6.54	4.62	3.33	0
1.67	5.45	7.00	5.50	6.54	6.15	6.67	0
2.00	5.45	5.00	7.00	6.54	3.46	0	0
2.33	6.36	4.00	4.00	2.69	5.00	5.00	0
2.67	5.91	12.00	8.50	4.23	4.62	8.33	0
3.00	2.73	0	6.50	3.08	3.46	1.67	0
3.33	3.64	4.00	3.50	3.85	2.69	3.33	0
3.67	4.09	3.00	3.00	2.69	2.69	6.67	0
4.00	7.27	7.00	5.00	1.92	1.92	1.67	0
4.33	6.82	1.00	.50	1.92	.77	0	0
4.67	2.73	6.00	2.50	3.08	1.92	0	0
5.00	6.82	8.00	4.50	3.46	2.69	0	0

[1] *Society of American Foresters forest cover type designation No. 230.*

Table 22. — Signal strength frequency distribution by aspect angle for white spruce test area[1]

Relative signal strength	Aspect angle (degrees)						
	0	10	20	30	40	50	60
0	1.79	1.67	5.82	9.69	21.04	45.00	0
.33	.36	1.11	2.73	5.00	9.38	12.73	0
.67	1.43	1.67	3.18	4.69	9.79	9.55	0
1.00	6.79	6.67	12.27	20.00	22.50	15.00	0
1.33	5.00	7.22	6.36	8.13	7.50	4.09	0
1.67	6.07	5.00	8.18	5.94	5.42	3.18	0
2.00	4.64	5.56	10.91	10.31	6.25	3.64	0
2.33	6.43	9.44	7.27	10.31	4.38	1.82	0
2.67	9.29	6.67	5.91	5.00	4.79	2.27	0
3.00	6.43	3.89	6.36	4.69	2.08	.91	0
3.33	7.86	11.67	8.64	4.69	2.92	.45	0
3.67	7.86	9.44	5.00	4.06	2.50	.45	0
4.00	8.93	11.67	5.91	2.50	1.04	.45	0
4.33	7.14	3.33	3.64	3.75	.42	0	0
4.67	4.29	10.00	4.55	.31	0	0	0
5.00	15.71	5.00	2.27	.94	0	0	0

[1] *Society of American Foresters forest cover type designation No. 201.*

Table 23. — Signal strength frequency distribution by aspect angle for western white pine test area[1]

Relative signal strength	Aspect angle (degrees)						
	0	10	20	30	40	50	60
0	11.88	13.00	12.00	20.83	27.50	33.75	50.00
.33	3.13	0	4.00	3.33	3.00	1.25	0
.67	2.50	4.00	0	2.50	6.50	6.25	10.00
1.00	15.63	17.00	22.00	23.33	28.00	26.25	0
1.33	1.88	4.00	5.00	4.17	7.00	8.75	5.00
1.67	5.00	4.00	4.00	6.67	2.50	0	10.00
2.00	8.75	6.00	13.00	9.17	5.50	6.25	5.00
2.33	1.88	4.00	6.00	2.50	4.50	5.00	5.00
2.67	4.38	3.00	7.00	5.00	5.50	2.50	10.00
3.00	11.88	8.00	3.00	5.00	2.00	2.50	5.00
3.33	5.63	5.00	5.00	2.50	1.00	1.25	0
3.67	5.00	5.00	7.00	5.00	2.00	6.25	0
4.00	9.38	7.00	4.00	3.33	.50	0	0
4.33	2.50	2.00	2.00	1.67	1.50	0	0
4.67	5.00	7.00	2.00	2.50	2.50	0	0
5.00	5.63	11.00	4.00	2.50	.50	0	0

[1] *Society of American Foresters forest cover type designation No. 215.*

Table 24. — Signal strength frequency distribution by aspect angle for lodgepole pine test area[1]

Relative signal strength	Aspect angle (degrees)						
	0	10	20	30	40	50	60
0	4.17	15.63	12.50	12.07	16.07	14.06	21.88
.33	2.08	6.25	6.73	5.60	6.55	7.81	17.19
.67	2.08	0	.96	6.90	6.55	9.38	17.19
1.00	7.64	0	5.77	14.22	8.33	4.69	15.62
1.33	7.64	0	.96	4.31	10.71	1.56	4.69
1.67	9.03	9.38	2.88	11.64	8.33	3.13	9.38
2.00	13.89	15.63	3.85	11.21	3.57	6.25	9.38
2.33	15.28	6.25	6.73	9.91	5.95	9.38	3.13
2.67	7.64	0	11.54	6.47	7.74	12.50	0
3.00	7.64	6.25	5.77	5.60	4.76	3.13	0
3.33	4.17	3.13	10.58	3.02	3.57	14.06	1.56
3.67	6.25	3.13	19.23	3.02	1.79	6.25	0
4.00	4.17	6.25	2.88	2.16	4.17	6.25	0
4.33	2.78	3.13	5.77	2.16	7.14	1.56	0
4.67	1.39	15.63	3.85	.43	1.79	0	0
5.00	4.17	9.38	0	1.29	2.98	0	0

[1] *Society of American Foresters forest cover type designation No. 218.*

Table 25. — Signal strength frequency distribution by aspect angle for aspen test area[1]

Relative signal strength	Aspect angle (degrees)						
	0	10	20	30	40	50	60
0	11.67	6.67	2.50	12.50	11.50	17.50	25.00
.33	1.67	3.33	0	5.00	4.50	4.17	10.63
.67	0	5.00	2.50	5.00	7.00	11.67	5.63
1.00	15.00	16.67	25.00	18.75	33.50	38.33	25.63
1.33	3.33	8.33	2.50	3.75	4.00	7.50	6.88
1.67	6.67	0	0	3.75	5.50	1.67	6.25
2.00	11.67	5.00	2.50	7.50	7.00	4.17	3.13
2.33	6.67	8.33	5.00	7.50	7.00	5.00	3.13
2.67	6.67	6.67	15.00	7.50	4.00	2.50	3.75
3.00	6.67	1.67	2.50	6.25	4.50	2.50	3.13
3.33	8.33	5.00	2.50	7.50	2.50	.83	1.88
3.67	1.67	8.33	12.50	2.50	2.50	1.67	2.50
4.00	5.00	5.00	7.50	3.75	1.50	0	1.88
4.33	3.33	3.33	2.50	3.75	1.50	.83	.63
4.67	0	5.00	10.00	3.75	2.50	.83	0
5.00	11.67	11.67	7.50	1.25	1.00	.83	0

[1] *Society of American Foresters forest cover type designation No. 16.*

Table 26. — Signal strength frequency distribution by aspect angle for Northern Hardwoods test area[1]

Relative signal strength	Aspect angle (degrees)						
	0	10	20	30	40	50	60
0	19.38	21.00	23.89	25.00	33.50	36.67	50.71
.33	5.63	5.00	6.11	7.78	7.00	7.08	7.14
.67	6.25	6.50	5.56	7.22	6.50	3.75	2.86
1.00	21.25	17.50	13.33	26.67	22.50	24.58	18.57
1.33	1.88	3.50	6.11	3.89	4.00	5.00	2.14
1.67	4.38	2.50	5.56	4.44	4.50	1.25	1.43
2.00	11.25	9.00	8.89	6.67	5.50	7.08	7.86
2.33	.63	4.00	3.33	3.33	4.50	3.75	1.43
2.67	3.13	1.00	3.33	.56	3.00	2.08	1.43
3.00	3.75	3.50	6.11	2.78	1.00	2.50	3.57
3.33	2.50	6.00	5.56	2.78	3.50	3.75	1.43
3.67	6.88	10.50	2.78	1.67	.50	1.25	0
4.00	5.63	4.50	2.78	3.33	2.00	.83	.71
4.33	1.25	.50	1.11	1.67	1.50	.42	.71
4.67	1.88	4.50	2.22	1.67	0	0	0
5.00	4.38	.50	3.33	.56	.50	0	0

[1] *Society of American Foresters forest cover type designation No. 25.*

Table 27. — Signal strength frequency distribution by aspect angle for pin oak-sweetgum test area[1]

Relative signal strength	Aspect angle (degrees)						
	0	10	20	30	40	50	60
0	3.33	9.44	8.33	11.67	18.13	0	0
.33	.83	1.11	2.50	6.67	6.25	0	0
.67	1.67	2.22	5.83	10.00	9.38	0	0
1.00	22.50	15.56	20.83	24.17	33.75	0	0
1.33	2.50	7.22	10.83	9.17	5.00	0	0
1.67	4.17	7.78	9.17	6.67	3.75	0	0
2.00	6.67	7.22	4.17	2.50	6.25	0	0
2.33	6.67	11.11	2.50	9.17	3.13	0	0
2.67	8.33	5.56	5.00	3.33	1.25	0	0
3.00	5.83	6.11	7.50	4.17	6.25	0	0
3.33	10.83	7.78	5.83	6.67	3.75	0	0
3.67	5.83	3.33	5.00	1.67	2.50	0	0
4.00	6.67	2.78	5.00	.83	.63	0	0
4.33	1.67	4.44	1.67	2.50	0	0	0
4.67	2.50	2.22	2.50	0	0	0	0
5.00	10.00	6.11	3.33	.83	0	0	0

[1] *Society of American Foresters forest cover type designation No. 65.*

Table 28. — Signal strength frequency distribution by aspect angle for gum-oak test area[1]

Relative signal strength	Aspect angle (degrees)						
	0	10	20	30	40	50	60
0	6.00	14.38	13.33	15.00	23.21	31.00	0
.33	3.00	2.50	2.50	2.50	5.00	6.00	0
.67	3.50	2.50	4.17	5.00	3.57	4.00	0
1.00	15.00	7.50	17.50	19.17	11.43	17.00	0
1.33	2.50	3.75	1.67	4.17	3.57	8.00	0
1.67	5.50	3.13	2.50	9.17	6.43	4.00	0
2.00	7.00	4.38	4.17	5.00	8.57	3.00	0
2.33	4.50	5.63	3.33	8.33	5.36	1.00	0
2.67	13.50	11.25	8.33	6.67	7.14	4.00	0
3.00	6.00	8.75	5.83	5.83	4.64	5.00	0
3.33	2.00	3.75	5.00	3.33	4.64	5.00	0
3.67	5.00	6.88	6.67	1.67	2.50	3.00	0
4.00	4.00	6.25	4.17	4.17	3.57	2.00	0
4.33	1.00	6.25	3.33	2.50	1.79	2.00	0
4.67	8.50	3.75	7.50	2.50	4.64	4.00	0
5.00	13.00	9.38	10.00	5.00	3.93	1.00	0

[1] *Society of American Foresters forest cover type designation No. 92.*

Table 29. — Signal strength frequency distribution by aspect angle for oak-hickory test area[1]

Relative signal strength	Aspect angle (degrees)						
	0	10	20	30	40	50	60
0	10.32	7.14	9.44	15.00	18.33	35.00	38.00
.33	5.32	5.00	6.11	3.46	7.50	5.00	9.00
.67	3.71	3.57	3.89	7.69	6.11	7.67	10.00
1.00	21.29	22.14	16.67	21.54	25.28	24.67	25.00
1.33	5.16	2.86	3.89	3.08	5.83	4.67	4.00
1.67	4.35	3.57	1.67	3.85	4.44	4.67	4.00
2.00	8.39	8.57	7.78	9.62	5.00	4.00	2.00
2.33	6.77	5.00	6.11	8.46	4.72	4.33	4.00
2.67	5.48	1.43	4.44	3.85	5.83	3.33	2.00
3.00	6.45	7.86	8.89	5.38	3.89	1.67	1.00
3.33	4.35	2.86	5.56	2.31	1.11	1.00	0
3.67	2.90	5.00	1.67	3.08	1.39	1.33	1.00
4.00	5.32	7.14	3.89	2.69	4.44	1.67	0
4.33	1.77	3.57	2.22	3.85	1.11	.67	0
4.67	1.45	2.14	2.78	1.54	1.94	.33	0
5.00	6.94	12.14	15.00	4.62	3.06	0	0

[1] *Society of American Foresters forest cover type designation No. 52.*

DETECTION PROBABILITY CURVES FOR 13 TEST AREAS

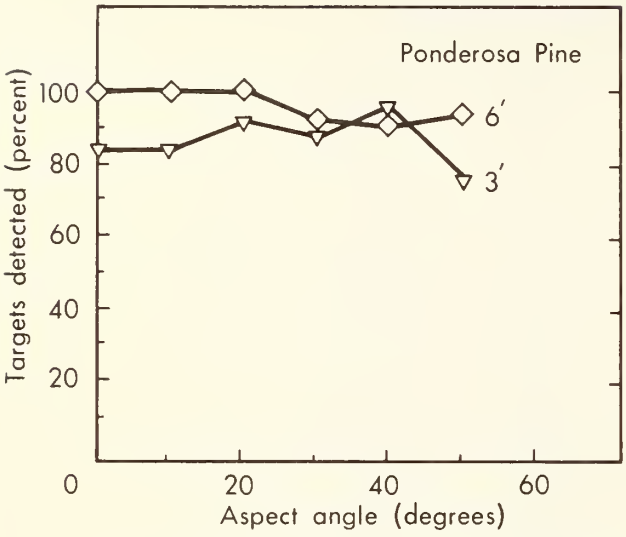

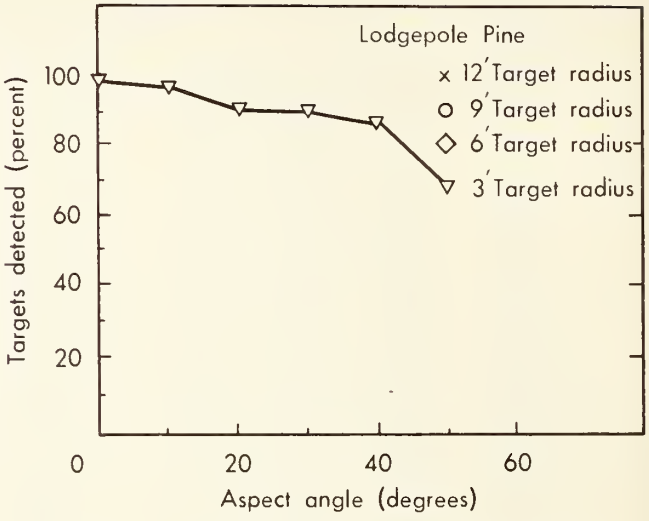

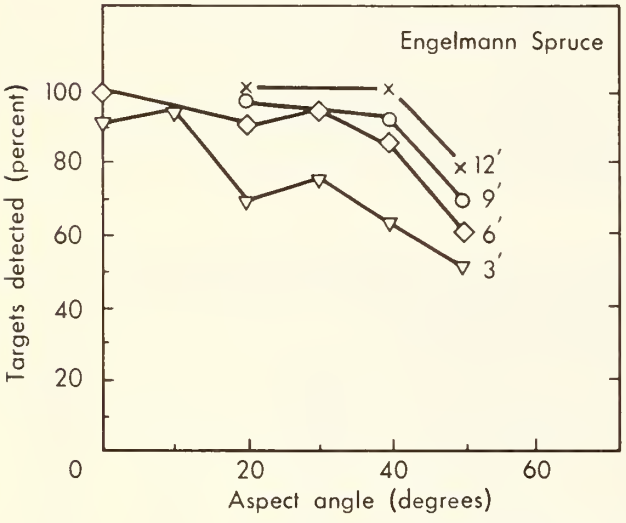

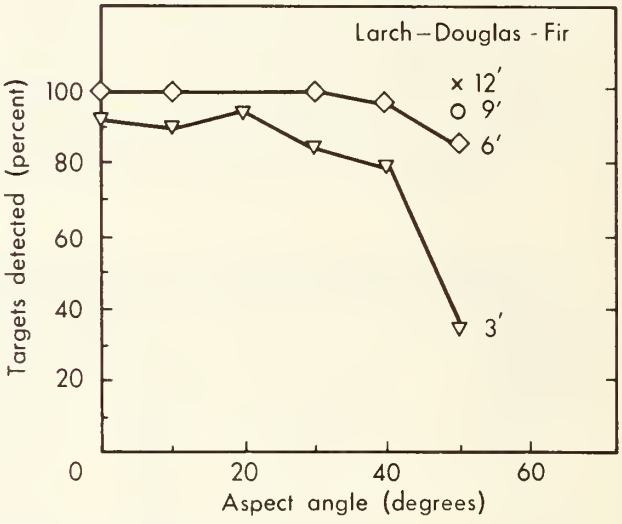

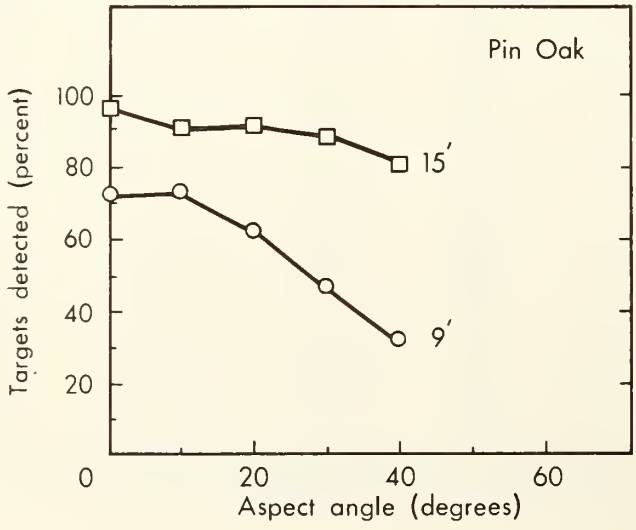

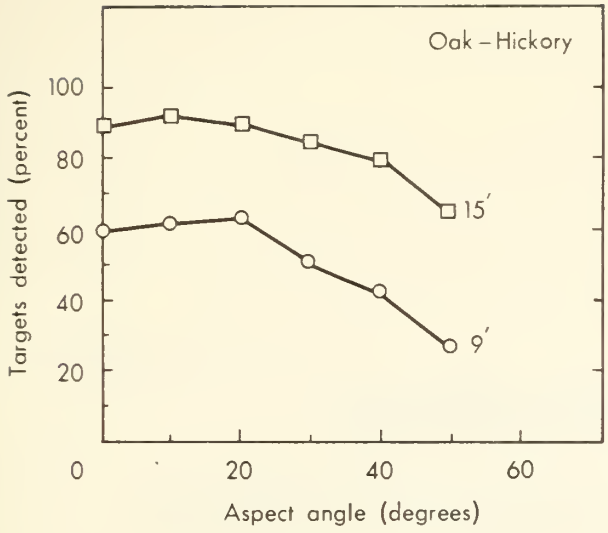
Oak – Hickory
Targets detected (percent)
100
80
60
40
20
0
20
40
60
Aspect angle (degrees)
15′
9′

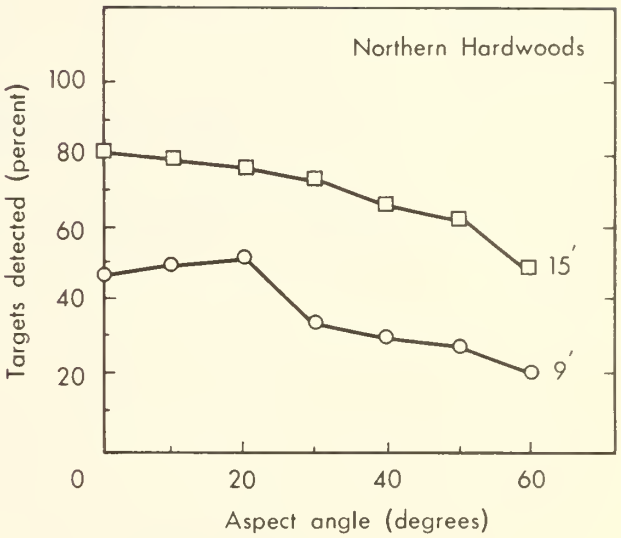
Northern Hardwoods
Targets detected (percent)
100
80
60
40
20
0
20
40
60
Aspect angle (degrees)
15′
9′

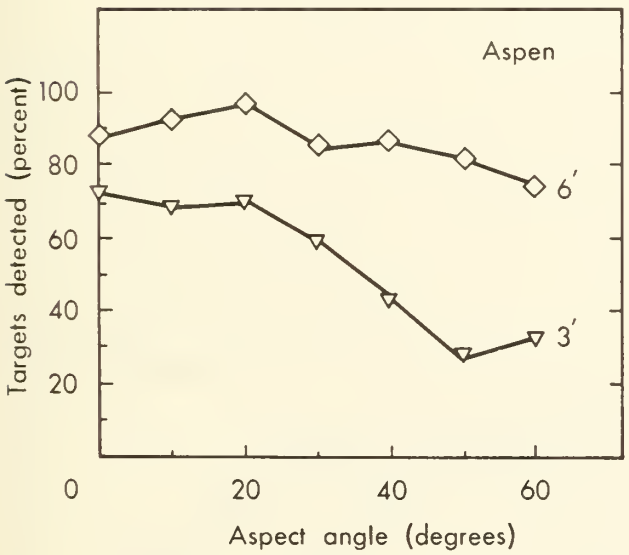
Aspen
Targets detected (percent)
100
80
60
40
20
0
20
40
60
Aspect angle (degrees)
6′
3′

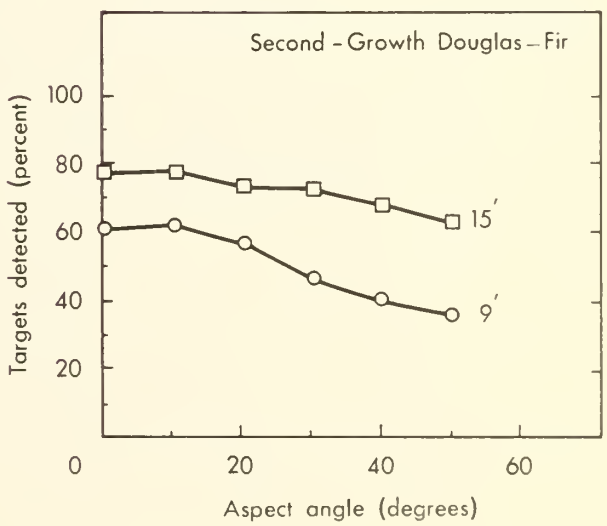
Second – Growth Douglas – Fir
Targets detected (percent)
100
80
60
40
20
0
20
40
60
Aspect angle (degrees)
15′
9′

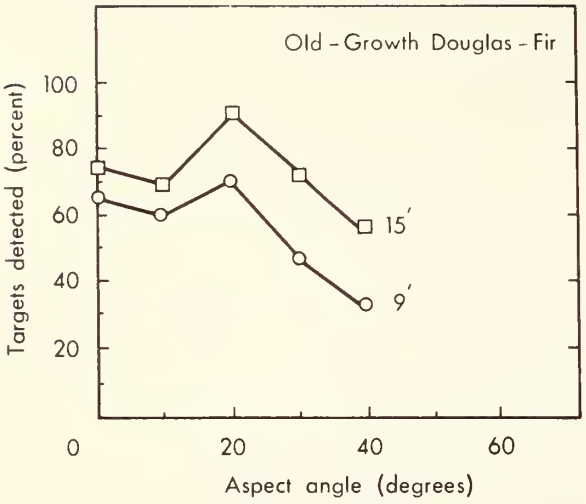
Old - Growth Douglas - Fir
Targets detected (percent)
100
80
60
40
20
0
20
40
60
Aspect angle (degrees)
15′
9′

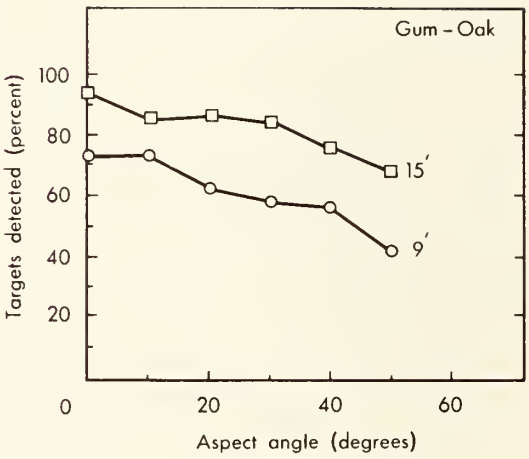
Gum - Oak
Targets detected (percent)
100
80
60
40
20
0
20
40
60
Aspect angle (degrees)
15′
9′

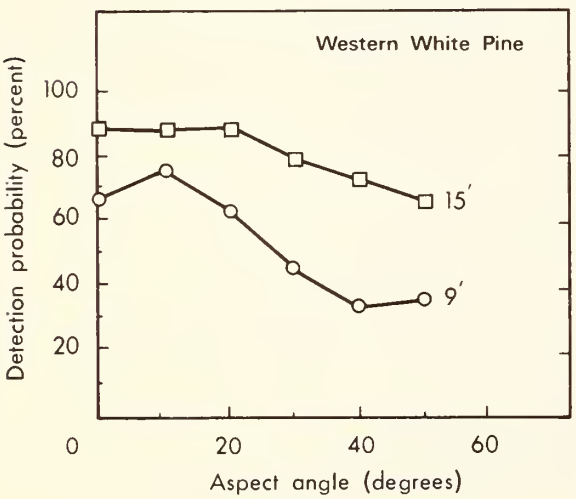
Western White Pine
Detection probability (percent)
100
80
60
40
20
0
20
40
60
Aspect angle (degrees)
15′
9′

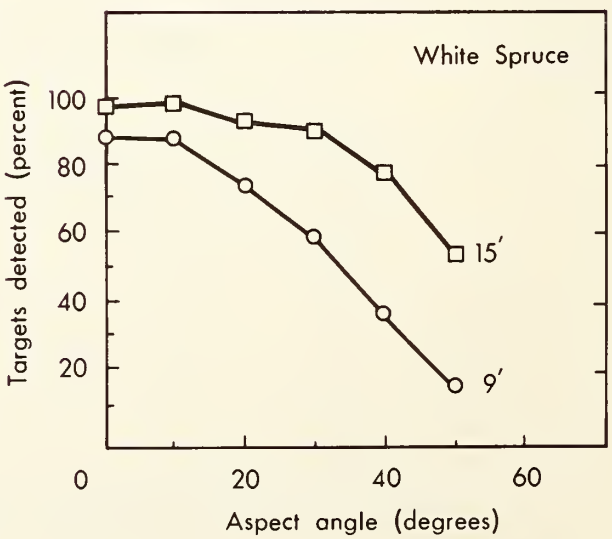
White Spruce
Targets detected (percent)
100
80
60
40
20
0
20
40
60
Aspect angle (degrees)
15′
9′

APPENDIX IV

Data From Operational Patrol Tests

Table 30. — Fire targets detected using airborne infrared equipment during the 1966 fire patrols

Fire no.	Date	Scan angle	Fire size	Time interval between IR scan and visual detection[1]	Fire manned[2]	Detection class[3]	Difference in location between IR and visual report	Remarks
				Hrs.:Mins.				
1	7/14	47°	Snag	—35:30	Yes	1	Same	In old burn, hot fire. Duff burning also.
2	7/15	40°	1 acre	—40:42	Yes	1	SE SE (NE SE)	Old-growth timber, hot fire.
9	7/26	10°	3 × 3 feet	+13:30	No	1	Same	In heavy brush field, very little fire.
10	8/5	30°	Spot	+ 4:00	No	1	Same	
13	8/5	42°	Unknown	—	No	1	—	Detected only on IR, never visually; nothing found on ground search.
14	8/5	38°	5 acres	—10:54	Yes	1	Same	Missed on morning patrol, burning hot when detected on evening patrol.
16	8/5	25°	Spot	+12:51	No	1	Same	
17	8/6	35°	200 acres	Unknown	Yes	1	Same	
18	8/6	50°	Spot	—13:00	Yes	1	Same	
19	8/15	23°	Snag	— 2:22	Yes	1	SW NE 27 (SE 28)	Lone snag on open ridge.
20	8/15	48°	1/4 acre	— 7:00	Yes	2	SW NW (NW NW)	In heavy timber and brush, fire out or cooled before flight.
21	8/15	30°	Spot	—	Yes	1	Same	Hotspot remaining in large fire on Cedar Creek.

[1] *Negative means that detection was first made visually.*
[2] *Whether or not fire was already being suppressed when first detected using airborne infrared equipment.*
[3] *See table 19 on pages 62, 63.*
[4] *Location in parentheses taken from official Forest Service fire suppression reports.*

Table 31. — Fires not detected using airborne infrared equipment during the 1966 fire patrols

Fire no.	Date	Scan angle	Fire size	Time interval between IR scan and visual detection[1]	Fire manned[2]	Detection class[3]	Remarks
				Hrs.:Mins.			
3	7/15	25°	Unknown	— 6:20	Yes	1	Pulse-height circuit not operating on patrol. Heavy brush, possible target on film, no overstory, may have been out at time of patrol.
4	7/14	10°	Treetop	+ 4½ days	No	1	Pulse-height circuit not operating on patrol. In top of live tree, possible target on film.
5	7/15	35°	Tree	+13½ days	No	1	In live tree, no pulse-height circuit, nothing on film.
6	7/16	30°	Tree	— 8:00	Yes	2	Pulse-height circuit not operating on patrol. No target on film. Fire may have been out at time of patrol.
7	7/16	20°	Tree crotch	— 5:20	Yes	1	Same as above.
8	7/16	25°	Spot in duff	— 5:21	Yes	1	Same as above.
14	8/5	35°	Unknown	+ 7:30	No	1	
22	8/15	15°	Tree crotch	+ 2½ days	No	2	Smoldering in tree fork. Did not trip pulse-height alarm.

[1] *Negative means that detection was first made visually.*
[2] *Whether or not fire was already being suppressed when first detected using airborne infrared equipment.*
[3] *See table 19 on pages 62, 63.*

Table 32. — Priority of National Forests for flight patrols

Order of priority	National Forest	Fire frequency per million acres	Average No. forest fires per storm	Priority factor[1]
		REGION 1		
1	Clearwater	53.4	4.11	3.74
2	St. Joe	64.9	4.33	3.74
3	Bitterroot	53.8	2.56	2.40
4	Nezperce	57.8	2.27	2.13
5	Coeur d' Alene	44.8	2.17	1.83
6	Kootenai	35.9	1.69	1.66
7	Kaniksu	36.4	1.67	1.54
8	Colville	31.2	1.56	1.50
9	Lolo	38.8	1.44	1.36
10	Helena	32.0	.94	.87
11	Flathead	19.5	.92	.86
12	Custer	29.6	.85	.83
13	Deerlodge	12.7	.43	.42
14	Lewis & Clark	12.9	.41[2]	.40
15	Gallatin	9.9	.31[2]	.30
16	Beaverhead	8.6	.29	.28
		REGION 2		
1	Bighorn	6.8	.49[2]	.48
2	Shoshone	5.1	.36[2]	.34
		REGION 4		
1	Boise	52.9	2.59	2.32
2	Cache	17.3	2.47	2.30
3	Payette	36.4	2.53	2.27
4	Salmon	32.2	1.53	1.36
5	Caribou	10.4	.94	.88
6	Bridger	8.2	.77	.73
7	Sawtooth	13.2	.63[2]	.59
8	Challis	13.8	.63[2]	.58
9	Targhee	9.5	.58	.54
10	Teton	6.5	.38	.36
		REGION 6		
1	Malheur	106.0	5.76	5.64
2	Ochoco	78.1	5.10	4.87
3	Deschutes	46.1	4.61	4.43
4	Fremont	50.2	4.18[2]	4.15
5	Gifford Pinchot	16.7	5.57	3.83
6	Umatilla	69.3	3.96[2]	3.59
7	Wenatchee	49.8	3.61	3.33
8	Mt. Hood	20.8	4.16[2]	2.97
9	Wallowa-Whitman	49.5	2.92	2.72
10	Snoqualmie	16.0	2.67[2]	2.60
11	Okanogan	25.6	2.41[2]	2.11
12	Winema	39.4	2.08	2.02
13	Mt. Baker	11.1	1.48	1.04

[1] *Development of priority factor is explained on page 28.*
[2] *Based on estimated storm occurrence.*

Flight No. 16

Zone A

Date 8-21-67

Elevation 5,000

Strip Interval 7

PROJECT FIRE SCAN FIRE DETECTION PATROL

NAVIGATOR'S FORM

Forests Covered: CLEARWATER, NEZPERCE, BITTERROOT, LOLO

VOR: MISSOULA VOR to start of run: Course 252.6° Distance 57 3/4

Strip 1: Course: 170.3 Distance: 84 1/4 Slate: Start 4 End 4 of run

Checkpoint. LOCHSA RIVER Miles to go 35 1/2

Strip 2: Course: 350.3 Distance: 84 1/4 Slate: Start ___ End ___ of run

Checkpoint LOCHSA RIVER Miles to go 43 3/4

Strip 3: Course: 170.3 Distance: 84 1/4 Slate: Start ___ End ___ of run

Checkpoint LOCHSA RIVER Miles to go 49 1/2

Strip 4. Course: 350.3 Distance: 84 1/4 Slate: Start ___ End ___ of run

Checkpoint LOCHSA RIVER Miles to go 28 1/2

Strip 5: Course: 170.3 Distance: 84 1/4 Slate: Start ___ End ___ of run

Checkpoint LOCHSA RIVER Miles to go 60 3/4

Strip 6: Course: 350.3 Distance: 84 1/4 Slate: Start ___ End ___ of run

Checkpoint LOCHSA RIVER Miles to go 2.1

Strip 7: Course. 170.3 Distance. 84 1/4 Slate: Start ___ End ___ of run

Checkpoint WHITE SAND CREEK Miles to go 64 1/4

Strip 8: Course: 350.3 Distance: 84 1/4 Slate: Start ___ End ___ of run

Checkpoint BIG SAND LAKE Miles to go 30 1/4

REMARKS:

Figure 40. — Typical completed form with course, distance, and checkpoints detailed for each patrol leg.

Target No. 5

Flight No. 1

Date 7-5-67

PROJECT FIRE SCAN FIRE DETECTION PATROL

TARGET DATA SHEET

Strip 2 Mile Marker: ___

District Challis Forest Challis State Idaho

Sec. NWNE 23 T. 16N R. 18E

Local Landmarks: ON BEAR CREEK SIDE OF DIVIDE AT EDGE OF TIMBER

Time: 0040 (7-6-67) Scan Angle: 36° Heading: 62° TRUE

Plane: R X L ___ of fire

Fire X Campfire ___ House ___ Other ___

Image quality: GOOD Detected X Undetected ___ by IR

Time 0700 Date 7-6-67 reported to Forest.

Time ___ Date ___ reported by Forest. NOT DETECTED

Detected by Air Patrol NO Lookout ___ Other ___

Origin: Time 1900 C.S.T. Date 7-4-67

REMARKS:

Figure 41. — Typical completed form used to document reported fires.

Table 33. — Number of targets detected on 1967 patrol flights by kind

Flight patrol no.	Wildfires		Slash fires	Oil waste	Campfires	Hot springs	Towns	Houses	Trains	Mills	Fires not found[1]	False alarms	Missed by photo-interpreter	Fires never verified	Total
	Initial detection	Second reports													
1	2				8			1	1	1				1	14
2					17	1		5		3	1	2			29
3					20	1	2	6		2		1		2	34
4				4	7	1	1	3					3		19
5	9		3		17	3	2	1		1	3	4	2	2	47
6	1	5			3	2	1	2							14
7	9	1			17	1	4	6		2	6	2			48
8			1		16		1	6							24
9	2		1		17	4	4	1		2	1	14	3		49
10			1		18	1	2	1		1		3			27
11					3	1	3	8	4	2			5		26
12	3		3		17	1	7	11	3	3	1	3		1	53
13	2		3	1	14	2	3	2		3		1	4	1	36
14			4		6	1		1				1			13
15					5			5		1					11
16	44				5	2	2				5	1			59
17	2	8			1		4	5		3	1				24
18	9				1	1	1	1		1					14
19	4				12		2	5		1	1	2			27
20	2				3	3	1			4	2				15
21					11	2	2	3							18
Total targets	89	14	16	5	218	27	42	73	8	30	21	34	17	7	601

[1] *See table 35 on page 84.*

Table 34. — Confirmation of target identification of campfires and wildfires reported to the National Forests

Identification	Number	Percent
TARGETS REPORTED AS WILDFIRES		
Wildfires confirmed by Forest	84	56.3
Second reports on a previously detected fire	14	
Campfires	21	12.1
Slash burning	14	8.0
Miscellaneous hot targets	11	6.3
Unconfirmed reports	30	17.2
Total	174	
TARGETS REPORTED AS POSSIBLE WILDFIRES		
Wildfires confirmed by Forest	3	7.7
Campfires	7	17.9
Miscellaneous hot targets	4	10.3
Unconfirmed reports	25	64.1
Total	39	
TARGETS REPORTED AS POSSIBLE CAMPFIRES		
Confirmed as wildfires	2	
Reported as campfires or miscellaneous	95	
Total	97	

Table 35. — Targets detected on the 1967 fire patrols, but never found by suppression forces

Date	Fire no.	SAF timber cover type	Elevation	Remarks
			Feet	
7/6	21-2	Douglas-fir	8,000	Fire found near area on 7/19, but location given makes it impossible to be the target.
7/13	88-5	Alpine fir	7,000	High, rocky area.
7/13 7/14	95-5	Alpine fir and lodgepole pine	7,000	Detected on two flights. High alpine and goat rock area.
7/13 7/14	98-5	Alpine fir	7,000	Detected on two flights. High alpine and goat rock area.
7/14	117-7	Ponderosa pine	6,000	Lookout reported lightning strike and burst of flames—fire never found.
7/14	124-7	Alpine fir	8,000	High alpine and goat rock area.
7/14	134-7	Lodgepole pine	7,000+	
7/14	140-7	Alpine fir (?)	7,000+	High, rocky area.
	143-7	Alpine fir (?)	7,000	High, rocky area.
7/14	154-7	?	7,000	
7/17	183-9	Lodgepole pine	5,000+	Even stand of lodgepole pine.
7/23	272-12	Douglas-fir, larch, and lodgepole pine	6,000+	High, rocky country with pockets of good timber. Broken up by rockslides and cliffs.
8/21	362-16	?	5,000+	Appears to be heavy timber.
8/21	364-16	?	7,000	
8/21	386-16	NCF[1]	6,000	Appears to be high, rocky country.
8/21	401-16	Alpine fir (?)	7,000+	High, rocky country.
8/21	405-16	Alpine fir (?)	6,000+	High and rocky.
8/22	435-17	NCF	7,000	
8/28	487-19	Juniper (?)	4,000	Fire reported. Never found.
8/30	492-20	Ponderosa pine	5,000	
8/30	495-20	Douglas-fir	7,000	Lightning hit tree in average stand of Douglas-fir.

[1] *Noncommercial forest, no information on site.*

Table 36. — 1967 wildfires detected by IR before visual detection

Fire no.	IR detected		Time reported to forest		Visually detected		Found by suppression forces		Size
	Date	Time	Date	Time	Date	Time	Date	Time	
5-1	7/6	0400		0700	Not detected		7/8	0930	2,700 sq. ft.
69-5	7/13	0210		0830	Not detected		7/13	1110	<.25 acre
92-5	7/13	0505		0830	Morning		7/13	1940	<.25 acre
93-5	7/13	0505		0830	Morning		7/13	1435	<.25 acre
94-5	7/13	0505		0830	Morning		No action taken		Snag
176-9	7/18	2310	7/19	0730	7/19	1655	7/19	2015	<.25 acre
273-12	7/23	2220	7/24	0530	Not detected		7/24	1520	800 sq. ft.
459-18	8/28	0317		0730	9/1	1621	9/1	1730	2.3 acres
460-18	8/28	0330		0730	8/28	0830	8/28	0900	.03 acre
489-19	8/29	0347		0800	Not detected		8/29	1010	360 sq. ft.
498-20	8/31	0345		0700	8/31	0725	8/31	1145	.1 acre

Table 37. — IR detection performance by timber classes and aspect angle

Timber detection class[1]	Aspect angle						
	0°-10°	10°-20°	20°-30°	30°-40°	40°-50°	50°-60°	Total
				DETECTED FIRES			
1	1	6	2	3	0	1	13
2	2	2	2	2	1	0	9
3	0	0	0	0	0	0	0
Total	3	8	4	5	1	1	22
				UNDETECTED FIRES[2]			
1	0	1	0	0	0	0	1
2	0	1	0	0	2	1	4
3	0	0	0	0	0	0	0
Total	0	2	0	0	2	1	5
				COMPLETE MISSES (NO TARGET ON IMAGERY)			
1	0	0	2	1	2	1	6
2	0	0	2	1	2	1	6
3	0	0	0	0	0	0	0
Undetected							
Total	0	2	4	2	6	3	12

[1] *See definition of these classes on page 33.*
[2] *Target recorded on imagery but alarm on automatic target discriminator failed to trip.*

APPENDIX V

Equipment and Instrumentation

Under certain environmental conditions, we might expect that the minimum and maximum temperatures of the terrain background could be T_{min}=290° K and T_{max}=310° K. Thus, the maximum temperature difference, ΔT_{max} = 20° K.

The effective radiation difference can be calculated by equation (2) on page 15. $\Delta W(20°K)$=1.8 watts/(cm^2 steradian °K). The radiation difference available at the scanner aperture from the background would be $\Delta W_A(20°K) = 2.4 \times 10^{-10}$ watts/cm^2 assuming a spectral band pass of 3 to 6 microns, an atmospheric transmission of 50 percent, and a scanner resolution of 4×10^{-6} steradians.

A 700° K fire target has a radiant power, W(fire) (between 3 and 6μ with 50 percent attenuation), W(f)=.095 watts/cm^2 steradian. The radiation from the fire that is available at the scanner is $W_A(f)$, and $W_A(f)=\omega_f W(f)$ where ω_f is the solid angle subtended by the fire target from the scanner. The criterion for this fire to be detected is that its radiation output, $W_A(f)$, must exceed the background radiation signal $W_A(20°K)$; $\omega_f W(f) > \Delta W_A(20°K)$ or

$$\omega_f > \frac{\Delta W_A(20°K)}{W(f)}$$

$$= 2.5 \times 10^{-9} \text{ steradians.}$$

Then, for a scanner resolution, $\omega_s = 4 \times 10^{-6}$ steradians, $\omega_f/\omega_s > 6 \times 10^{-4}$. Thus, we conclude that a 700° K fire is detectable from a 20° K terrain background if it exceeds 6/10,000 of the instantaneous field of view (IFOV) of the scanner.

The following equation, which is based on equations (2) and (7) (see pages 15 and 36), provides a more exact solution for detection criterion:

$$\frac{\text{Fire Area}}{\text{IFOV Area}} > \frac{\int \frac{dW(\lambda,T_{BG})}{dT} \Delta T_{max} \tau(\lambda) R(\lambda) d\lambda}{\int W(\lambda,T_f)\ \tau(\lambda) R(\lambda) d\lambda} \qquad \text{Eq. 11}$$

IR Scanner, Receiver, Optics, Filters

Most of the optical-mechanical scanners that are commercially available are adequate for general thermal mapping. Our present scanner (Texas Instruments, Inc. FFS-1) is a modified version of the Texas Instrument RS-7 (table 38). It has an effective aperture of about 100 cm^2, a focal length of 16.5 cm, and a field stop of 0.0625 cm^2. The scanner (including the 3-to 6-micron filters) has a typical transmission of 70 percent (filters are changed from time to time). We can characterize its response function (see page 14) as an "optical gain," G_O, which is defined as the output-to-input ratio of radiant flux density. For our scanner,

$$G_O = \frac{100 \text{ cm}^2}{.0625 \text{ cm}^2} (.7) \approx 1.1 \times 10^3$$

This optical gain is a constant. It is not subject to "saturation" or "roll off," nor does it affect the noise threshold of our complete detection system. These are logical concepts; for example, it is conceivable that the input flux could be large enough to cause a decrease in transmission or a "roll off" in optical gain. In this sense, the filters are used to control the spectral band pass of the system (i.e., optical gain is a function of spectral wavelength).

Scanning systems of the RS-7 type sweep the resolution element across the object plane at twice the rotational speed of the scanning mirror. Our mirror rotates at 4,000 r.p.m. The lateral resolution, α, is 2 mrd. (determined by focal length and field stop). The active scan, or total field of view, is 120° (nominally 2 radians).

The 4,000 r.p.m. mirror provides a scan rate

$$\dot{\theta} = \frac{2\pi}{60} 4{,}000 \times 2 \approx 800 \text{ rad/sec.}$$

The dwell time, τ, of each resolution element is

$$\tau = \alpha/\dot{\theta} = \frac{2 \times 10^{-3}}{800 \text{ rad/sec}} = 2.5\mu\text{sec.}$$

The scanning rate and the geometrical configuration of the resolution element completely specify the modulation function, $\delta(r\text{-}\dot{r}t)$, of the scanner. The rectangular resolution element is determined by the square field stop. The field stop produces a square wave modulation for a point source by means

Table 38. — History of development of equipment for IR forest fire detection system

Year	Aircraft	Equipment	Results
1962	Beechcraft AT-11	AN/AAS-5 scanner	First imagery obtained through smoke. Preliminary look at detection of small fires under forest canopy.
1963	Beechcraft AT-11	AN/AAS-5 (modified for Polaroid readout)	16 flights over wildfires, imagery dropped to fire bosses. Data collected on detection probability versus scan angle in four coniferous types.
1964	Aero Commander 500B	AN/AAS-5, Polaroid	49 flights over wildfires, gained experience in use of imagery for fire control.
	Convair T-29	AN/AAS-5, KD-14 rapid film processor	No data due to equipment problems.
1965	Aero Commander 500B	Reconofax XI scanner	Preliminary equipment evaluation, no operational data due to equipment problems.
	Convair T-29	RS-7 scanner, Litton CRT, KD-14, Tape recorder	Data collected on detection probability versus scan angle in three coniferous and three deciduous timber types.
1966	Aero Commander 500B	Reconofax XI, Dual Polaroid	System delivered to Div. Fire Control for operation.
	Convair T-29	RS-7, Litton CRT, KD-14, Tape recorder, APN 81 Doppler	Data collected on detection probability versus scan angle in one coniferous and two deciduous timber types. First fire patrols.
1967	Aero Commander 500B	Reconofax XI, Dual Polaroid	Operational, R&D terminated.
	Convair T-29	RS-7, Litton CRT, KD-14, Target discrimination module Bendix DRA-12 Doppler	21 fire detection patrols.
1968	Convair T-29	RS-7, Litton CRT, KD-14, TDM, DRA-12 Doppler	Equipment modified for 2-color system and to reduce size and weight for installation in smaller aircraft.
1969	Beechcraft King Air	RS-7, Litton CRT, KD-14, TDM, DRA-12 Doppler, 2-color temperature discriminator	Equipment tested. 25 operational fire detection patrols.

of the displacement vector, (r-ṙt). The width of the square wave (δ) is α in the object space and τ in the time domain. The resultant resolution on the IR imagery depends on the fidelity of subsequent processing of this square wave signal.

Detectors

Several types of detectors have adequate response in the 3- to 6-micron spectral region around the 1,000°K (fire) blackbody peak. Selected examples of photoconductive (PbS, PbSe, and InSb) detectors have produced good fire detection imagery. Since 1964 we have used photovoltaic (PV) InSb detectors exclusively for fire detection. We have had consistently good performance from the PV, InSb detector; thus, our electronic problems (coupling detectors to preamplifiers) were minimized by standardizing on one good type of detector.

Manufacturers publish typical response curves for their detectors (fig. 42). PV, InSb detectors develop a short circuit current, which is directly proportional to the number of effective photons, and also develop an open circuit voltage, which is proportional to the log of the number of effective photons. Like all photodiodes, PV, InSb detectors do not require the use of bias current for signal generation.

Standard procedures for system design generally recommend that detector detectivity, D*(λ), be used for analysis such as in equation (3) on page 15 and for detector procurement specifications. However, there is a very real danger in this procedure. D* (Jones, Goodwin, and Pullan 1960) is a normalized signal-to-noise, S/N, measurement from the detector for given incident power. A given detector material (e.g., InSb or Ge:Hg) has an inherent responsivity, R, (volts/watt) that is determined by the type of material and, more or less, by the *art* of detector manufacture.

Solid state technology has improved the D* of detectors primarily by lowering the internal detector noise approaching the background noise limit ("BLIP" detectors). Thus, a detector with large D* may not have as high *responsivity* as another detector with poor D*.

The quality of a scanning system is determined by the S/N ratio at the output terminals of the system. The cryogenic IR detector enjoys an inherently lower noise level than the electronic load that it is trying to drive; and therein lies the danger. We have *never* observed this detector noise at the output of an operational system. Good IR scanning systems are almost invariably noise limited in the first preamplifier stages of the electronic chain. Thus, if we desire a large S/N ratio at the system output, we must start with a large detector responsivity at the input and not necessarily the best D*.

If the average responsivity, R, of our detector is taken as 1×10^6 volts per watt between 3 to 6 microns for ambient temperature sources, we can estimate the signal from the detector as follows: Recall

$$\frac{\Delta W_A}{\Delta T} = 1.2 \times 10^{-11} \text{ watts/(cm}^2 \text{°K)}$$

then

$$\frac{\Delta S}{\Delta T} = \frac{\Delta W_A}{\Delta T} \cdot G_o \cdot A \text{ (detector)} \cdot R \text{ (detector)}$$

$$= 7.5 \times 10^{-6} \text{ volts/°K.}$$

The signal representing a 20°K contrast would be $\Delta S_{20°K} = 150$ μvolts, and the signal from a 700° K fire that is big enough to *fill the field of view* will exceed $S_f > 250$ millivolts.

The time varying signal will have components whose amplitude will depend on their thermal contrast and whose duration will depend on their size. The sizes will range in extent from a full scan line (for a broad uniform source) equivalent to a time duration of about 2½ msec, down to a small point (smaller than the resolution element) that will produce a pulse whose width is 2.5 μsec. (i.e., the dwell time of the resolution element). The above response and modulation requirements are well within the capabilities of PV, InSb detectors.

Several detector-preamplifier coupling techniques are appropriate for IR line scan thermal mappers. Each technique has particular advantages:[5]

[5] *Texas Instruments. Infrared devices. 33 p., illus.*

Figure 42. — Characteristics of InSb detectors: A, Frequency response; B, responsivity; and C, spectral detectivity.

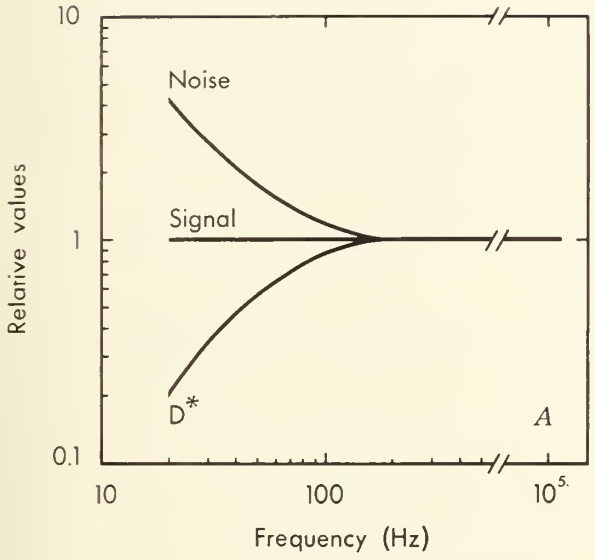

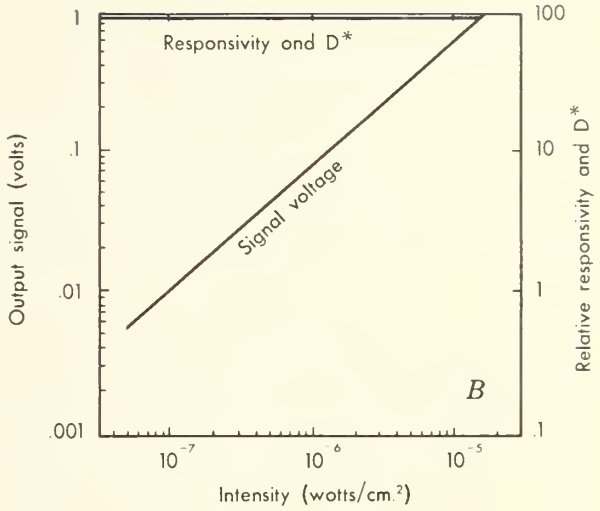

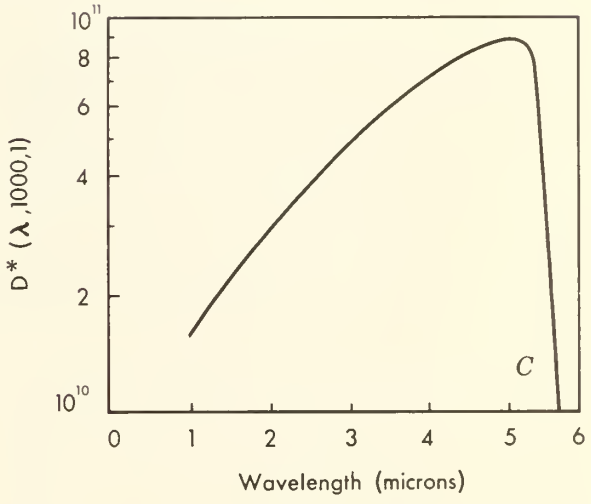

1. The detector may be operated directly into the preamplifier through a d.c. blocking condenser. This method is advantageous for small detectors, or in cases where spectral band-pass filter has reduced the input radiation and, as a result, also reduces the short circuit current of the detector to less than 1 μamp.

2. The detector may be operated in series with a variable bias supply and in parallel with a fixed load resistor whose resistance is much larger than that of the detector. Low noise, solid state circuitry must be used in the preamp. The preamp should be designed for a minimum noise figure for the parallel load. This technique complements high responsivity detectors.

3. The detector may be operated into a preamp load resistance much lower than that of the detector. This technique reduces the RC time constant of the circuitry and utilizes the fast intrinsic response speed of InSb photodiodes.

4. The detector may be coupled directly into a current gain preamp that will automatically maintain the zero bias condition of the detector as the input irradiance changes.

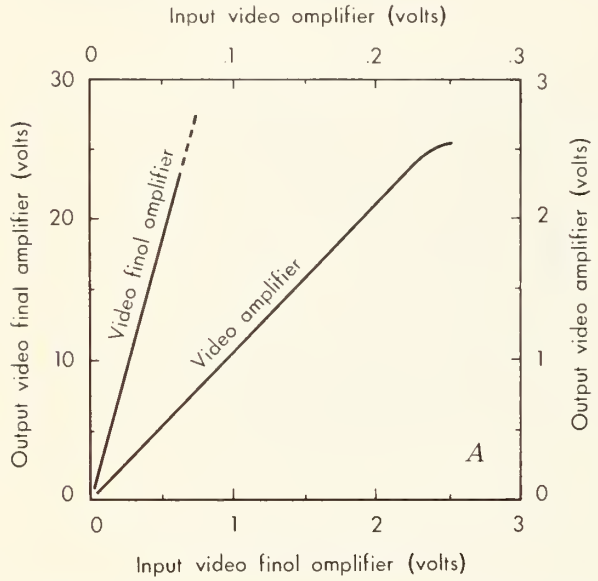

Figure 43. — Characteristics of the video amplifier: A, Gain; and B, frequency response.

Preamplifiers, Amplifiers, and Video Signals

The electric signals from the detector are time dependent. Following standard engineering practice, the modulation characteristics of electronic components are designed and evaluated in the time-frequency domain through the LaPlace transform $S(f) = \int S(t)e^{i2\pi ft}dt$.

The spatial resolution of the scanner is dependent on amplifier frequency bandwidths, etc. In this regard, IR line scanners require relatively wide bandwidths. The high frequency

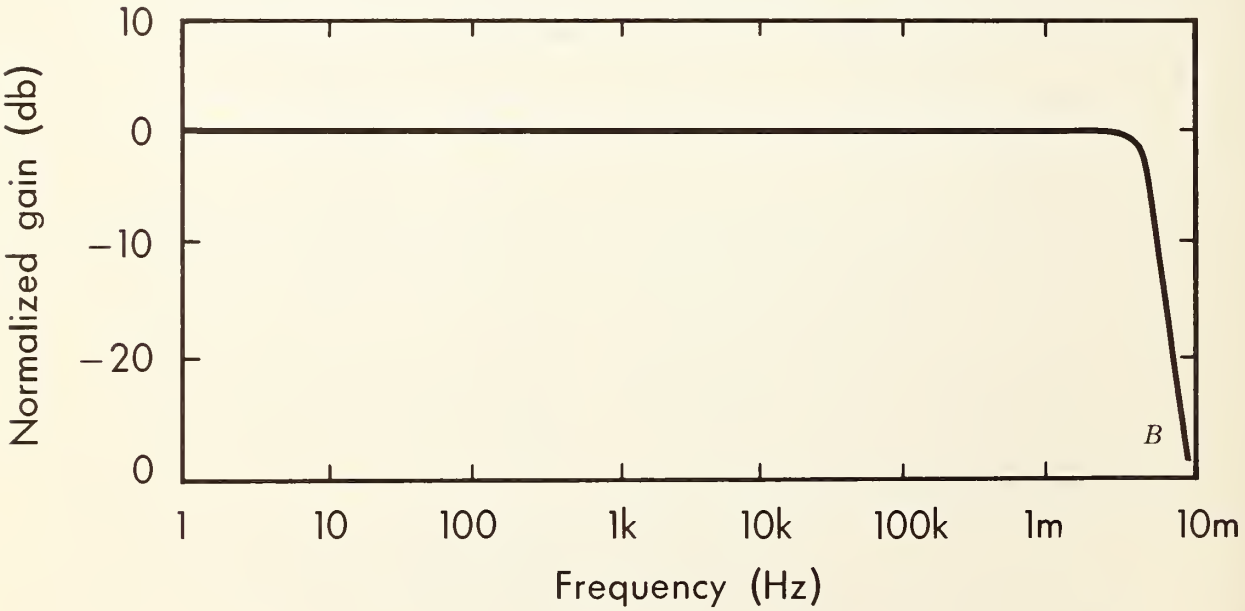

limit is determined by the fidelity with which the square wave resolution element is to be reproduced. Recall it has a pulse width, $\tau \approx 2.5$ μsec. Each full cycle would be 5 μsec long and an upper frequency limit of 200 kc would be adequate, if one were to reproduce a cyclic input signal representing alternate hot and cool sources, each one resolution element wide.

Another high frequency limit, $f = n/\tau$, is indicated if the requirement is to respond with a signal, S, to a hot point target (smaller than the resolution element) signal, S_o. $S = S_o(1\text{-}1/e)$ within 1/n of the dwell time, τ. Or, one might require 1 mc upper frequency limit if the requirement is to reproduce the resolution element's square wave response to a hot point source with the fidelity required by the fifth harmonic of the fundamental frequency.

On the low frequency side of the modulation function, we must reproduce the profile of the 120° scan line, 200 Hz square wave without slope or distortion of any kind. A d.c. lower limit is desirable for this purpose; however, we have made satisfactory imagery with capacitive coupling and a 2.0 Hz low frequency cutoff (for exceptions, see Hirsch and others 1968, app. IV, p. 41).

The "response" function, or gain of an amplifier, is the ratio of output-to-input signals (S_{out}/S_{in}) and is generally unitless (volts/volt, etc.). In some cases (as in the current mode detector-amplifier circuit), the units may be volts of output per amperes of input. Gains of electronic components are a function of the amplitude of the signal being processed (fig. 43). The electronic components are saturated by large signals.

In a well-designed system, the practical limiting noise is most likely the thermal ($T\Delta fR$) noise from the load resistance in the early stages of amplification. This noise is most noticeable because it is amplified by all succeeding stages. When the limiting noise is measured at the system output and compared to an equivalent input temperature contrast, it determines the system NET.

The dependence of gain on signal amplitude and signal frequency may be used to advantage in many cases. For example, we faced the problem of maintaining enough sensitivity to observe small signals of background contrast and yet restricting large amplitude signals from hot targets to the dynamic range of the film. This was easily solved by proper selection of amplifier gain versus signal amplitude curve.

The time dependent output signal, $S(t')$, is determined by the inverse LaPlace transform, $S(t') = \int S(f)e^{-i2\pi ft'}df$, which takes into account all applicable amplitude and bandwidth limitations on $S(f)$. The gain of the electronic system is $G_e = S(t')/S(t)$. The performance characteristics of some of the amplifiers we have evaluated are shown in fig. 44.

Target Discrimination Module

Our early development of automatic target discriminators exploited the unique character of the hot target signals. These targets are much smaller than the instantaneous field of view (IFOV) and thus produce a pulse width, τ, the IFOV dwell time. The signal amplitude of the targets exceeds the maximum background contrast if the targets are hot enough and exceed some small fraction of the scanner resolution element (700°K and $6 \times 10^{-4}\,\omega_{scanner}$ in the case developed on page 88). Our first discrimination circuits were simple signal threshold discriminators whose performance was very poor because of the many false alarms generated by high amplitude random noise pulses from aircraft electronic and radio frequency sources. The technique of narrow band filtering was incorporated into a pulse height/pulse width discrimination circuit. The resistance/capacitance filter networks created many false alarms by differentiating the sharp thermal edges of lakes, roads, ridgetops, etc. Although these circuits produced excessive false alarm rates they were successful in detecting signals of hot fire targets.

In the summer of 1967 we added a target discrimination module (TDM) to our system. It takes advantage of the overscanning capability of the system (fig. 45). Signals from the video electronics are amplified and filtered to obtain signals that are scaled to threshold levels and pulse width limits of interest for detection. The

signal is fed to a pulse selector that produces logic pulses coinciding with any signal element above a selected amplitude threshold and signal elements within selected minimum and maximum pulse widths. The logic pulses are delayed in a serial memory for one scan line and are compared at the comparator with logic pulses produced by the corresponding portion of the following scan line. If a pulse occurs in the same place on two successive scan lines, the comparator activates the output driver, which in turn triggers an external alarm and marks the target on the imagery.

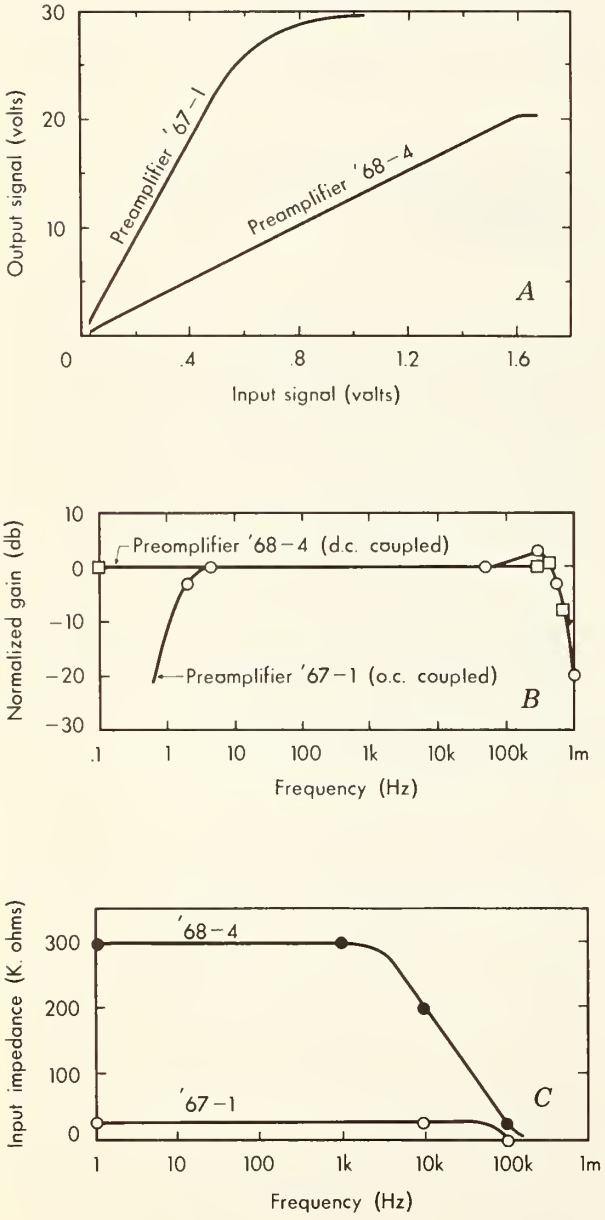

Figure 44. — Characteristics of detector preamplifiers: A, Gain; B, frequency response; and C, impedance.

Cathode Ray Tube, Camera, and Recording Film

The cathode ray tube (CRT) transforms an electronic signal to light intensity. The analogous time-space transform is made by electromagnetic deflection of the CRT spot, $\delta'(r\text{-}\dot{r}t)$, which is the inverse of the scanning mirror operation.

The CRT sweep, or beam deflection system, is responsible for keeping the video signal in register on the output IR imagery. The four major criteria for undistorted imagery are:

1. The CRT spot must be synchronized with the scanning mirror to very close toler-

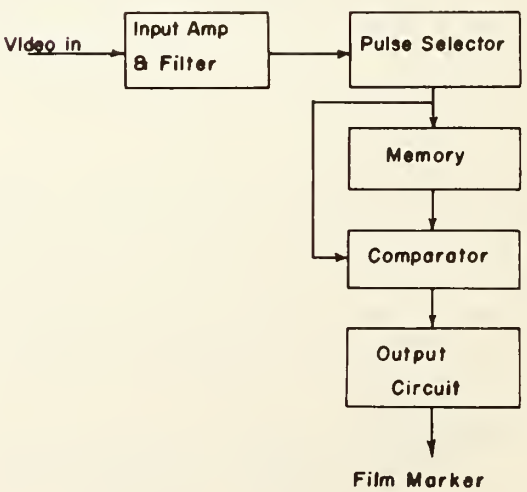

Figure 45. — Block diagram of target discrimination module.

ances. These tolerances are referred to the system input and specified typically as ±1/10 of the resolution element (or ±.2 mrd).

2. The sweep is also stabilized for aircraft roll. In our system the imagery is corrected for ±10° of aircraft roll by electronic stabilization from a vertical gyro reference.

3. The constant scanning speed, $\dot{\theta}$, produces a nonlinear displacement, $\dot{r} \propto \sec^2 \theta$ (where $\theta \propto \dot{\theta}t$) across the terrain. We rectilinearize our imagery (i.e., correct this lateral angular distortion) by electronically driving the CRT spot at a velocity, $\dot{r}' \propto \sec^2 \theta$, such that distance on the imagery is proportional to distances on the ground.

4. The film slew rate must be adjusted relative to the operational V/H of the aircraft. The basic requirement is that the ratio of the lateral and longitudinal components of the image printing vector, $\dot{r}'$, must equal the ratio of the respective components of the scanning vector, $\dot{r}$. Geometrically, it follows that the film slew rate equals $\frac{V}{H}\frac{d}{2} \cot \frac{\pi}{3}$,
where d = width of the imagery.

The size and shape of the CRT spot, δ', (fig. 46) is different than that of the scanning (δ); it is circular and is nearly constant in size (d), as it is displaced over the face of the CRT. When we drive the CRT sweep, $\dot{r}' \propto \sec^2 \theta$, for rectilinearization, we produce a nonlinear dwell time, τ', for the CRT spot. Geometrically $\tau' = d/\dot{r} \propto \cos^2 \theta$.

The exposure of the film is proportional to the product of the light flux density transmitted to the film by the relay camera lens from the CRT spot and the dwell time of the spot, $E \propto I \cdot \tau'$.

To maintain constant exposure across the film, we must remove the $\cos^2 \theta$ dependence of exposure. This is done by electronically generating a $\sec^2 \theta$ intensity correction. The effect of the intensity correction and rectilinearized sweep is that the CRT spot is brighter and moves faster at the edges of the scan line while it is dimmer and moves slower in the center.

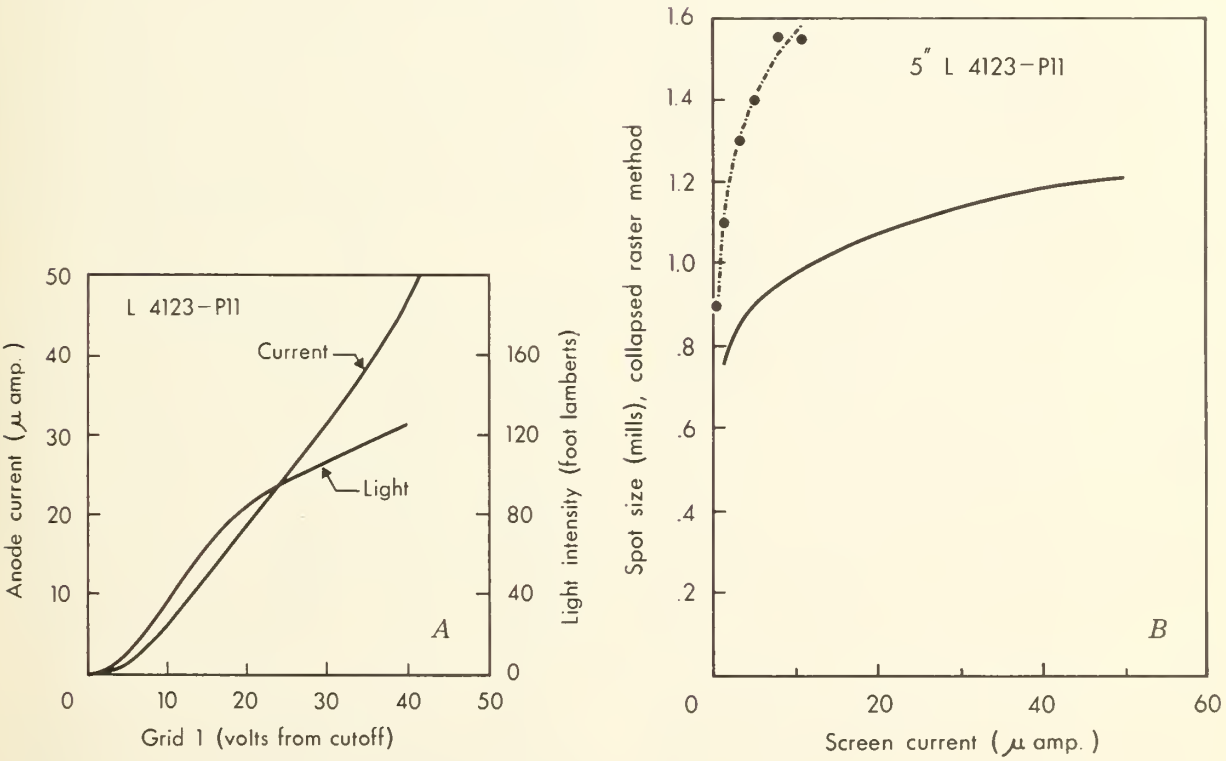

Figure 46. — Characteristic curves of the CRT: A, Response function; and B, resolution.

The camera relay lens is a 6-inch focus f/1.9 Cathode Ray Navitar (ELGEET Optical Co., Rochester, New York) with an adjustable iris to f/16. The resolving power of this lens greatly exceeds the resolution requirements of the system (i.e., its modulation transfer function (MTF) is constant — approximately 100 percent) over the range of spatial frequencies of interest. The magnification ratio (photo image/CRT image = 3.5 in./4.5 in.) is approximately 0.8. The lens response function and photographic exposure of the film depend on the adjustment of f/stop.

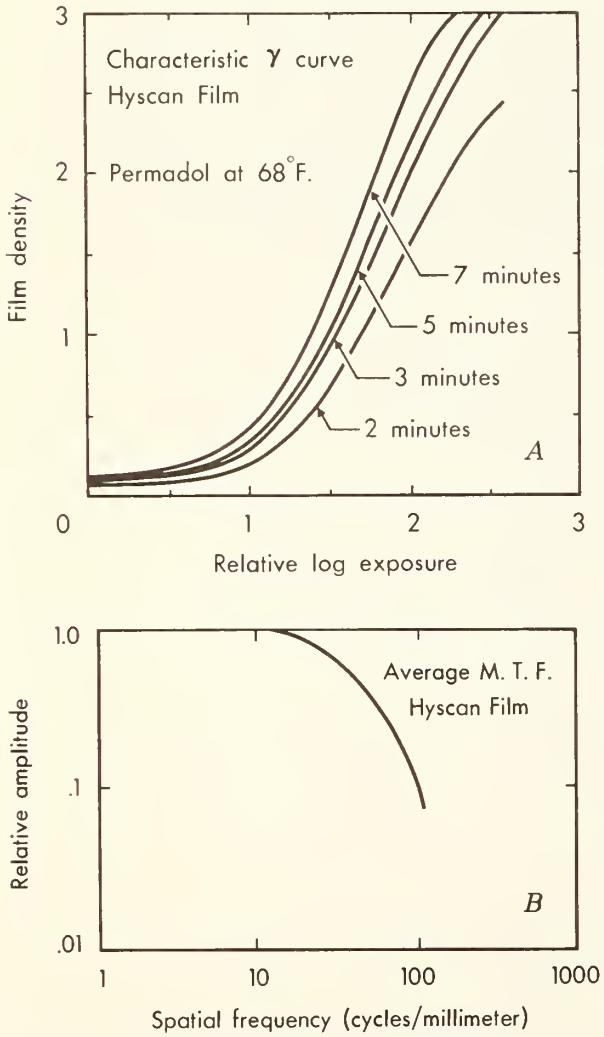

Figure 47. — Characteristics of Hyscan film: A, ν curve (response function; B, resolution function (MTF); and C, spectral response of Hyscan film and P-11 phosphor.

Our IR imagery is recorded on high resolution, high contrast films designed for high temperature, rapid access processing. General Aniline and Film Corporation's Hyscan film characteristic γ curve and transfer function are given in fig. 47. A rigorous calculation of exposure is almost impossible because of ambiguous definitions of light flux density (Biberman 1967). A rough judgment of the response of Hyscan film to P-11 phosphor on the CRT can be made from the spectral curves of figure 47. but it is difficult to relate this sensitivity to the ordinate of the CRT response function (foot candles) of figure 46. In addition, the film speed depends on the processing and exposure conditions. At the beginning of each flight operation, a series of test exposures under prevailing conditions is made to determine CRT brightness, lens f/stop, etc. The dynamic ranges and shapes of these curves (figs. 42 through 47) are useful in system design to properly engineer the total system response. In particular, the electronic amplifiers (where we have considerable design freedom and latitude) must be adjusted so that the desired background thermal sensitivity, dynamic range, and resolution are properly reproduced on the IR imagery.

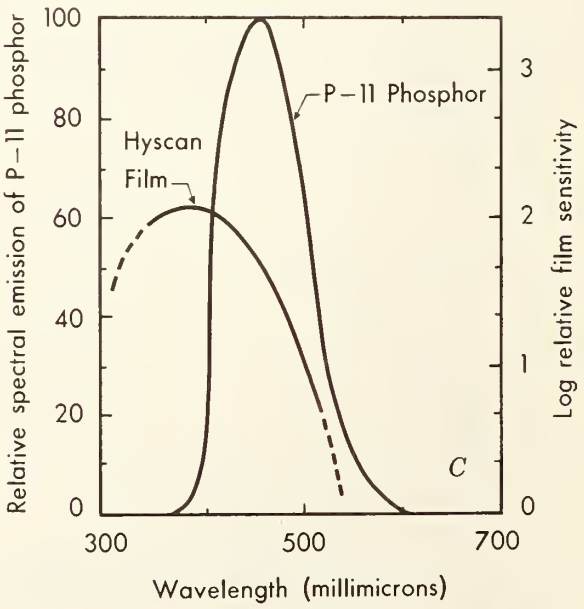

Standard Performance Parameters

It is standard practice to calculate a well defined set of performance parameters (Wolfe 1965) for the purposes of evaluating and comparing airborne IR line scanners. The characteristic parameters of our system follow.

- 120° total field of view (TFOV)±10° for aircraft roll correction.

- 2-mrd optical resolution determined by ¼-mm^2 detector area in the image plane of a 6.5-inch focus collector. The optical system is capable of much better resolution (<.5 mrd); however, we have compromised at 2-mrd optical resolution because of practical considerations of resolution, signal/noise ratios, scanning rates, etc.

- 200 line scans per second. For contiguous scanning, the ultimate capability of the system is 0.4 rad/sec (velocity/height ratio) if the longitudinal optical resolution is 2×10^{-3} radians. The V/H concept is a source of much confusion and ambiguity in the literature (e.g., we normally *operate* our system in the neighborhood of .02 rad/sec-15,000 to 20,000 feet over terrain at 250 to 300 m.p.h.). This produces an overscan such that each point of terrain is scanned or observed about 20 separate, unique, independent times.

- Approximately 2° C noise equivalent temperatures (NET) measured in the laboratory under conditions equivalent to the 0.4 rad/sec scan rate with ambient backgrounds. A statistical integration occurs on the output imagery when we operate at 0.02 rad/sec. We would observe $(S/N)_1 = 1$ for one scan observation if we were to observe a 2°C background temperature difference in the presence of an effective 2°C noise. If we overscan 20 times, $(S/N)_{20} = 1 \cdot \sqrt{20} = 4.5$. Thus, our observed NET is less than ½°C.

- A figure of merit, $n = R/(\Delta T \cdot \Delta\alpha)$, is determined by the system limited resolutions, ΔT = NET, and $\Delta\alpha$ = IFOV, and the field sampling rate R (i.e., the rate at which independent thermal measurements are made). When the performance parameters are properly interpreted, the figure of merit, n, of our system between 1964 and 1967 was approximately $n = 4 \times 10^5$ (sec °K mrd)$^{-1}$.

Because fast scanners and detectors are available, it is not necessary to degrade the other performance parameters of the system just to improve thermal resolution (e.g., one might be tempted to slow the scan speed to produce contiguous scanning at V/H = 0.02 rad/sec and give the detector time to make the ½°C temperature measurement by "one look" contiguous scanning, as recommended by design-tradeoff philosophy).

The improvement in effective NET by overscan has a fortunate effect on image quality when we significantly change altitude. As we go to higher altitudes, the resolution element projected on the ground increases in size. We would expect from equation (2) on page 15 that the observable thermal contrast, T_{BB}, between adjacent resolution elements would decrease because T_{BB} is averaged over larger terrain areas. By overscanning, this lower thermal contrast remains observable.

Another alternative that we have speculated about might be to utilize the full 0.4 rad/sec contiguous scan capability to improve our optical resolution by decreasing the size (× 1/20) of the resolution element and argue that individual measurements in 20 smaller, adjacent areas will provide just as good an average thermal measurement as before. However, consider the convolutions (equations (3) and (5) on pages 15 and 16, respectively) and the sets of orthogonal scanning functions, δ and δ' in the case of the 20 times overscan. If the scanning functions are in phase and register (i.e., $\dot{r}t \equiv \dot{r}'t'$ within tolerances required by the 1/20 resolution scan), then the overscan generates 20 *complete* sets of contiguous imagery — thermal distribution functions that have a unique value at each resolution element. The 20 sets are interlaced such that the maximum cross correlation that can exist between corresponding resolution elements of consecutive sets is about 0.95 (i.e., no two sets overlap more than 19/20). By the same reasoning, the minimum cross correlation is 0.5 (50-percent overlap between the first and eleventh scan lines).

If we superimpose these 20 sets of imagery in exact register (recall that they are not completely correlated spatially), we should observe an improved spatial resolution. In principle, special δ's can be designed that have zero correlation; thus, the ultimate resolution would be determined only by the displacement between scan lines. However, we have the following practical engineering limitations such as: (1) The synchronization and register are difficult to achieve; (2) the video electronic bandwidths that would be required are the same as those required of a 20-times resolution system; and (3) the transforms, δ and δ', are not exact inverses of one another (i.e., δ is generally determined by the area of the detector in the focal plane of the scanner and is a rectangular spatial function with unknown contour, while δ' is usually a circular CRT spot).

Brute force methods, such as more horsepower to turn a scan mirror faster, have a limit. With *good design technique*, system performance depends on the *tolerances* of such parameters as scan sync-register and signal processing fidelity at least as much — probably more — than it depends (1) on scan rate, (2) the V/H ratio at which the system is operated, or (3) the optical resolution. Furthermore, one must have some insight to properly handle these tradeoffs in order to design a better than average system.

Later Equipment Development

The equipment used through 1967 was optimized to detect small, hot targets in wildland terrain. We performed extensive field tests of its operational capability. However, the critical question still remained, "Is it an effective operational tool for finding small, hot targets?" The answer depended in part on the specific operational goals: How small are the targets? How reliable must they be detected? We concluded that the system of 1967 was at the margin of effectively detecting the small targets of interest to the Forest Service.

Our studies demonstrated that a large number of these small, marginal targets does exist. If the small target signals were buried in the background contrast, the target was not detectable. However, even for many small targets a temperature discrimination between target and background could be made by comparing the relative amplitudes of target and background signals in two spectral regions. Furthermore, the system was readily adapted to a two-color temperature discrimination technique.

Since 1967 we have added a second spectral channel to our system (fig. 48). This channel operates in the 8.5- to 11-micron region of the ambient background radiance peak. An Hg:Ge detector is placed in the focal plane of the scanner beside the InSb (3- to 4.1-micron) detector and brought into scan register by electronic-time delay. Thus, both channels look simultaneously at the same IFOV.[6]

The two spectral bands (3- to 4.1-micron and 8.5- to 11-micron) were very carefully chosen to eliminate the effects of changes in concentration of atmospheric moisture on the relative signal amplitudes in the two channels. The effective blackbody temperatures defined in equation (2) on page 15 emphasize the concept of the $T_{BB}(\lambda)$ average over the IFOV at the two widely different wavelengths.

The electronic signal in channel A is adjusted (by a factor K) relative to channel B such that $KS_{Amax} = S_{Bmax}$, or:

$$K \int \frac{dW}{dT}(\lambda, t)\, \Delta T_{max}\, \Upsilon(\lambda)\, R_A(\lambda)\, d\lambda = \int \frac{dW(\lambda T)}{dT}\, \Delta T_{max}\, \Upsilon(\lambda)\, R_B(\lambda)\, d\lambda$$

at the A and B inputs to a differential amplifier. $\Delta T_{max} = T_2 - T_1$ is determined by the warmest and coolest IFOV's of the background, respectively. The output signal of the differential amplifier, S_{KA-B}, from internal calibration sources, is nulled (zero contrast) for the temperatures, T_1 and T_2. The contrast, $\Delta T = T_2 - T$ is not zero for any other background temperature, $T \neq T_1$. Fig. 49 shows computed values of the relative signal, S_{KA-B}, as a function of background temperature for various values of K.

This bispectral difference signal enhances the target signal-to-background signal ratio. A comprehensive description of this system and a performance analysis are being prepared for publication.

[6] *By convention, the InSb (3- to 4.1-micron) channel is "A" channel and the Hg:Ge (8.5- to 11-micron) channel is "B" channel.*

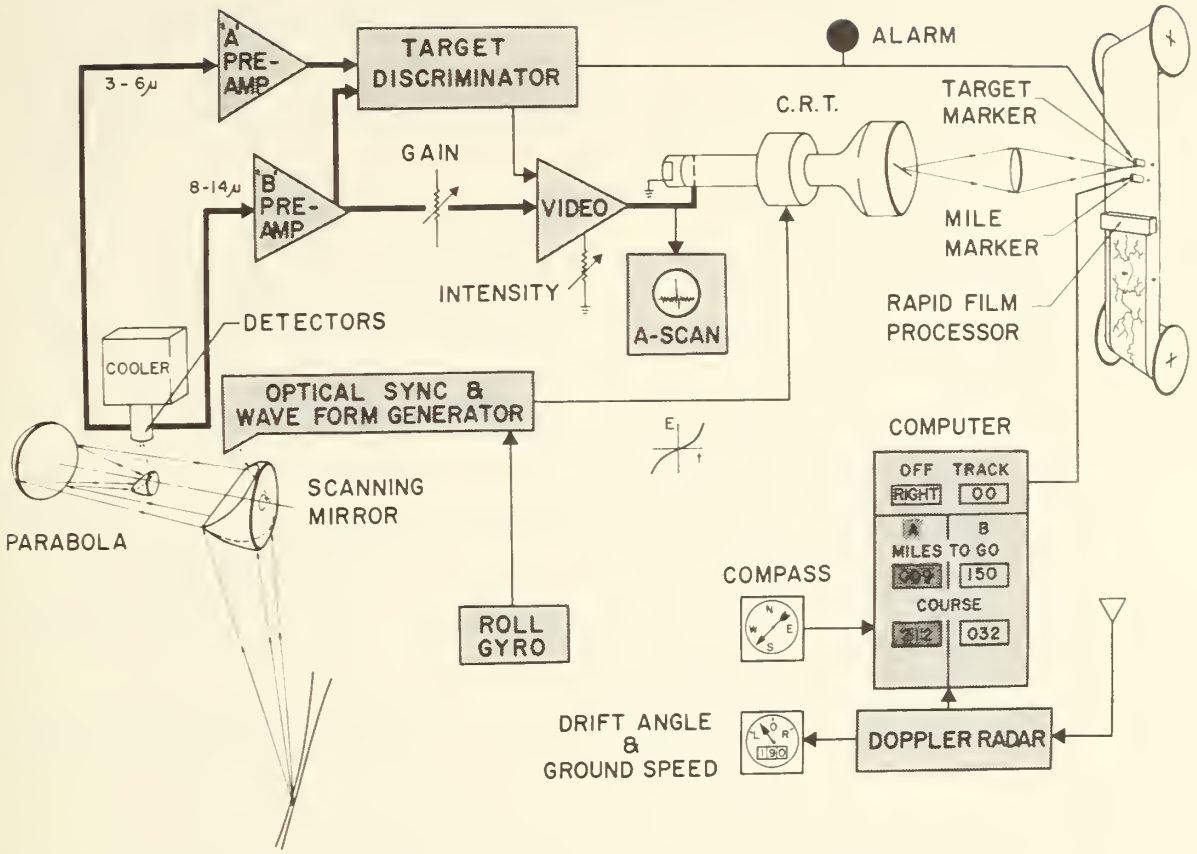

Figure 48. — Schematic of two-color IR fire detection system.

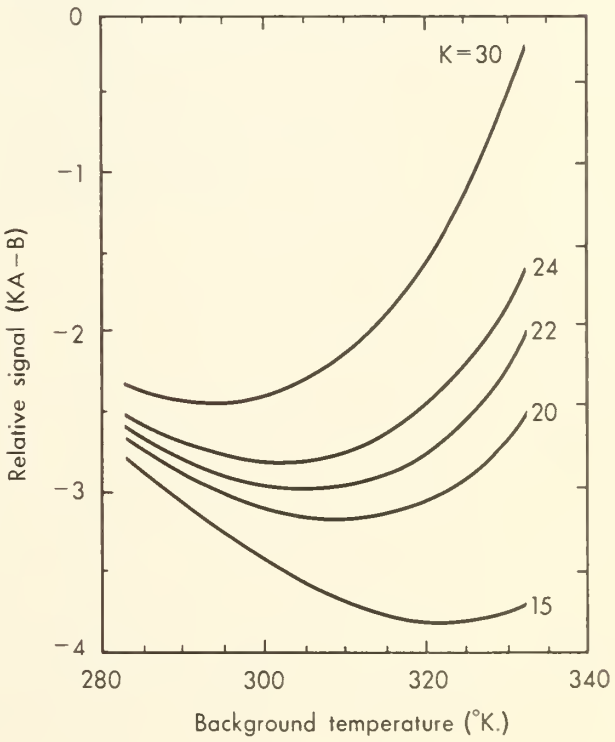

Figure 49. — Computed values of the relative signal (KA-B) as a function of background temperature for various values of K.

Security Classification

DOCUMENT CONTROL DATA - R&D

(Security classification of title, body of abstract and indexing annotation must be entered when the overall report is classified)

1 ORIGINATING ACTIVITY *(Corporate author)*
USDA Forest Service
Intermountain Forest & Range Exp. Station
Northern Forest Fire Laboratory, Missoula, Montana

2a. REPORT SECURITY CLASSIFICATION
Unclassified

2b GROUP

3 REPORT TITLE

Airborne Infrared Forest Fire Detection System: Final Report

4 DESCRIPTIVE NOTES *(Type of report and inclusive dates)*
Final Report, April 1962 to December 1967

5 AUTHOR(S) *(Last name, first name, initial)*
Wilson, Ralph A. Madden, Forrest H.
Hirsch, Stanley N. Losensky, John B.

6. REPORT DATE	7a. TOTAL NO. OF PAGES	7b. NO. OF REFS
May 1971	99	38

8a. CONTRACT OR GRANT NO.
OCD-OS-72-174
b. PROJECT NO. ARPA ORDER #636
Work Unit 2521A
c.
d. ARPA Program Code No. 5860

9a. ORIGINATOR'S REPORT NUMBER(S)
Research Paper INT-93, 1971

9b. OTHER REPORT NO(S) *(Any other numbers that may be assigned this report)*

10 AVAILABILITY/LIMITATION NOTICES

Distribution of this document is unlimited.

11. SUPPLEMENTARY NOTES Study Title: "THE EVALUATION OF AN AIRBORNE INFRARED MAPPER AS A TOOL FOR DETECTING AND MEASURING FIRES."

12. SPONSORING MILITARY ACTIVITY
Dep. of the Army, Office of the Secretary
Office of Civil Defense
Washington, D. C. 20310

13 ABSTRACT

Outlines the basic requirements for an airborne infrared forest fire detection system and discusses the capability of the system to detect hot fire targets in natural forest backgrounds.

DD FORM 1 JAN 64 1473

Security Classification

14. KEY WORDS	LINK A		LINK B		LINK C	
	ROLE	WT	ROLE	WT	ROLE	WT
airborne infrared line scanners detection probability target obscuration forest fire spectral response background noise						

INSTRUCTIONS

1. ORIGINATING ACTIVITY: Enter the name and address of the contractor, subcontractor, grantee, Department of Defense activity or other organization *(corporate author)* issuing the report.

2*a*. REPORT SECURITY CLASSIFICATION: Enter the overall security classification of the report. Indicate whether "Restricted Data" is included. Marking is to be in accordance with appropriate security regulations.

2*b*. GROUP: Automatic downgrading is specified in DoD Directive 5200.10 and Armed Forces Industrial Manual. Enter the group number. Also, when applicable, show that optional markings have been uaed for Group 3 and Group 4 as authorized.

3. REPORT TITLE: Enter the complete report title in all capital letters. Titles in all cases should be unclassified. If a meaningful title cannot be selected without classification, show title classification in all capitals in parenthesis immediately following the title.

4. DESCRIPTIVE NOTES: If appropriate, enter the type of report, e.g., interim, progresa, summary, annual, or final. Give the inclusive dates when a specific reporting period is covered.

5. AUTHOR(S): Enter the name(s) of author(s) as shown on or in the report. Enter last name, first name, middle initial. If military, show rank and branch of service. The name of the principal author is an absolute minimum requirement.

6. REPORT DATE: Enter the date of the report as day, month, year; or month, year. If more than one date appears on the report, use date of publication.

7*a*. TOTAL NUMBER OF PAGES: The total page count should follow normal pagination procedures, i.e., enter the number of pages containing information.

7*b*. NUMBER OF REFERENCES: Enter the total number of references cited in the report.

8*a*. CONTRACT OR GRANT NUMBER: If appropriate, enter the applicable number of the contract or grant under which the report was written.

8*b*, 8*c*, & 8*d*. PROJECT NUMBER: Enter the appropriate military department identification, such as project number, subproject number, system numbers, task number, etc.

9*a*. ORIGINATOR'S REPORT NUMBER(S): Enter the official report number by which the document will be identified and controlled by the originating activity. This number must be unique to this report.

9*b*. OTHER REPORT NUMBER(S): If the report has been assigned any other report numbera *(either by the originator or by the sponsor)*, also enter this number(s).

10. AVAILABILITY/LIMITATION NOTICES: Enter any limitations on further dissemination of the report, other than thoae imposed by security classification, using standard statements such as:

(1) "Qualified requesters may obtain copies of this report from DDC."

(2) "Foreign announcement and dissemination of this report by DDC is not authorized."

(3) "U. S. Government agencies may obtain copies of this report directly from DDC. Other qualified DDC users shall request through _____."

(4) "U. S. military agencies may obtain copiea of this report directly from DDC. Other qualified uaera shall request through _____."

(5) "All distribution of thia report is controlled. Qualified DDC users shall request through _____."

If the report has been furnished to the Office of Technical Services, Department of Commerce, for sale to the public, indicate this fact and enter the price, if known.

11. SUPPLEMENTARY NOTES: Use for additional explanatory notes.

12. SPONSORING MILITARY ACTIVITY: Enter the name of the departmental project office or laboratory sponsoring *(paying for)* the research and development. Include address.

13. ABSTRACT: Enter an abstract giving a brief and factual summary of the document indicative of the report, even though it may also appear elsewhere in the body of the technical report. If additional space is required, a continuation sheet shall be attached.

It is highly desirable that the abstract of classified reports be unclassified. Each paragraph of the abstract shall end with an indication of the military security classification of the information in the paragraph, represented as *(TS)*, *(S)*, *(C)*, or *(U)*.

There is no limitation on the length of the abstract. However, the suggested length is from 150 to 225 words.

14. KEY WORDS: Key words are technically meaningful terms or short phrases that characterize a report and may be used aa index entries for cataloging the report. Key words must be selected so that no security classification is required. Idenfiers, such as equipment model designation, trade name, military project code name, geographic location, may be used as key words but will be followed by an indication of technical context. The assignment of links, rules, and weights ia optional.

AFLC/HAFB Ogden

Headquarters for the Intermountain Forest and

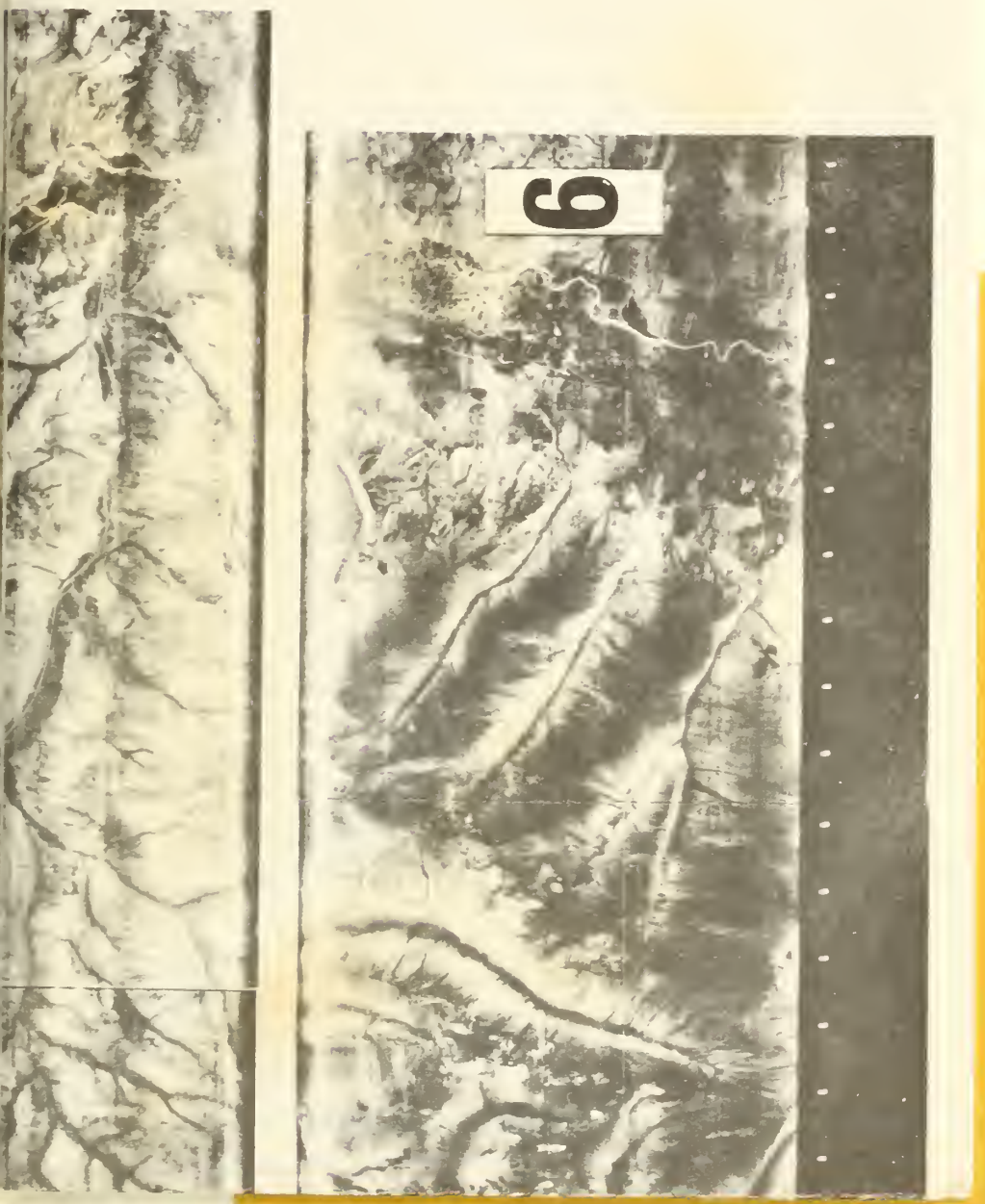

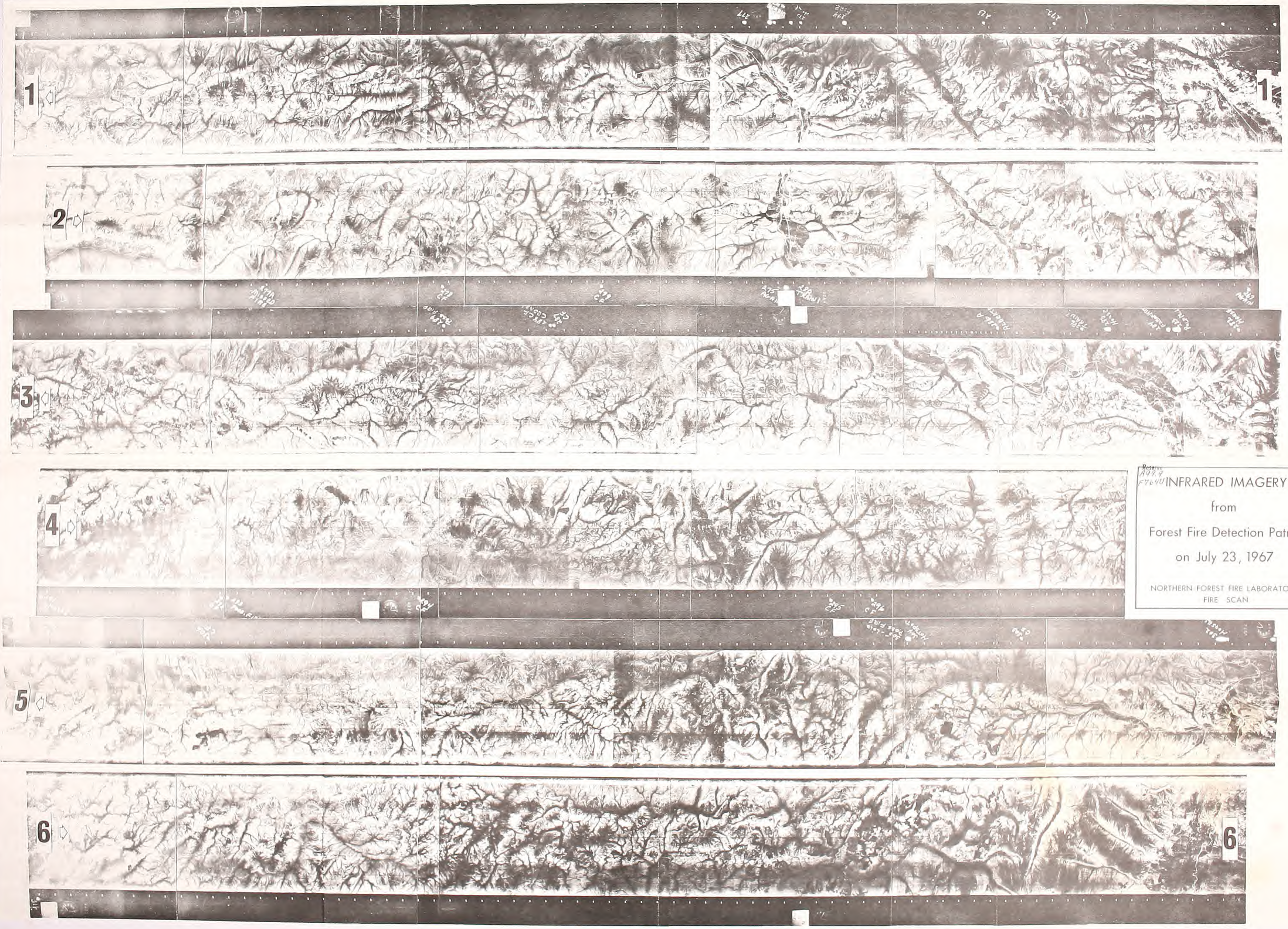

Reserve
A99.9
F764U

INFRARED IMAGERY

from

Forest Fire Detection Patrol

on July 23, 1967

NORTHERN FOREST FIRE LABORATORY
FIRE SCAN

Headquarters for the Intermountain Forest and Range Experiment Station are in Ogden, Utah. Field Research Work Units are maintained in:

Boise, Idaho
Bozeman, Montana (in cooperation with Montana State University)
Logan, Utah (in cooperation with Utah State University)
Missoula, Montana (in cooperation with University of Montana)
Moscow, Idaho (in cooperation with the University of Idaho)
Provo, Utah (in cooperation with Brigham Young University)

WOOD · WATER · FORAGE
WILDLIFE · RECREATION
FOREST SERVICE
U S
DEPARTMENT OF AGRICULTURE